DOCTOR OF PHILOSOPHY

Depth Modulation in Radiotherapy

Baugh, Gareth

Award date:
2016

Awarding institution:
Coventry University

Depth Modulation in Radiotherapy

Gareth Baugh

September 2016

A Thesis submitted in partial fulfilment of the University's requirement for the degree of Doctor of Philosophy.

Faculty of Engineering, Environment and Computing, Coventry University
in collaboration with University Hospitals Coventry and Warwickshire (UHCW), NHS Trust.

Abstract

Intensity Modulated Radiotherapy (IMRT) has been a major field of research over the last thirty years and is today the standard in radiotherapy treatment of cancer. The introduction of IMRT into the clinical environment has greatly improved the ability of the treatment team to conform the radiation dose to the tumour volume. Alongside improvements in image guidance, IMRT has led to a reduction in side effects for patients and opened up the possibilities of dose escalation and hypofractionation. IMRT is however by no means perfect. IMRT and derivatives such as Volumated Arc Therapy (VMAT) are limited by the exit dose from the X-ray beams and deliver a significant amount of radiation dose to normal tissues. The much publicised alternative to IMRT is proton therapy. Proton therapy beams deposit dose over a narrow range resulting in minimal exit dose. The future of radiotherapy certainly involves a significant contribution from proton therapy but the availability to patients is likely to remain limited for a long time to come. The research in this thesis considers the possibility of further improving IMRT by modulating radiotherapy beams along their direction of travel as well as across their intensity, i.e. the so called 'Depth Modulation' of the thesis title. Although there are numerous possible ways to achieve depth modulation, this work proposes a combination of X-ray beams with electron beams of different energies with both modalities delivered with a conventional medical linear accelerator. The research in this thesis is concerned with developing a proof of principle for this method. It is to some extent a theoretical study, however at each step the possibility of practical implementation has been considered with the view that the method is only a viable proposition if it can be effectively implemented into clinical practice.

The technique proposed in this work is to use electron beams delivered through X-ray MLC with a standard patient set up. To reduce scatter and photon contamination it is proposed to remove the scattering foils from the beamline and to employ optimisation of the electron and photon components to compensate for any remaining penumbra broadening. The research has shown that improvements to dosimetry through removal of the scattering foil would allow delivery without reducing the source to surface distance, making a single isocentre synergistic

delivery for both the electron and photon components practical. Electron dose segments have been calculated using Monte Carlo radiation transport and a procedure to optimise dose for the combined photon and electron IMRT technique has been developed. Through development of the optimisation procedure the characteristics of the mixed modality technique have been examined. A number of findings are demonstrated such as the benefit of gaps between electron segments, the benefits of optimising for energy in three dimensions and the dependence of the cost function minimum on the electron to photon ratio. Through clinical examples it has been shown that for tumours close to the surface the mixed modality technique has the potential to reduce the dose to normal tissues, particular in the low dose wash. Calculations of relative malignant induction probability demonstrate that this reduction in dose has the potential to reduce the incidence of secondary cancer induction. Possible treatment sites for application of the technique include breast, head and neck, brain and sarcomas.

Acknowledgement

A number of people have been of great help, assistance and inspiration during the course of this research. First I would like to thank Dr. John Mills of UHCW for inspiring me to embark upon a PhD by research six years ago. From this time forward I have enjoyed continued support from Coventry University and I would like to express my sincerest gratitude to my supervisors Prof. Keith Burnham and in particular Dr. Olivier Haas, formerly of CTAC and currently with the Mobility and Transport Research Centre, for the opportunity to pursue this research project and their academic support of my studies. I would also like to thank Prof. Adrian Wilson, Dr. Nigel Williams and Dr. John Sage of UHCW for their continued encouragement and support in pursuing this research on part time basis. I would like to thank the physics staff at UHCW who have been a great help either directly by engaging in discussion of the topic or indirectly by ensuring that there was no effect on the service during the time I dedicated to this research. I would particularly like to thank Bob Crichton and the engineering team at UHCW for their assistance in configuring a clinical linac to run in scattering foil free electron mode, often out of hours. I would also like to acknowledge the work of Paul Johnson and Thomas Roussi whose undergraduate projects contributed to aspects of the optimisation work in this research. For his encouragement to pursue a topic that is perhaps not mainstream I would like to thank Prof Mikael Karlsson from Umeå University.

And finally, a special thanks to my family. I couldn't do it without your support and understanding.

Contents

Abstract ii

Acknowledgement iv

Contents v

Glossary of Abbreviations xi

List of Figures xiii

List of Tables xviii

Chapter 1 .....

Introduction and outline of approach 1

1.1. Introduction 1

1.2. Background to the problem 1

1.2.1. Radiotherapy 1

1.2.2. Radiobiology 2

1.2.3. Hardware 3

1.2.4. Treatment Planning 7

1.2.5. Treatment Technique 8

1.3. Motivation for research 9

1.4. Research aim and objectives 12

1.5. Thesis outline 14

1.6. Contributions of the thesis 15

1.7. Publications 17

Chapter 2 .....

Critical review of depth modulation in radiotherapy 18

2.1. Introduction 18

2.2. Depth Modulation in Radiotherapy 18
2.2.1. X-ray energy modulation 18
2.2.2. Heavy charged particle energy modulation 19
2.2.3. Very high energy electrons (VHEE) 20
2.2.4. Modulated electron radiotherapy (MERT) 21
2.2.5. Mixed X-ray and Electron Therapy 24
2.2.6. Summary 26
2.3. Optimisation 27
2.4. Practical IMRT planning 31
2.4.1. Physical Constraints 31
2.4.2. Objective function 32
2.5. Clinical Evaluation 34
2.5.1. Isodose 34
2.5.2. Dose-volume data 34
2.5.3. Equivalent uniform dose (EUD) 35
2.5.4. Normal tissue complication probability (NTCP) 36
2.5.5. Malignant induction probability (MIP) 36
2.6. Discussion and conclusions 37
Chapter 3 .....
Dosimetric characteristics of xMLC shaped scattering foil free electron beam 39
3.1. Introduction 39
3.2. SSD 39
3.3. Methods 40
3.4. Electron beam delivery through xMLC 42
3.5. Scattering foil free electron beam 43
3.6. Dose rate 49

3.7. Peripheral doses 51

3.8. Segment size 53

3.9. Discussion and conclusions 54

Chapter 4 .....

Monte Carlo modelling of an xMLC scattering foil free electron beam 55

4.1. Introduction 55

4.2. BEAMnrc scattering foil free model 56

4.3. Monte Carlo transport parameters 58

4.3.1. Electron-step algorithm= PRESTA-II 58

4.3.2. Spin effects= On 59

4.3.3. XIMAX = 0.5. 59

4.3.4. ESTEPE = 0.25 59

4.3.5. Boundary crossing algorithm= PRESTA-I 59

4.3.6. Skin depth for BCA= default 60

4.3.7. Global ECUT= 0.7, Global PCUT= 0.01, Global SMAX= 5 60

4.3.8. Sensitivity study 60

4.4. Parallel processing 62

4.5. Tuning the beam model 63

4.6. Small fields 65

4.7. SSD 67

4.8. Energy 68

4.9. CT calibration 69

4.10. Conclusions 70

Chapter 5 .....

Optimisation 71

5.1. Introduction 71

5.2. Problem formulation 71
5.2.1. Limitations and assumptions 72
5.2.2. Constrained minimisation problem 72
5.3. Methods 73
5.3.1. Radiotherapy treatment planning environment 73
5.3.2. Optimisation solvers 74
5.3.3. Common set up for optimisation solvers 76
5.3.4. Phantoms used to evaluate the approach 76
5.4. MERT 79
5.4.1. MERT Introduction 79
5.4.2. Electron matrix resolution 79
5.4.3. Electron intensity modulation 82
5.4.4. Electron energy modulation 85
5.5. exIMRT 88
5.5.1. exIMRT Introduction 88
5.5.2. Treatment plan set up for the cylindrical phantom 90
5.5.3. Optimisation solvers 90
5.5.4. exIMRT optimisation 94
5.6. Results of exIMRT comparison with IMRT 101
5.7. Discussion and conclusions 102
Chapter 6 .....
Clinical treatment plan comparison 103
6.1. Introduction 103
6.2. Assumptions and approximations 104
6.2.1. RBE 104
6.2.2. X-ray photon dose calculation and segmentation 104

6.3. Case descriptions 105
6.3.1. Case descriptions: Introduction 105
6.3.2. Description: Case 1 - Paraspinal sarcoma 106
6.3.3. Description: Case 2 – Brain 106
6.3.4. Description: Case 3 – Concomitant breast boost 107
6.3.5. Description: Case 4 – Head and Neck re-treatment 108
6.4. Results 110
6.4.1. Results: Introduction 110
6.4.2. Results: Case 1 - Paraspinal sarcoma 110
6.4.3. Results: Case 2 – Brain 113
6.4.4. Results: Case 3 - Concomitant breast boost 114
6.4.5. Results: Case 4 – Head and Neck re-treatment 117
6.5. Radiobiology 118
6.5.1. Radiobiology: Case 1 119
6.5.2. Radiobiology: Case 2 119
6.5.3. Radiobiology: Case 3 120
6.5.4. Radiobiology: Case 4 121
6.5.5. Conformity and Malignant induction probability (MIP) 122
6.5.6. Discussion and conclusion 124
Chapter 7 .....
General conclusions and further research perspectives 125
7.1. General conclusions 125
7.2. Further research perspectives 127
7.2.1. Robustness 127
7.2.2. Planning studies 128
7.2.3. Clinical implementation and validation 128

References 129

Appendix A .....

Optimisation Algorithms 138

Appendix B.....

Dose-volume data 143

Appendix C.....

Radiobiology 146

Glossary of Abbreviations

This section presents the notational conventions used for abbreviations in this thesis.

3D-CRT	Three-dimensional conformal radiotherapy
CAX	Central axis
CI	Conformity index
CT	Computed tomography
CTV	Clinical target volume
DVH	Dose-volume histogram
EUD	Equivalent uniform dose
eMLC	Electron MLC
exIMRT	Combined electron and X-ray IMRT
GTV	Gross tumour volume
IAEA	International Atomic Energy Agency
ICRU	International Commission on Radiological Units and Measurements
IEC	International Electrotechnical Commission
IMRT	Intensity-modulated radiotherapy
kV	Kilovoltage
LET	Linear energy transfer
MC	Monte Carlo
MIP	Malignant induction probability
MLC	Multi-leaf collimator
MU	Monitor units
MV	Megavoltage
NTCP	Normal tissue complication probability

OAR	Organ at risk
PRV	Planning organ at risk volume
PTV	Planning target volume
RBE	Relative biological effectiveness
R_{50}	Half value depth
relMIP	Relative malignant induction probability
RF	Radiofrequency
SSD	Source to surface distance
ssIMRT	Step and shoot IMRT
TCP	Tumour control probability
TPS	Treatment planning system
UHCW	University Hospital Coventry and Warwickshire
VMAT	Volumetric modulated arc therapy
xMLC	X-ray MLC

List of Figures

Figure 1.1 The variation of dose with depth in the patient for X-rays and for electrons at energies commonly used in Radiotherapy..... 6

Figure 1.2 Examples of dose gradients in radiotherapy treatment. a) Ideal step function with an immediate drop to zero dose after PTV. b) Taken from a clinical bilateral Head and Neck VMAT plan showing the drop in dose from the target to the adjacent parotid gland. c) The penumbra at the edge of single direct 6MV X-ray 10cm square field at 10cm depth in the patient d) a 230MeV direct proton field depth dose taken from (Cai et al., 2015) e) 10MeV 10cm square field electron depth dose curve..... 11

Figure 1.3 A comparison of 3D conformal radiotherapy (3DCRT), Intensity Modulated Radiotherapy (IMRT) and the proposed mixed modality exIMRT approaches 13

Figure 1.4 flow chart illustration contributions of theses 16

Figure 3.1 X-ray field orthogonal to MERT at 60cm SSD (left) and 80cm SSD (right), tumour not covered by maximum field size at 60cm SSD 40

Figure 3.2 Elekta scattering foil carousel with empty space 42

Figure 3.3 Measured off axis profiles in water for a 10MeV electron beam (scattering foils in place) at 95cm SSD, field defined by a 10x10cm applicator and by 10x10cm (set field size) Jaws and MLC (measurement in the MLC direction, Elekta MLCi 1cm wide leaves)..... 42

Figure 3.4 Measured electron fluence across half the field at 60cm SSD for a 10MeV field, scattering foils removed jaws and MLC set at 40x40cm in orthogonal planes and across the diagonal. 44

Figure 3.5 Profiler measurements of field symmetry with scattering foils removed. Taken directly from Sun Nuclear Profiler software and showing measured profile (red), measured profile mirrored about the central axis (blue) and the % difference (purple), plotted against distance off axis (a) A-B and (b) G-T direction, 25x25cm set field size. 44

Figure 3.6 Measured off axis profiles in water for a 10MeV electron beam at 90cm SSD 2cm deep, 40x40cm Jaws and MLC (set field size). With and without the scattering foils across the A to B (similar profiles measured in the G to T and diagonal axis). 45

Figure 3.7 Measured off axis profiles in water for a 10MeV electron beam at 90cm SSD 2cm deep, 10x10cm Jaws and MLC (set field size). With and without the scattering foils across the A to B axis (left) and across the G to T axis (right). 46

Figure 3.8 Measured off axis profiles in water for a 10MeV electron beam 2cm deep, 2x2cm Jaws and MLC (set field size) across the A to B axis. With and without the scattering foils at 90cm SSD. 47

Figure 3.9 Measured percentage depth dose for a 10MeV electron field delivered through the jaws and MLC at 90cm SSD for a 2x2 cm field with and without scattering foils to show reduction in X-ray contamination 48

Figure 3.10 Measured off axis profiles in water for a 10MeV electron beam 2cm deep, 2x2cm Jaws and MLC (set field size) across the A to B axis. With and without backup jaws. 49

Figure 3.11 Variation of dose rate with field offset in the B direction for a 10MeV 2x2 xMLC scattering foil free electron beam at 90cm SSD relative to a clinical 10MeV 10x10 field delivered with an applicator at 95cm SSD 51

Figure 3.12 Dose distal to the field edge measured using a 0.6cc Farmer chamber and 6MV build up cap. Distance from the field edge towards G (a), towards T (b) and towards B(c). Detail with and without build up cap (d). 52

Figure 3.13 EDR2 radiochromic film measurements of 10MeV profiles at 90cm SSD and 2cm deep 1x1cm and 2x2cm profiles overly each other and 5x1cm (across the 1cm direction) is wider. 53

Figure 4.1 Monte Carlo Simulation of a 10MeV parallel electron beam incident on the nickel exit widow and a 0.07mm Tantalum primary scattering foil (left) and the exit window alone (right). Electrons tracks are shown in blue, contaminant X-ray photons in yellow as they enter the opening of the primary collimator. Disks represent the planes of the foils. 57

Figure 4.2 10MeV 2x2cm Monte Carlo calculated depth dose in a water/air/water/bone/water phantom with different boundary crossing algorithms 62

Figure 4.3 10MeV Energy tuning using 10x10cm field depth dose curve at 90cm SSD. See Table 4.3 for corresponding modelling parameters. 64

Figure 4.4 Comparison of measured and Monte Carlo calculated dose for a 2x2cm field at 90cm SSD, (a) profiles at 4 depths, (b) detail of depth dose and (c) detail of profile at 3cm

deep both with error bars from Monte Carlo variance and gamma index overlaid in green. 66
Figure 4.5 Comparison of measured and Monte Carlo calculated dose for a 2x2cm field at 90cm SSD 3cm deep offset from the central axis by 6cm in the A-B direction (offset defined at 100cm SSD). Error bars from Monte Carlo variance and gamma index overlaid in green. 67
Figure 4.6 Comparison of measured and Monte Carlo calculated depth dose curves for a 10x10cm field at 80cm SSD. 68
Figure 4.7 comparison of measured and Monte Carlo calculated dose for a 10x10cm field at 90cm SSD 6MeV, 10MeV and 15MeV. 68
Figure 4.8 CT calibration curve for Monte Carlo dose calculations 70
Figure 5.1 Cylindrical software phantom to test exIMRT optimisation 79
Figure 5.2 Matching of two 90cm SSD 10MeV 2cm segments at 2cm deep a) no gap, b) 1cm gap, c) 2cm gap and d) matched to 50% isodose (gap size defined at isocentre). 81
Figure 5.3 Matching of two 90cm SSD 10MeV 2cm beamlets at 2cm deep. Field edge position with gap (gap size defined at isocentre). 82
Figure 5.4 Intensity modulation to create a flat dose distribution. Calculated profile for a 5x5 matrix of 2cm electron segments optimised for uniformity at 2cm depth 90cm SSD 10MeV electron beam compared to measured 10MeV 10x10 field collimated with jaws and MLC and a measured clinical 10MeV field collimated with a 10x10cm applicator at the water surface also at 2cm deep 83
Figure 5.5 The effect of energy on the segment weighting required to produce a flat field. Composite profiles and the constituent segments for a) 6MeV, b) 10MeV, and c) 15MeV at 90cm SSD 1.5cm, 2cm and 3.0cm deep respectively. The optimisation leads to segment 2 and 4 having zero weighting for 6MeV and 10MeV. Composite profile is for a 2d matrix so also includes a contribution from segments not in this plane. 84
Figure 5.6 Intensity modulation of segments to conform dose to 2D shapes as seen from the beams eye view. 90cm SSD 10MeV 2cm deep. 85
Figure 5.7 Isodose lines for abutting segments of dissimilar energy without optimisation. Without a gap, with a 2cm gap and with a 2cm gap and manual increase of the 6MeV segment weight. 86

Figure 5.8 Dose distribution for a stepped PTV used to demonstrate energy modulation of the MERT beam. Energy fixed at 6, 10 then 15 MeV across the PTV (range selection) or left to the optimiser to choose between the three energies (free optimisation)..... 87

Figure 5.9 Fluence maps for a stepped PTV used to demonstrate energy modulation of the MERT beam. Energy fixed at 6, 10 then 15 MeV across the PTV (range selection) or left to the optimiser to choose between the three energies (free optimisation)..... 88

Figure 5.10 Illustrative dose distributions calculated with XiO treatment planning system pencil beam model for overlaid 6MV X-rays and 15MeV electrons. 6MV X-ray beam intensity modulated to offset the wide penumbra of the electron beam and produce a uniform dose distribution at 1.5cm deep. At 10cm combined electron and X-ray dose has dropped to less than 5% on the central axis but the X-ray only dose is 68%..... 89

Figure 5.11 Plot of cost function value *F(x)* against function counts for an IMRT problem with the MATLAB fminsearch simplex search and fmincon interior-point and SQP algorithms..... 92

Figure 5.12 Plot of cost function value *F(x)* against function counts for an IMRT problem with genetic algorithm, particle swarm optimisation (PSO), Firefly and MATLAB fmincon interior-point algorithms..... 94

Figure 5.13 Plot of cost function value *F(x)* against function counts for an exIMRT problem with Firefly and MATLAB fmincon interior-point algorithms. 96

Figure 5.14 Plot of cost function value *F(x)* against the electron weighting factor *m*. X-ray beam Gantry angles have been set to maximise the benefit of the exIMRT plan (0, 62, 104, 256 and 298 degrees). 98

Figure 5.15 Flow chart depicting two stage exIMRT optimisation processes..... 100

Figure 5.16 Dose distribution on the central slice for the phantom study for the 6MV X-ray photon IMRT plan and a) the MERT component, b) the 6MV X-ray photon IMRT component and c) the total dose for exIMRT (a+b=c)..... 101

Figure 6.1 Case 1: Dose distribution on the isocentre slice for paraspinal sarcoma plan in the axial (top) and sagittal plane (bottom) for Monaco 6MV VMAT, xIMRT and exIMRT treatment plans. 111

Figure 6.2 Case 1: DVH for paraspinal sarcoma plan Monaco 6MV VMAT (top), xIMRT (bottom) and exIMRT treatment plans..... 112

Figure 6.3 Case 1: OAR mean doses for Monaco 6MV VMAT, xIMRT and exIMRT treatment plans. 112
Figure 6.4 Case 2: Dose distribution on the isocentre slice for brain plan in the axial plane for Monaco 6MV ssIMRT (left) and exIMRT (right) treatment plans. 113
Figure 6.5 Case 2: DVH for Brain plan Monaco 6MV ssIMRT and exIMRT treatment plans. 114
Figure 6.6 Case 2: OAR mean doses for Monaco 6MV VMAT, xIMRT and exIMRT treatment plans. 114
Figure 6.7 Case 3: Dose distribution on the isocentre slice for concomitant breast boost plan in the axial plane for Monaco 6MV ssIMRT (left) and exIMRT (right) treatment plans. 115
Figure 6.8 Case 3: DVH for concomitant breast boost plan Monaco 6MV ssIMRT and exIMRT treatment plans (with detail at under 10Gy). 116
Figure 6.9 Case 3: OAR mean doses for Monaco 6MV ssIMRT, xIMRT and exIMRT treatment plans. 116
Figure 6.10 Case 4: Dose distribution on the isocentre slice for head and neck re-treatment plan in the axial plane for Monaco 6MV ssIMRT (left) and exIMRT (right) treatment plans. 117
Figure 6.11 Case 4: DVH for head and neck re-treatment plan Monaco 6MV ssIMRT and exIMRT treatment plans. 118
Figure 6.12 Case 4: OAR mean doses for Monaco 6MV ssIMRT, xIMRT and exIMRT treatment plans. 118

List of Tables

Table 2.1 Summary of MERT+IMRT studies for <20MeV electrons 27
Table 3.1 Reduction of penumbra width for a 2x2 field by reduction of SSD and by removal of scattering foils 47
Table 3.2 Dose rate relative to Clinical 10x10 10MeV beam, all at 2cm depth in WTe Solid Water measured with an Advanced Markus ionisation chamber 50
Table 4.1 Sensitivity of calculated dose and calculation time to Monte Carlo transport parameters 61
Table 4.2 Sensitivity of calculation time to Boundary Crossing algorithm 62
Table 4.3 Modelling parameters for energy tuning as displayed in Figure 4.3 65
Table 5.1 Calculated field penumbra width and flatness for a modulated and un-modulated electron beam at 2cm deep (2cm segment spacing unless stated) 84
Table 5.2 Dose data for a stepped PTV used to demonstrate energy modulation of the MERT beam. 5x7 matrices of 2cm square segments with 0.5, 1cm or 2cm segment spacing. Dose normalised to mean dose to PTV. 88
Table 5.3 Results of errors for three optimisation algorithms and three test functions with 30 variables 93
Table 5.4 Objectives contributing to the cost function. Where $C(y) = 1$ for $y > 0$ and $C(y) = 0$ for $y \leq 0$, $N < \mathrm{DPTVmin}$ is the number of voxels with value less than DPTVmin , $N > \mathrm{DPTVmax}$ is the number of voxels with value greater than DPTVmax and all other variables are defined in the text or assigned a target value in the table. 95
Table 5.5 Solutions to the IMRT and exIMRT problem. The final value of the cost function for objectives detailed in Table 5.4 is given along with the fraction of the PTV dose from the electron component. 99
Table 5.6 Dose-volume data for phantom study showing the benefits of using exIMRT 102
Table 6.1 Contribution of the electron component to the mean PTV dose for exIMRT treatment plans 109
Table 6.2 Radiobiology: Case 1 119
Table 6.3 Radiobiology: Case 2 120
Table 6.4 Radiobiology: Case 3 121

Table 6.5 Radiobiology: Case 4 122
Table 6.6 Conformity index for clinical Case 1, 2 and 3 123
Table 6.7 Relative Malignant Induction Probability (relMIP) for exIMRT compared to the Monaco IMRT/VMAT plan 123
Table A1 Functions used for tuning and evaluation of the optimisation algorithms 134
Table A2 Optimisation algorithm parameters used for IMRT problem 137
Table B1 Dose-volume data: Case 1 Paraspinal Sarcoma 138
Table B2 Dose-volume data: Case 2 Brain 139
Table B3 Dose-volume data: Case 3 Breast 139
Table B4 Dose-volume data: Case 4 Head and Neck re-treatment 140
Table C1 Parameters for NTCP calculations 142
Table C2 Parameters for relMIP calculations 143

Chapter 1

Introduction and outline of approach

1.1. Introduction

This chapter introduces the background to the problem by describing current practice in the use of radiotherapy for the treatment of cancer. It introduces the concept of depth and energy modulation for external beam radiotherapy to help the reader understand the current issues in radiotherapy treatment planning and delivery addressed in this work. Following the description of the motivation, the research aims are identified before describing the contributions and resulting deliverables. The outline of approach is then given to provide the reader with a concise description of the organisation of this thesis as well as the logical connections between chapters.

1.2. Background to the problem

1.2.1. Radiotherapy

Radiation therapy or radiotherapy is used as part of cancer treatment either as a curative treatment or as a palliative treatment to control symptoms and improve quality of life. Radiotherapy can be as a standalone treatment or used in conjunction with other forms of treatment such as chemotherapy and surgery. Controlled amounts of ionising radiation are used to destroy malignant cancer cells. The best way to deliver the dose of radiation will depend on the type and location of the cancer:

a) External beam radiotherapy (teletherapy): delivers the required radiation dose from a source of ionising radiation outside of the patient.
b) Brachytherapy: delivers the required radiation dose from radioactive sources implanted in the patient close to or inside the cancer location.
c) Intraoperative: delivers the required radiation dose to the tumour bed during surgery.

d) Unsealed Source Therapy: delivers the required radiation dose from a radioactive substance swallowed or injected into the patient.

The nature of methods b), c) and d) are such that they are only relevant for a small subset of tumours. This work, will therefore consider external beam radiotherapy which constitutes the majority of radiotherapy treatments delivered in the UK/world. Henceforth, for conciseness, the term 'radiotherapy' will be used to refer to 'external beam radiotherapy'.

The history of radiotherapy starts with the discovery of X-rays in 1895. Just weeks after Wilhelm Roentgen's discovery Emil Grubbé, a student doctor in Chicago, became the first person to use ionising radiation to treat cancer. Applying ionising radiation to a tumour can destroy the cancer cells making them unable to divide, reproduce and supplant the surrounding healthy cells. Today radiotherapy has developed into an integral part of cancer treatment. It has been estimated that the addition of radiotherapy to cancer treatment improves 5 year survival by 16% (Barton et al., 1995). In comparison the 5 year survival contribution from chemotherapy drugs is estimated at 2% (Morgan et al., 2004), making radiotherapy second only to surgery in its effectiveness.

1.2.2. Radiobiology

Radiotherapy strives to destroy as many cancer cells as possible, while limiting damage to the healthy tissue. This is accomplished by directing, with great precision, high energy photons to the target volume defined by the clinician. The photons travel some distance in the patient before interacting with the tissue leading to a partial or total transfer of the photon energy to electron energy. Subsequent ionisations cause damage to the cell molecules either directly or through the creation of free radicals. A small fraction of the damages are non-repairable, which results in cells that eventually die. DNA is thought to be the most important subcellular target molecule and it is DNA double strands breaks that most closely correlate with cell death.

Unfortunately as with other forms of treatment radiotherapy is not without its side effects. Side effects result from damage to normal tissues as X-rays pass through the patient. In general the amount of damage and the severity of the side effects will increase with dose and the volume irradiated. The time from treatment to injury will depend on the rate of turnover of cells in the

organ. Tissues that have a rapid turnover manifest acute effects with a timescale of days or weeks following treatment. Late effects with a timescale of months or years occur in tissues with a slow turnover. Both early and late reactions can result in permanent effects ranging in severity from changes to the appearance of the skin to spinal cord injury resulting in paralysis. The severity of injury will also be influenced by the organisation of functional subunits within the organ. Damage to a small volume of an organ with serially arranged subunits, such as the bowel, will result in change to the whole organ. Organs where subunits are arranged in parallel, such as the kidney, can sustain damage to a larger volume as each subunit acts independently. In addition to the significant risk of side effects there is a potential small risk that irradiation of normal tissues will induce a secondary cancer at a later stage.

In order to maintain a high 'tumour control probability' (TCP) it is necessary to deliver as much dose as possible to the target in order to kill all of the cancer cells. The radiation dose delivered in the path of the ionising radiation will also damage surrounding normal tissues and this dose must be minimised to give a low 'normal tissue complication probability' (NTCP). Hence when designing a radiotherapy treatment technique, the aim is to increase TCP and reduce NTCP, or to maximise the 'therapeutic ratio' of TCP over NTCP.

One way to improve the therapeutic ratio is through fractionation. In general early responding tissue cells damaged by ionising radiation can repopulate faster than the radiosensitive cancer cells. Most radiotherapy is therefore given in multiple small doses or 'fractions' with time in between treatments to allow for the repair of normal tissues.

1.2.3. Hardware

Protocols for dose and fractionation schemes are being continuously reviewed and updated based on evidence derived from clinical research. However for any given dose and fractionation scheme the technical challenge of how to deliver the dose to the tumour volume whilst minimising the dose to surrounding normal tissues remains. Attempting to meet these conflicting goals by improving the spatial distribution of dose in the patient has been a major motivation for the technological advances in radiotherapy. In turn, as the conformity of dose distributions to the tumour volume improves, the next step is to review dose and fractionations schemes to permit

higher tumour dose to be achieved through a reduced number of fractions without increasing side effects.

In the early days of radiotherapy some sparing of normal tissues was achieved by collimating the applied X-ray beam to the area to treat by using lead shielding on the surface of the patient. This conforms the dose distribution in the plane of the lead shielding but does not change the distribution of dose with depth in the patient. The distribution of dose with depth is characterised by an approximately exponential drop off as the X-ray photons are attenuated and as the X-ray intensity drops due to the inverse square law as the distance from the source of radiation increases (see Figure 1.1). Due to this slow drop off in dose with depth, a tumour at some depth in the patient will receive less dose than the preceding tissues.

Higher energy, more penetrating, X-ray beams can be used to reduce the dose towards the surface relative to the tumour dose for deep tumours. Hence, one of the early drivers for radiotherapy technology was to increase the energy from 100kV X-ray tubes to 1 MeV cobalt-60 machines to up to 25MeV linear accelerators (Thwaites and Tuohy, 2006).

The medical linear accelerator or linac is the current workhorse of radiotherapy departments. A linac produces ionising radiation by generating electrons and accelerating them in a pulsed RF field along a tuned waveguide. In X-ray mode the electrons are directed towards a tungsten target where bremsstrahlung X-ray photons are produced.

Increasing the X-ray beam energy to 'megavoltage' levels has the additional benefit of reducing skin dose due to the so called build-up effect. The dose at the surface of the patient is actually less than the dose at depth due to the relatively long range of energetic secondary charged particles (electrons and positrons) that are first released in the patient by photon interactions and then deposit their kinetic energy in the patient downstream of the initial interaction. This region between the surface and depth of maximum dose in megavoltage X-ray beams is referred to as the dose build-up region (see Figure 1.1).

However, this build-up region is a few centimetres deep at most. To deliver a cumulative dose higher at the tumour depth than at the surface it is necessary to combine several beams, from different angles of incidence, overlapping over the tumour location. This is achieved in a modern linac by mounting the linac head through which the X-rays are directed onto a gantry. The gantry is able to rotate around the patient permitting X-ray beams to be delivered from different directions

without moving the patient. The gantry rotation is centred at a point referred to as the isocentre and the machine calibrated such that the radiation isocentre is coincident with the mechanical isocentre. The gantry enables the direction of the beams to be in a direction coplanar with the gantry rotation and perpendicular to the patient that is typically lying on a patient support system. Non coplanar beam arrangement are possible by changing the orientation of the patient support systems. The approach developed in this work can be applied to either coplanar or non-coplanar beam delivery, however, it is demonstrated for the coplanar case only.

It is also possible to run the linac in electron mode. In electron mode the X-ray target is retracted from the linac such that the accelerated electrons pass directly to the patient. Electrons are particles with a negative elementary charge and a mass that is 1/1836 that of a proton. When a charged particle enters a medium the energy it deposits is approximately inversely proportional to the square of its velocity, so as the particle slows the probability of causing ionisation events increases. The resultant rapid accumulation of ionisation events due to decreasing velocity at the end of the particles path causes a dose peak known as a Bragg peak. However, as electrons have extremely small mass they undergo multiple scattering events on their path into the patient. At each scattering event the electron will change direction and the energy deposition is spread in the transverse direction as it progresses forward in the initial direction. Hence no Bragg peak is seen for electrons. Megavoltage electron beams will deliver close to maximum dose at the patient's surface rising to a plateau and steeply falling off with depth after a few centimetres. The dose gradient for lower electron energies is steeper than that for higher electron energies, because the lower energy electrons are scattered at a greater angle away from their initial directions. For electron energies less than 20MeV the steep dose gradient can be exploited to spare normal tissues beyond the range of the electrons. Such characteristics only allows treatment to superficial tumours up to 7cm deep (see Figure 1.1).

Linac X-ray energy is defined by the maximum energy in the spectrum of the beam. For example, a linac with an energy distribution of up to 6 MeV would be described as '6 MV'. In electron mode there is less spread in the energy spectrum and an electron beam with approximately 6MeV energy would be described as '6 MeV' in electron mode. For both X-ray and electron mode these are convenient approximate terms only. Accurate definition of the beams energy is achieved using parameters derived from the characteristics of its distribution of dose with depth or 'depth dose'.

Shaping of the beam is necessary to further minimise dose to normal tissues. High energy X-rays need several cm of lead for shielding. Linac employ, within the head of the machine, moveable components made of heavy metal to block unwanted radiation and shape the radiation to conform to the target as seen from the beams eye view. Two sets of movable jaws can form rectangles and multi leaf collimators (MLC), that are composed of 80 to 160 4 to 10mm wide interlocking motorised leafs (depending on design) can form complex shapes to conform the dose to the tumour volume. MLC can also be moved dynamically to modulate the amount of radiation passing through, (see Section 1.2.5). The head of the linac is typically about 40 to 50cm from the patient surface. In order to minimise scatter of electrons in the air between the linac head and the patient, electron beams are collimated using additional applicators or cones that bring the shaping of the beam close to the patient surface. This is made easier by the fact that a reduced thickness of shielding is required for electron beams compared to megavoltage X-ray beams.

The amount of radiation absorbed by the tissue is called dose and has the unit Gray (abbreviated as Gy), with 1 Gy = 1 J/kg. If a linac runs at a constant dose rate then the amount of dose received in the patient will be proportional to the amount of time the X-ray beam remains on. Rather than using time, the output of the linac is monitored in real time using a monitoring ionisation chamber and the machine calibrated in terms of monitor units (MU). Typically the linac will be carefully calibrated to give 1Gy per 100 MU in specific reference conditions. If deviation from the reference conditions is known then the MU to give a required dose at the specified point can be calculated.

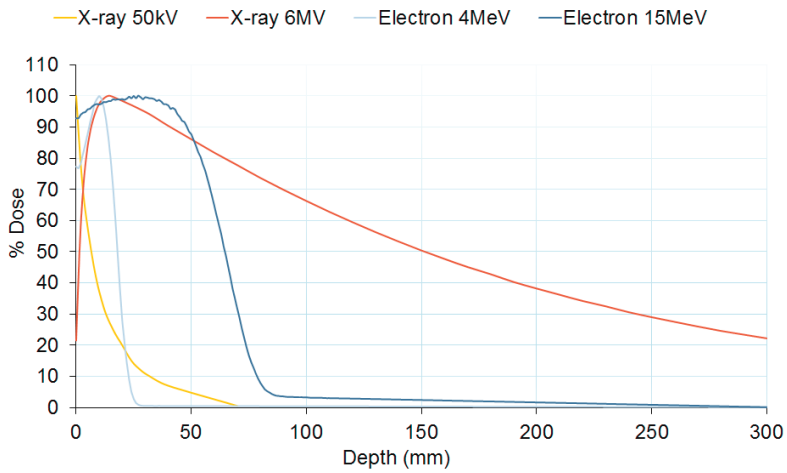

Figure 1.1 The variation of dose with depth in the patient for X-rays and for electrons at energies commonly used in Radiotherapy.

1.2.4. Treatment Planning

The process of using computer aided design to plan the delivery of the treatment is known as treatment planning. To plan a treatment it is necessary to delineate the volume to be treated and the key anatomical structures to consider and if possible spare. Such information can be obtained by imaging the patient in 3D using CT as well as a number of other imaging modalities. In cases where organ motion is critical, it is also possible to create 3D movies of the relevant patient anatomy.

Using such information, a clinician will define a volume corresponding to the tumour mass or gross tumour volume (GTV). This GTV may then be expanded to include subclinical microscopic disease to create the clinical target volume (CTV). To account for errors in setting up the patient, movement of the patient, internal movement of the CTV, or potential changes in size or shape of the CTV during treatment an additional margin for error is added to form the planning target volume (PTV). This PTV is a tool to shape the dose distribution and ensure with a clinically acceptable probability that an adequate dose will actually be delivered to all parts of the CTV.

The aim of treatment planning is to determine the most appropriate setting for the linac parameters to create the spatial distribution of dose in the patient that delivers the required dose to the PTV whilst minimising dose to normal tissues, with specific care being taken of critical anatomical structures. Specific organs at risk (OAR) may be defined with associated planning constraints to ensure treatment is safe. A margin may be added to the OAR in a similar way to the PTV to create a planning risk volume (PRV) to ensure that adequate sparing of OAR will actually be achieved with a reasonable probability.

Recommendations for the definition of GTV, CTV, PTV and PRV volumes along with methods for dose prescribing and reported are provided by the international committee on radiation units and measurement (ICRU) in (ICRU50, 1993, ICRU62, 1999, ICRU83, 2010). These guidelines help standardise the process of treatment planning allowing direct comparison of techniques internationally.

Treatment planning is a complex process due to the large number of variables to consider, including beam energy, beam modulation, beam angle of incidence and rotation of the patient support system. In addition the optimisation of these variables by the treatment planner cannot be

achieved in isolation from the clinical context. For example uncertainties in the delivery of the radiotherapy need to be included in the treatment plan.

For complex beam modulation an inverse planning approach is required. Rather than relying on the skill of the treatment planner to set the linac parameters a prescription is defined and an algorithm used to determine the beam intensity required to deliver that prescription. Inverse planned intensity modulated radiotherapy (IMRT) is now the current standard in radiotherapy.

1.2.5. Treatment Technique

There are a number of techniques available to deliver external beam radiotherapy treatment, all of which aim to conform the dose distribution to the PTV. 3D conformal radiotherapy (3DCRT) aims to conform to the shape of the PTV as seen from the beam's eye view. Prior to 3DCRT, treatments aimed to match the height and width of the tumour perhaps with a minimal amount of shielding. Advances in imaging technology have made it possible to locate and treat the tumour more precisely and advances in hardware allow shaping of the beams with MLC.

An improvement to 3DCRT, referred to as intensity modulated radiation therapy (IMRT) can be made by modulating the intensity across each beam. Individual beams are modulated using MLC to intentionally deliver a non-uniform dose to the target. When dose distributions from individual beams are superimposed the combined dose distribution is uniform and shaped to the target. The additional degrees of freedom are utilised to achieve a better target dose conformity and/or better sparing of normal tissues.

The natural evolution of IMRT is to have one continuous gantry arc rather than multiple static beams and this technique is known as volume modulated arc therapy (VMAT). At the time of writing, VMAT is rapidly taking over from static field IMRT as, thanks to the high level of linac automation, it is much quicker to deliver and can potentially produce improved dose distributions (Teoh et al., 2011).

IMRT and VMAT are conventional linac based technologies, however there are others treatment machines available. For example TomoTherapy® employs a rotating compact linac and delivers the dose slice by slice like a CT scanner. CyberKnife® uses a compact linac attached to a robotic arm to allow freedom of movement in three dimensions.

All these variations on the IMRT approach have their advantages and disadvantages but all use 4 to 25MV X-ray photons and work on a similar principle. They can produce highly conformal dose distributions sparing normal tissues but retain the limitations of the X-ray beam physics which dictates that a certain amount of dose will be deposited before and after the tumour as the beam passes through.

The leading alternative to X-ray external beam radiotherapy is heavy charged particle therapy (CPT). Protons and other heavy charged particles have a definite range and the dose delivered is maximum over the last few millimetres of the particles range known as the Bragg peak. Proton therapy dose distributions can therefore achieve very low doses distal to the tumour and low integral dose (Jones, 2008). Unfortunately, the availability of accelerators capable of delivering high energy proton therapy is limited.

There is a charged particle treatment option available with standard linacs and that is electron beam therapy. Historically a number of techniques have been described that use the properties of electron fields to conform the dose with depth and reduce normal tissue doses. For example abutting X-ray and electron fields have been used to treat head and neck cancers, where the sharp fall off in dose for the electron field is utilised to minimise the dose to the spinal cord (Sun et al., 1998). In recent years, however, this type of treatment has largely been replaced by IMRT. There has been some interest in complex electron beam therapy around the use of scanning electron beam treatment machines but the popularity of these machines diminished following a series of fatal accidents due to the failure of the scanning system (Israelski and Muto, 2004). Today electron beam treatment is predominantly confined to simple treatment of small skin cancers and additional boost fields for breast treatments. The latter are also on the decline and are being replaced by integrated boost IMRT. Advanced electron beam therapy is confined to few small research groups (Mikael and Rockwell, 2013).

1.3. Motivation for research

Modern X-ray IMRT techniques can produce highly conformal dose distributions that spare organs at risk (OAR) and minimise side effects. What is less well understood is the effect of the low level ‘dose wash’ received by OAR and other normal tissues. In particular, some studies estimate the

risk of developing a secondary cancer due to this dose wash at up to 2.5% (Verellen and Vanhavere, 1999, Hall and Wuu, 2003, Ardenfors et al., 2014).

At the time of writing about 3% of the U.S. population are cancer survivors, corresponding to 11 million people, a figure projected to grow to 18 million by 2022 (de Moor et al., 2013). About half these people will have had Radiotherapy as part of their treatment. As the pool of people potentially effected is so large, even small increases in risk should be considered and reduced to levels as low as reasonably practical.

It is currently not physically possible to deliverer the required dose to the tumour whilst delivering zero dose outside the tumour. To aid discussion of what is achievable a representation of the dose gradients for different modalities is presented in Figure 1.2. An ideal dose distribution of 100% dose in the PTV and an immediate drop to zero dose in normal tissues is shown in Figure 1.2, curve a). Representative curves either in the direction of or perpendicular to the direction of the beam path are shown, offset to put the zero depth at the 95% dose level.

X-ray IMRT techniques are represented in Figure 1.2, curve b) by the gradient of the dose at the junction between the PTV and an OAR (the parotid gland) taken from a typical VMAT head and neck plan. This dose gradient is sufficient to reduce the dose to the parotid gland below a threshold level (and consequently reduce the incidents of Xerostomia (Nutting et al., 2011)). The gradient is however limited by the way X-ray dose varies with depth (see Figure 1.1) and by the penumbra at the edge of the field. The penumbra at the edge of the field, represented in Figure 1.2 curve c), results from the finite source size but also scatter in the head of the machine and scatter in the patient. The combination of scattered dose and entrance and exit dose results in a significant level of 'dose wash' in the VMAT planed dose distribution. The dose does not immediately drop to zero but stays at the 20-30% level over several cm.

By contrast the Proton depth dose curve, Figure 1.2 curve d), has a definite range and drops to less than 10% in just 1cm. It is the potential to exploit this physical characteristic of the proton beam to improve normal tissues sparing that drives the current interest in proton therapy (Newhauser and Zhang, 2015).

The dose fall off for the electron beam depth dose curve, is not as steep as for the proton beam but does drop to less than 10% in 2cm, see Figure 1.2 curve e).

The curves in Figure 1.2 illustrate that the steepest dose gradients can be achieved with proton therapy. There is however some uncertainty in the long term role of proton therapy, largely due to scepticism about its cost-effectiveness (Newhauser and Zhang, 2015). At the time of writing there are no proton therapy facilities in the UK and just two NHS centres and a handful of small private centres planned for the in the next 2 to 3 years. Even when these centres are in operation radiotherapy patients with access to proton therapy has been estimated at roughly 1 % of the total number of patients currently receiving radiotherapy (DOH, 2012)

As proton therapy is not available for all patients, the work in this thesis will reconsider the role of the electron beam. Although the fall off in dose for the electron beam is not as steep as the proton beam and although electron beams have other significant disadvantages (primarily limited range) electron beams have the significant advantage of being readily available. Perhaps by combining electron beams with X-ray photon beams to achieve 'Depth Modulation' as well as intensity modulation radiotherapy, IMRT dose distributions can be further improved.

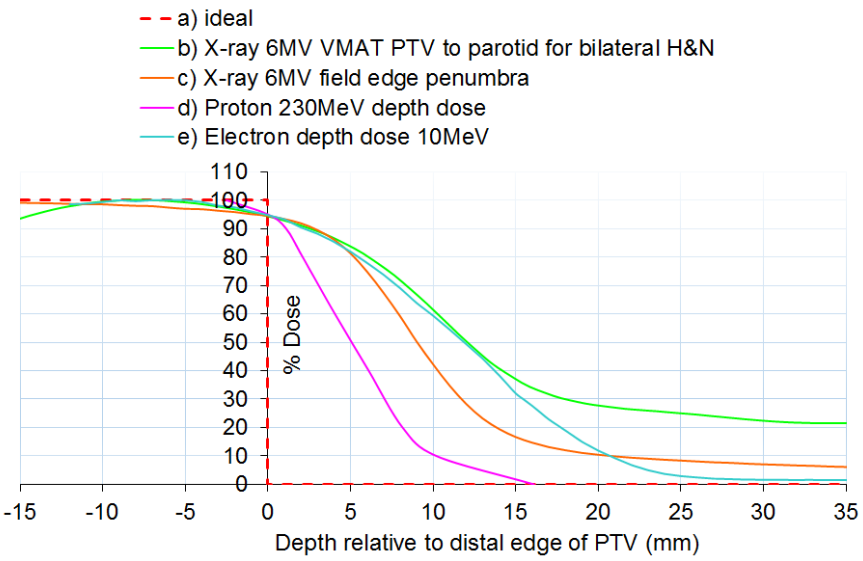

Figure 1.2 Examples of dose gradients in radiotherapy treatment. a) Ideal step function with an immediate drop to zero dose after PTV. b) Taken from a clinical bilateral Head and Neck VMAT plan showing the drop in dose from the target to the adjacent parotid gland. c) The penumbra at the edge of single direct 6MV X-ray 10cm square field at 10cm depth in the patient d) a 230MeV direct proton field depth dose taken from (Cai et al., 2015) e) 10MeV 10cm square field electron depth dose curve

1.4. Research aim and objectives

The primary aim of this work is to answer the following question:

- Can radiotherapy dose distributions be improved through a novel depth modulated X-ray and electron therapy treatment technique?

The literature review (Chapter 2) revealed a number of studies investigating complex combined X-ray and electron treatments but none which have been successful in making the transition to the clinical setting. The aim of this study was therefore refined to answer the following research question:

- Is an isocentric combined X-ray and electron therapy treatment possible with no modifications to equipment and can it be used to improve radiotherapy dose distributions?

Existing studies require add on electron MLC or a compromise in patient positioning to put the patient close to the X-ray MLC. It is suggested that to have a practical complex combined electron and X-ray treatment technique it would be desirable to have a single isocentre (point of rotation) and no add on components to reduce the need for intervention between the electron and X-ray dose delivery. Hence the aim of this work is to produce a novel mixed X-ray and electron treatment technique with the electron component treated isocentrically through the X-ray MLC.

The solution proposed in this work is to use electron beams delivered through MLC at standard SSD but reduce scatter and photon contamination by removing the scattering foils from the beamline and to employ optimisation of the electron and photon components to compensate for any remaining penumbra broadening. This mixed modality technique will be referred to as *ex*IMRT (see Figure 1.3). To achieve this solution the following objectives were addressed:

- Create a radiotherapy treatment planning system (TPS) that is capable of implementing the proposed technique. The TPS development will require the following:
    - To select a programming environment for radiotherapy research.
    - To develop and validate an accurate electron beam model to model the specific features of this work.
    - To develop an optimisation scheme to optimise electron and photon concurrently.
- Use the developed TPS for treatment planning studies, initially involving simple phantoms, to demonstrate the principle prior to applying to a range of clinical case studies.
- Critically evaluate the performance of the proposed combined X-ray and electron plans to X-ray only treatment plans to determine whether the novel treatment technique developed has the potential for improving dose distributions in the patient.

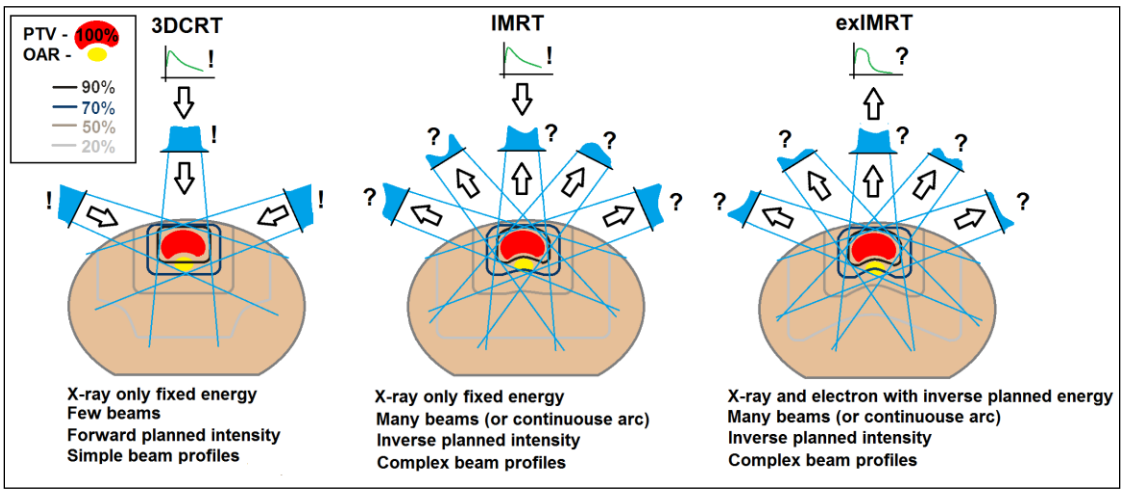

Figure 1.3 A comparison of 3D conformal radiotherapy (3DCRT), Intensity Modulated Radiotherapy (IMRT) and the proposed mixed modality exIMRT approaches

1.5. Thesis outline

The thesis is organised as follows:

Chapter 2 presents a short review of the depth modulation for the different modalities used in radiotherapy before focusing on modulated electron radiotherapy (MERT) and the combination of MERT with IMRT. This is followed by a review of published solutions to optimisation of the spatial dose distribution in radiotherapy. Finally a review of the methods for evaluating planned dose distributions is presented. The chapter concludes with a justification of the material and methods researched in this work.

Chapter 3 introduces the concept of electron beam delivery collimated with X-ray MLC with scattering foils removed. This scattering foil free mode of operation is examined for an Elekta Synergy MLCi linac at UHCW through a series of measurements. It is shown that a stable beam with a useful field size (FWHM) of 18cm can be produced with scattering foils removed. It is then demonstrated that by removing the scattering foils photon contamination and lateral scatter is reduced. Such reduction makes delivery of small MLC collimated electron beams at isocentric SSD feasible. The ideal size of these segments is discussed and a 2x2cm square suggested. It is shown that acceptable dose rates are achievable over a useable treatment area and that the level of scatter/leakage dose in the patient plane outside the treatment field is similar to or less than X-ray therapy. Both the dose rate in field and unwanted dose outside the field are shown to improve with scattering foil removal.

Chapter 4 presents the modelling of the scatting foil free electron beam using the Monte Carlo radiation transport software tool BEAMnrc. The model is adjusted to achieve good agreement with depth doses and profile measured in water. In addition the sensitivity to different modelling parameters is presented.

Chapter 5 describes the development of an approach to optimising the combined electron and photon dose distribution. A novel two stage approach is used to make best use of the electron dose component. The development of this approach is presented including a comparison of different optimisation solvers.

Chapter 6 presents the application of the proposed technique to four different clinical cases. It is shown that in all cases the proposed technique is able to produce acceptable PTV coverage and uniformity whilst, at the same time reducing dose distal to the tumour volume. It is shown that reduced normal tissues dose with the proposed technique has the potential to reduce the risk of secondary cancer induction.

1.6. Contributions of the thesis

The contributions to the thesis are first described as a list of bullet points and then presented in Figure 1.4 to illustrate the relationship between the chapter organisation and the contributions arising from this work.

- Performed a thorough survey of relevant literature. (Chapter 2)
- Proposed a novel approach to reduce lateral scatter, reduce photon contamination and increase dose rate for MLC modulated electron beams by removing the electron scattering foils. (Chapter 3)
- Showed that the proposed approach is feasible through a series of measurements. (Chapter 3)
- Created a Monte Carlo beam model to calculate dose distributions generated by the proposed solution and shown that accurate dose calculation is possible. (Chapter 4)
- Developed a novel method to optimise dose distributions using the Monte Carlo calculated electron dose and pencil beam calculated X-ray photon dose. (Chapter 5)
- Shown through clinical examples that the proposed solution has the potential to reduce dose distal to the target for relatively superficial tumours. (Chapter 6)

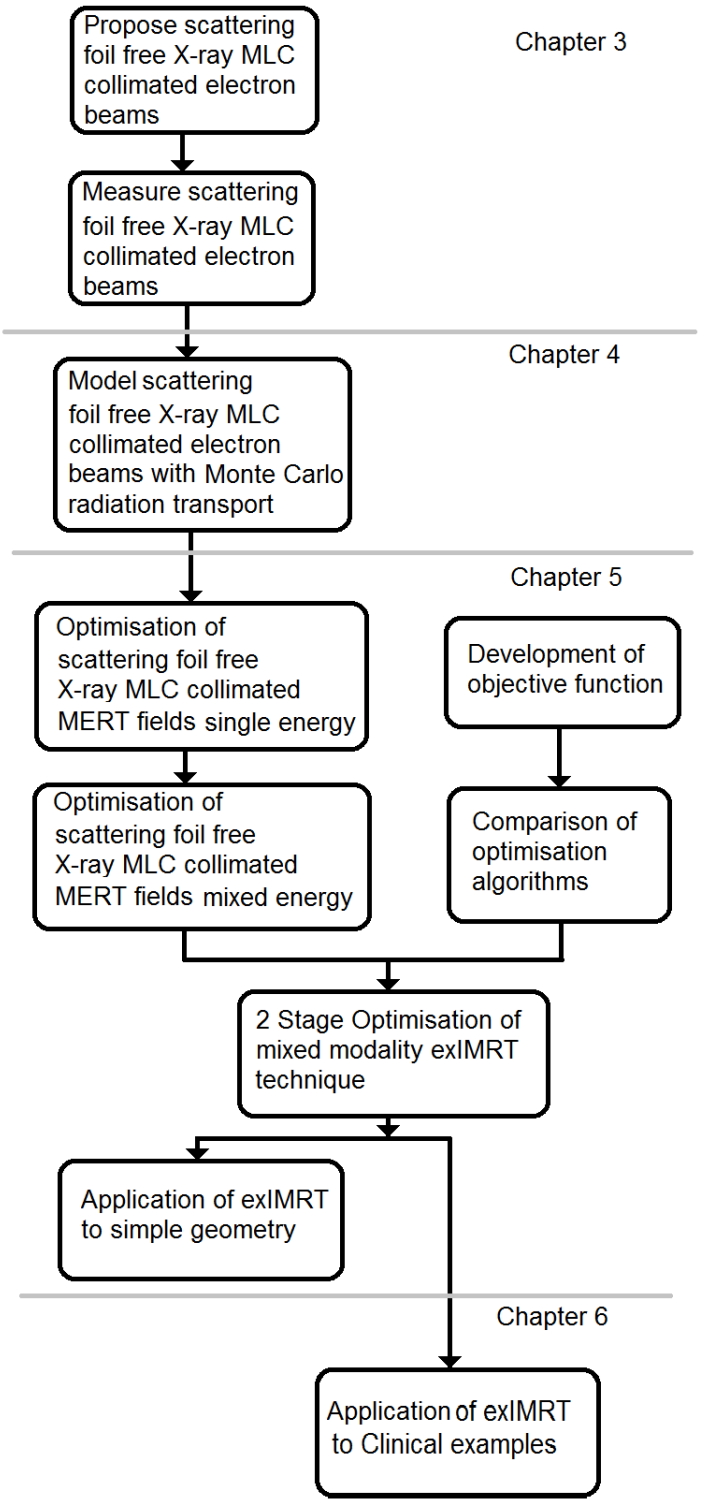

Figure 1.4 flow chart illustration contributions of theses

1.7. Publications

The work has led to the following publications:

Baugh, G.M., Haas O.C.L (2013) 'Optimisation of combined electron and photon IMRT using standard photon MLC', poster presented at 2nd ESTRO Forum, Geneva, Switzerland, Rad. Onc. 106(S2), S225-226

Baugh, G.M., Haas O.C.L (2015) 'Isocentric combined electron and photon IMRT using standard photon MLC', paper presented at UKRO 2015, Coventry, UK

Chapter 2

Critical review of depth modulation in radiotherapy

2.1. Introduction

This chapter presents a short review of depth modulation for the different modalities used in radiotherapy before focusing on modulated electron radiotherapy (MERT) and the combination of MERT with IMRT. This is followed by a review of published solutions for the optimisation of the spatial dose distribution in radiotherapy. A review of the methods for evaluating planned dose distributions is then presented before offering conclusions that justify the approach undertaken.

2.2. Depth Modulation in Radiotherapy

The title of this thesis is 'Depth Modulation in Radiotherapy'. This title arose from the initial intention of investigating the modulation of dose in the direction of the beam as well as modulating the intensity of the beam perpendicular to the beam direction. To this end a review of depth modulation for different radiotherapy modalities was performed.

2.2.1. X-ray energy modulation

For X-ray photon beams the variation of dose with depth can be modified by the choice of energy or by using combinations of the different energies available. Standard clinical linacs are supplied to the user's specifications with a choice of energies between 4 MV and 25 MV. The advantages of increased penetration and increased skin sparing with higher energy photons (10-25MV) to treat

deep seated tumours is well known. However, for IMRT an increase in the beam-on time relative to conventional radiotherapy has led to concerns about secondary malignancies arising from increased neutron dose. This risk becomes greater at higher energies where there is a greater neutron contribution. Hence, most centres use 6-10 MV for IMRT (de Boer et al., 2007). Even so, some studies have demonstrated that using higher energies can produce a reduction in normal tissue dose away from the target area outweighing the increased neutron dose (de Boer et al., 2007, Park et al., 2011, St-Hilaire et al., 2009). In addition, it has been shown in (Kry et al., 2007) that neutron production can be reduced by 69% for an IMRT plan by removing the flattening filter. It follows then that there may be benefits in modulating the photon energy (or rather finding the optimum mix of energies).

A feasibility study for an energy modulated photon radiotherapy (EMXRT) technique was performed in (Zhang et al., 2016). The techniques used an energy selection algorithm that selected the energy from a look up table according to effective path length and tumour size. It would seem that this algorithm tended to select lower energies to minimise exit dose. The technique appeared to have some small benefits, for example in a lung tumour study the V_5 for the whole lung, that is the percent volume of lung receiving a dose of 5 Gy, was decreased from 18.8% to 16.9%.

As well as increased penetration higher energy X-ray beams exhibit an increased skin sparing effect. When combining X-ray beams with electron beams this increased skin sparing could be used to offset the increase in dose over the first 1cm of tissue with electrons. However, it is suggested in (Butson et al., 1997) that the skin sparing of higher energy beams is compromised by electron contamination such that there is negligible reduction of the delivered dose to the basal cell layer (0.1 mm). Whilst a small increase in skin sparing at the dermal layer (1 mm) was found, the authors pointed out that this was negated by the increased exit dose from an opposing field of the same energy.

2.2.2. Heavy charged particle energy modulation

Depth modulation for proton therapy and other heavy charged particle therapies is achieved by combining multiple Bragg peaks to create a spread out Bragg peak (SOBP). By varying the number of peaks the extent of the uniform region can be can be varied. Technically this is achieved with energy stacking (energy changed up stream of the beam exit nozzle) realised by passing the beam

through either a range modulator wheel or a ridge filter. There is some uncertainty in the final range of the SOBP which has to be built into the planning volume. However, both the absence of dose distal to the uniform region and the lower dose proximal to the uniform region result in a lower integral non-target dose when compared to X-ray therapy (Newhauser and Zhang, 2015).

2.2.3. Very high energy electrons (VHEE)

By contrast to the complex beam arrangement routinely used in X-ray therapy, electrons are generally used for single direct fields for superficial treatment (Hogstrom and Almond, 2006). Key to reaching deep seated tumour sites is being able to produce high energy electrons. Current clinical machines have the potential to produce up to 20 MeV electrons. Historically, some treatment machines were capable of up to 50 MeV (Karlsson and Zackrisson, 1997). However, it has been suggested that very high energy electron beams of 50-200 MeV (VHEE) would have advantages over X-ray photons. VHEE is a distinct category of treatment to electrons beams of energy less than 20MeV as the properties of the dose distributions produced differ greatly. High energy electron beams are highly penetrating (>40cm for 150MeV), but do not exhibit the steep drop off in dose at a definite range. By contrast to lower energy electrons, very high energy electrons exhibit a lack of lateral scatter that results in reduced penumbra widths, smaller than MV X-ray beams. VHEE also has the advantage that there is no electron disequilibrium at the interface between materials of different densities. This results in an improvement in the dose distribution at the lung tissue interface when compared to X-ray treatments. Similar or improved dose distributions, when compared to VMAT, for a theoretical 100-200 MeV scanning electron beam have been obtained in (Palma et al., 2016, Bazalova-Carter et al., 2015). However the studies do not consider depth modulation, only selection of the appropriate energy which is not as critical as it is for low energy electron treatments. The greatest improvements seen is for large centrally located tumours that take advantage of the penetration of the high energy electrons. For an oesophagus plan, improved conformity was shown resulting in a reduction in OAR dose below 35Gy (76% of the prescribed dose). Mean dose to the heart was reduced by 20% and integral dose was reduced by 23%. Whether or not this level of improvement warrants the major investment that would be required to produce VHEE scanning electron machines remains to be seen.

2.2.4. Modulated electron radiotherapy (MERT)

A number of studies have looked at the potential of modulated electron radiotherapy (MERT) for electrons beams of energy less than 20MeV. X-ray IMRT uses multileaf collimators to modulate the intensity of the beam. Perhaps then the intensity of electron beams could be modulated in a similar way to produce MERT. Initial studies suggested that using the photon multileaf collimators (xMLC) for electron treatments was not practical (Klein et al., 1996). Electron scatter in the head of the machine and in the air between the head and the patient surface causes prohibitively high levels of penumbra broadening. To cut out this additional scatter the conventional method of shaping electron beams is to use collimation close to the patient surface. A fixed shape applicator or cone is attached to the linac head with a heavy metal cut-out added to conform to the tumour shape if required. As the shape is fixed there is no means to modulate the intensity of the beam using segmented fields in the manner of IMRT.

Modulating conventional electron beams is limited to varying the thickness of bolus on the patient's surface. For example the depth of penetration into the patient can be reduced by 1cm by adding a 1cm slab of wax on the surface of the patient. More complex modulation across the field can be achieved using bolus contoured to create varying thickness (Low et al., 1992, Kudchadker et al., 2002). Paraffin wax can be shaped by hand or plastics can be milled into a shape that has been designed either by inverse planning or more usually through a process of trial and error. Recently there has been increased interest in this method driven by the availability of 3D printers that can produce complex bolus shapes (Su et al., 2014, Zou et al., 2015). The use of 3D printed bolus increases the precision of manufactured contoured bolus allowing for more complex shapes and resulting in increased conformity of dose distribution. It is still however a time consuming process and does not lend itself either to energy modulation or combing MERT with IMRT as each electron energy would require its own contoured bolus to be manufactured and the bolus would need to be removed in between electron field and X-ray photon field delivery.

An alternative to contoured bolus is to use add-on electron multileaf collimators (eMLC) specifically designed to deliver MERT. These are positioned close to the patient surface to minimise the effects of scatter between the aperture and the patient. This approach has been investigated in a number of studies (Ma et al., 2000, Ma et al., 2003, Lee et al., 2001, Engel and Gauer, 2009). Hogstrom et al., (2004) proposed a retractable eMLC design but noted that eMLC

had the disadvantage of high cost and potential for patient collisions as located near to the patient surface. There is also some concern about the induced photon contamination from add-on devices (Olofsson et al., 2004).

To avoid the issues associated with eMLC a number of studies have looked into filling the linac head with inert gas and using a short source to surface distance (SSD) to minimise scatter when using standard X-ray MLC. Some scanning electron beam treatment machines use a Helium atmosphere to minimise scatter, as demonstrated by an increase in penumbra width when the Helium is replaced by air for a MM50 racetrack microtron (Karlsson et al. 1992). Using a Helium atmosphere has also been shown to reduce penumbra width for conventional linacs in Monte Carlo simulations (Karlsson et al., 1999, Blomquist et al., 2002). However such a method would require significant modifications to conventional linacs.

Through a series of measurements, it was shown in (du Plessis et al., 2006) that a useful field could be produced with electron beams through a standard Siemens Primus photon MLC without filling the head with inert gas. They demonstrated target dose conformity and tissue sparing with manual intensity and energy modulation using energies from 6 to 18MeV over an SSD range of 60-100cm. It was found that the most favourable SSD for MERT is 60cm.

It has also been shown in (Henzen et al., 2014) that it is possible to create a Monte Carlo based beam model to accurately predict dose distributions from xMLC electron beams for a Varian Millennium photon multileaf collimator. Henzen et al. (2014) did however highlight that for small electron fields the X-ray contamination of up to 10% could be prohibitive.

Klein et al. (Klein et al., 2008, Klein et al., 2009) have demonstrated that, by maintaining a short SSD and using Monte Carlo Calculations to correctly model the electron scatter, it is possible to implement MERT using standard X-ray MLC with no physical modifications. Klein et al., (2009) used a forward planning approach to successfully plan a chest wall case using: one gantry angle, 4 electron energies ranging from 6 to 15 MeV, and four segments at 70cm SSD. Comparison of calculations and measurements were presented with good agreement within ±2%/2mm.

In any electron therapy study, energy selection is important as it is the energy that will define the range and therefore the treatment depth. Some studies have taken this a step further by looking into the potential of modulating the electron energy by using a mixture of the available

electron energies over the treatment field. Theoretical advantages of electron energy modulation have been suggested in (Hyödynmaa et al., 1996, Mu et al., 2004, Olofsson et al., 2004). An inverse planning tool to select electron energy and modulate energy and intensity using bolus was devised in (Gentry et al., 2006). An inverse planning algorithm was used in (Ma et al., 2000, Ma et al., 2003) to optimise energy and intensity using a custom eMLC for MERT breast cancer treatment. An edge feathering technique was presented in (Eley et al., 2011) to improve homogeneity for abutting eMLC fields of different energies.

Jin et al. (2008) planned a MERT breast treatment on an anthropomorphic breast phantom at reduced (60cm) SSD for a Siemens Primus linac. They used Monte Carlo generated 1x1cm MLC beamlets with a 'gradient based' algorithm to adjust the beamlet weights. The plan produced, 22 segments with a mixture of 6, 9, 12 and 15MeV. Comparisons between measurement and calculation agreed within 2% or 1mm.

Surucu et al. (2010) demonstrated the advantages of energy modulated MERT with xMLC for chest wall treatments using a forward planning approach again with Monte Carlo dose calculation. Energy was selected across the field based on the calculated depth of the distal edge of the PTV and the electron energy range. MERT plans produced acceptable target coverage and lower doses to the heart in all 4 cases studied.

Salguero et al. (Salguero et al., 2009, Salguero et al., 2010) have demonstrated that inverse planned energy modulated MERT can be delivered with an MLC using a multi objective minimisation through a simulated annealing optimisation algorithm (Kirkpatrick et al., 1983). Four cases of shallow head and neck tumours were considered, a recurring squamous cell carcinoma in the oronasal region, a parotid mucoepidermoid carcinoma, a basal cell carcinoma in the right ear and a large B cell lymphoma of the parotid gland. For all cases DVH comparisons with conventional and IMRT plans demonstrated improvements in the dose delivered to the PTV and a reduction in the dose received by organs at risk. Comparisons of calculations and measurements for patient specific measurements analogous to the routine patient specific QC performed for IMRT were also presented. Gafchromic EBT radiochromic film was used for relative dose and a Roos PTW34001 plane parallel ion chamber for absolute dose. For the four cases studies absolute dose measurements were in agreement with calculations to ±2.0%**.** Good agreement between film

and measurement was found and a gamma analysis approach was suggested with 3%/3mm criteria, similar to that routinely used in patient specific quality control for IMRT.

2.2.5. Mixed X-ray and Electron Therapy

A few studies have looked at the potential advantages of mixing photon and conventional electron beams. Korevaar et al. (1999) demonstrated that photon fields could be used to sharpen the penumbra of a microtron electron beam. Li et al. (2000) developed a technique using IMRT and conventional electron fields for breast-conserving radiotherapy demonstrating reduced dose to the ipsilateral lung and the heart when compared to IMRT alone. Similarly, Van der Laan et al. (2010) found that incorporating conventional electron fields into post-mastectomy IMRT enables a dose reduction which can only be achieved with IMRT alone when allowing large irradiated volumes in the contralateral breast. Rosca (2012) combined conventional electron beams with IMRT plans to minimise the integral dose to other sites including brain, lung and thyroid cases.

These mixed electron and photon techniques have their advantages but there may be further improvements if IMRT is combined with MERT. Asell et al. (1999) demonstrated the possibility of improving dose conformity for electron beams by adding photon fields parallel or orthogonal to the electron beam by combining theoretical fluence profiles. Das et al. (2004) demonstrated that using an idealised electron beam fluence, mixed photon and electron IMRT could reduce the dose to critical structures.

There have also been studies that have considered combing eMLC MERT with IMRT. In a theoretically planning study Korevaar et al. (2002) found that the addition of high energy (15-50MeV) eMLC collimated electron beams could improve dose-volume histograms for the critical structures in an IMRT plan for deep seated tumours. This study by Korevaar et al. used the sequential quadratic optimisation of ORBIT (Löf, 2000) which was subsequently developed into a commercial X-ray IMRT optimisation solution. Al-Yahya et al. (2005) performed a study using a custom made ‘few leaf’ eMLC comparing MERT, IMRT and IMRT+MERT for two head and neck cases. In this study electron fluence and energy were modulated using the deterministic steep DVH minimisation algorithm (Hristov et al., 2002). The conclusion of the study was that the addition of energy modulated MERT systematically leads to a reduction of whole body dose equivalent (WBDE) while still meeting dose constraints

Mu et al. (Mu et al., 2004) demonstrated that, using a commercial X-ray IMRT algorithm and non-modulated electron beams with the beam's eye view shaped using xMLC, a lower integral dose outside the PTV could be achieved. They also commented: "It is reasonable to expect that if computerised optimisation tools were coupled with the mixed photon and electron beam technique, treatment goals would be more readily achieved".

The following three studies have been singled out as combing xMLC MERT with IMRT:

- The PhD thesis of (Weinberg, 2007) used 2x2 cm xMLC electron beamlets beam weight optimised along with intensity modulation of the X-ray component using the X-ray optimisation algorithm of a commercial treatment planning system (Pinnacle®). The electron energy was selected manually. Although it did not appear that a reduced SSD was used, no consideration was given to the increased penumbra, increased X-ray contamination or reduced dose rate. There was also no particular attempt to exploit the benefits of electrons and plans tended towards a relatively low contribution from the electron component. The mean electron target dose for MERT was 17% of the mean target dose for the partial breast irradiation plans studied. However, this study did show a small improvement in the dose distal to the target with the addition of the electron component for some plans. Mixed beam plans were selected as superior by a clinician for 6 of 9 partial breast plans.
- As part of the reduced SSD xMLC MERT study in (Surucu et al., 2010), a Pinnacle® IMRT plan was combined with a MERT plan for a chest wall treatment. The combination plan was created by simply adding the two plans in proportion but demonstrated clinically acceptable target coverage with increased OAR sparing (heart, contralateral lung and contralateral breast D_{20} were decreased by 48%, 43% and 49% respectively although the ipsilateral lung D_{20} was increased by 10%, when compared to IMRT alone). It was noted however that further investigations were required to provide tools for combed modality planning.

- Palma et al. (Palma et al., 2012) performed a successful study looking at combining the reduced SSD xMLC MERT technique developed by Salguero et al. with IMRT for partial breast irradiation. They found a reduction by a factor of 3.2-3.6 in the volume of Heart and Lung, receiving 5% and 15% of the prescribed dose respectively.

It is hypothesised that removing the scattering foil and carefully optimising the electron and photon component will produce a reduction in dose distal to the target without resorting to a reduced SSD. Removal of the scattering foils has previously been shown to reduce photon contamination for conventional electron beams (Eldib et al., 2014) and add on electron MLC (Connell et al., 2012) but may have additional benefits when utilising xMLC.

2.2.6. Summary

Depth modulation in one form or another is an important part of all radiotherapy treatment modalities. A number of studies have shown that it is possible to achieve depth modulation by combining electron and X-ray fields. Three of these studies have shown that Mixed X-ray and electron IMRT is credible without major modifications to existing standard treatment machines and these are summarised in Table 2.1 along with a summary of the proposed research.

Table 2.1 Summary of MERT+IMRT studies for <20MeV electrons

Reference	**MLC**	**Electron Dose Calculation**	**Scatter reduction**	**Electron Optimisation**	**Photon Optimisation**	**Energy Optimisation**
2007 Weinberg (Texas Uni.)	xMLC	BEAMnrc Monte Carlo	None	Pinnacle® (Sequential quadratic programming)		Manual
2010 Suruco (Washington Uni.)	xMLC	BEAMnrc Monte Carlo	≤70cm SSD	Manual	Pinnacle® (Sequential quadratic programming	Manual (Dose Slider)
2012 Palmer (Sevilla Uni. *CARMEN*)	xMLC	BEAMnrc Monte Carlo	≤70cm SSD	Simulated annealing		Range selection
Proposed research	xMLC	BEAMnrc Monte Carlo	Scattering foil removal	Iterative constrained optimisation		

2.3. Optimisation

Optimisation aims to find the values of a set of variables that will result in the most appropriate solution to the problem considered, whilst at the same time meeting various constraints in terms of both the possible values of the variables and defined objectives. The objectives represent the specific goals of the optimisation problem. To solve the problem using numerical methods, it is necessary to express these objectives using appropriate mathematical expressions. Key to the success is the ability to ask the correct question to the optimisation algorithm.

In the context of this work, namely radiotherapy treatment planning optimisation, the following features should be considered:

- The aim of the optimisation is to meet clinical objectives. The optimisation is therefore traditionally expressed as a minimisation problem, which aims to reduce the error between the value of the objectives achieved by the current solution and the value of the objectives

representing the clinical prescription.

- The variables optimised represent the energy delivered to the patient using various treatment modalities. It is not feasible to take away doses of radiation. This means that the variable representing the quantity of radiation delivered must be non-negative.
- To deliver the prescribed high dose of radiation to the planning target volume, all the tissues in the beam path will also be irradiated and receive some dose. This means that some solutions, whilst desirable, may not be physically realisable. For example, it is not possible to meet an objective that will specify a dose of 0 to tissues in the beam path. This implies that the objectives considered are competing and not mutually achievable. The solution will therefore be a compromise.
- Depending on the objectives considered, there can be several distinct sets of decision variables that can achieve apparently identical solutions due to the large number of variables that can be optimised.
- Some objective formulations aim to represent closely the clinical objectives. Their drawback is that they can have complex nonlinear formulation that are difficult to solve.
- Finally, depending on the approach adopted, the size of the optimisation problem could be very large with thousands of variables required to be determined.

Historically 3DCRT plans were optimised by hand with experienced planners shaping the beams and selecting weights to create the optimum dose distribution. Today, due to the complexity of an IMRT plan this is not possible and generally some algorithm is required to adjust the intensity of the applied X-ray beams in such a way that the spatial distribution of the dose distribution in the patient is optimised. Bortfeld (Bortfeld, 2006) provides a useful review of the development of IMRT up 2006 which is around the time IMRT became a widely used clinical technique. MLC based X-Ray IMRT is established as a standard clinical technique and there have been many studies investigating the formulation of the problem and the application of novel optimisation algorithms. Most current commercial planning systems used in the clinic employ an 'inverse planning' approach as suggested by Webb (Webb, 1989). The optimisation problem is formulated as:

$$\min F(x) \tag{2.1}$$

$$\text{subject to } x \geq 0$$

$$\text{subject to } C(x) \leq 0$$

where F denotes the objective function, C the inequality constraints evaluated at x and $x = x_1, \ldots, x_p$ is a vector of $p >> 1$ decision variables describing the X-ray intensity.

Optimisation of the IMRT plan can pose a challenge due to the size of the problem, the non-negativity bounds and potential inclusion of complex nonlinear objective functions. Various optimisation techniques have been employed to optimise dose distribution in IMRT planning (Bortfeld, 1999, Verhey, 2002, Webb, 2003). Current commercial solutions can generally be split into two distinct methodologies (Yu et al., 2006, Shepard et al., 2002)

- sequential optimisation
- direct aperture optimisation (DAO)

In the sequential method before an IMRT optimisation each beam is divided into a number of smaller 'beamlets', and the corresponding dose distributions computed as the sum of all weighted beamlets. The total dose to structure k can thus be written as:

$$d_k = \sum d_{k,i}\, x_i \tag{2.2}$$

where $d_{k,i}$ is the dose to structure k from beamlet i given the beamlet weight x_i. Beamlet weights are then optimised to produce the intensity map that minimises the objective function. The problem with this method is that a second stage is required to translate the ideal fluence map into apertures that are achievable under a given set of physical constraints. At this stage there is the risk of degrading the dose distribution to such an extent that the process has to be re-started. With DAO the physical constraints are included in the optimisation and aperture shapes and weights are optimised simultaneously. There is therefore no degradation of the plan due to a second segmentation stage. DAO also tends to produce fewer apertures, reducing treatment time (Shepard et al., 2002). However DAO is more difficult (non-convex) from a mathematical point of view and

is not guaranteed to find a global solution (Bortfeld, 2006). For this study DAO was not considered for the following reasons:

- Whilst physical constraints are considered, reducing treatment time and minimising plan complexity is not one of the aims of this project.
- There is a greater risk of becoming trapped in local minima with DAO.
- Sequential optimisation is computationally simpler to execute than direct aperture optimisation.

In beamlet based optimisation a solver is required to find the beamlets weight to minimise an objective function within the given constraints. The objective function is typically a quadratic equation and one potential method is to find a direct solution of the inverse problem using conventional quadratic objective functions. Unfortunately as no constraints are possible this method would result in negative weights. A solution with negative beamlet intensities is not feasible as taking away dose from the patient is not possible.

Goldman et al. did develop a fast inverse dose optimisation algorithm for IMRT via matrix inversion with non-negativity which showed positive results in two dimensions (Goldman et al., 2005). The objective function is reformulated such that the optimisation problem is reduced to a linear set of equations. The optimal set of intensities is found through a matrix inversion.

Typically however beamlet weights are optimised using some form of numerical search algorithm. Webb, (1989) introduced simulated annealing as an IMRT optimisation method. Simulated annealing is a metaheuristic that models the physical process of heating a material and then slowly lowering the temperature to decrease defects, thus minimising the system energy. Slow cooling is interpreted as a slow decrease in the probability of accepting worse solutions as it explores the solution space. Accepting worse solutions is a fundamental property of metaheuristics because it allows for a more extensive search for the optimal solution. Following on from this work other heuristic algorithms have been suggested, such as genetic algorithms (Ezzell, 1996, Wu and Zhu, 2001) and tabu search (Gilio, 1998). However Bortfeld et al., suggested that typical quadratic objective functions do not have local minima and fast gradient related methods can be used (Bortfeld et al., 1990, Spirou and Chui, 1998, Cotrutz et al., 2001, Chang et al., 2002). Recent advances in improving the speed of optimisation in commercial treatment planning systems have

been achieved through the use of an algorithm that incorporates sequential quadratic programming (SQP) (Löf, 2000). At a given approximate solution SQP models the problem as a quadratic sub problem then uses the solution from this sub problem to form a better approximate solution. This process is iterated to create a sequence of approximations that converge to the solution.

2.4. Practical IMRT planning

In practical terms the typical computer aided IMRT treatment planning process can be described as follows (James et al., 2008):

1. Set physical constraints.
2. Set beam orientation.
3. Define objective function (or cost function).
4. Automatically optimise beam intensity maps to minimise objective function.
5. Perform final dose calculation.
6. If plan achieves the clinical goals go to step 7, if not return to step 3 and redefine the objective function
7. Plan is approved for delivery by a clinician.

Step 4 defines the optimisation variable as the beam intensity, or fluence, maps but could potentially include any number of variables such as beam angle or patient/couch motion. The work in this thesis will expand step 4 to read:

4. Automatically optimise spatial variation of intensity, *modality and energy* to minimise the objective function.

2.4.1. Physical Constraints

The physical constraints are set to obtain a satisfactory dose distribution which can be practically delivered on the machine. First, limitations associated with the machine performance need to be considered. Geometrical constraints include the minimum distance between opposing leaves to avoid leaves crashing into each other. Dosimetric constraints include the minimum segment size

and the minimum segment MU. These are set to take into account limitations in the dosimetric performance of the machine. There are also a number of mechanical movements which need to be set. The collimator angle, couch angle, and in particular the number of beams must be chosen to obtain the optimum plan which can be practically treated. Increasing the complexity of the plan by increasing the number of mechanical movements can improve dose conformance but will reduce the efficiency of delivery. For IMRT the optimisation of these parameter is generally less critical than for conventional radiotherapy as the fluence can adapt to compensate for small changes (Bortfeld, 2006).

The selection of beam angles can be significant and some studies have looked at automating this process (Haas et al., 1998, Nazareth et al., 2009). However, the use of beam angle optimisation (BAO) algorithm in routine clinical practice is not yet widespread. Most clinics still adopt the method of placing a sufficient number of equispaced beams, which has been found to produce clinically acceptable dose distribution in many anatomic sites (Ranganathan and Maria Das, 2016).

2.4.2. Objective function

The treatment prescription entered into the treatment planning system describes the goals of the treatment. These goals can be expressed in either an objective function or in constraints. Constraints are restrictions on the set of solutions that are considered feasible. They define what is an acceptable solution and not necessarily an optimal solution. The most basic constraint in IMRT is that all of the beam weights must be non-negative. Constraints can also be used to fix the dose in a particular structure. However, each of these this constraints, which represents only a single threshold value, limits the freedom of the optimiser. If the constraints are conflicting there may not be any feasible solution.

Alternatively a simple objective function would be the square of the differences between the prescribed dose and delivered doses summed for all points:

$$F(x) = \sum_{n=1}^{N} (Dose\ delivered - Dose\ prescribed)^2 \tag{2.3}$$

This has the advantage that all points are considered rather than optimising for a single point. The quadratic sum results in a higher penalty on outliers e.g. hot and cold dose regions in the target. The treatment plan will in reality include multiple structures (targets and organs at risk) such that there are multiple objectives. The objective function then becomes the sum over *K* structures. It is possible to increase the importance of certain structures using relative weights, thus the equation becomes a weighted sum objective function:

$$F(x) = w_1 \sum_{n=1}^{N_1} (d_1 - D_1^{aim})^2 + w_2 \sum_{n=1}^{N_2} (d_2 - D_2^{aim})^2 \ldots + w_K \sum_{n=1}^{N_K} (d_K - D_K^{aim})^2 \quad (2.4)$$

where d is the calculated dose, D^{aim} is the objective value and *w* is the relative weight for each of the *K* structures. An additional factor can be included if it is desirable to penalise only values less than or greater than the objective value (see equation 5.5). To produce an optimal treatment plan the values of D^{aim} and *w* need to be carefully chosen by the treatment planner. Alternatively these parameter can be included into an automation routine such as the fuzzy reasoning approach suggested by Dias et al. (Dias et al., 2016).

In this study objective values were chosen based on the goals of the treatment plan, set slightly low or high (as appropriate) to increase the penalty as the solution approaches the required value. The relative weights of objectives were iteratively tuned in a trial and error approach until the resulting treatment plan was deemed acceptable. Priority was given to OAR dose tolerances and the plan was not deemed to be acceptable unless all OAR dose tolerances were met. The PTV dose objectives were of second highest priority with the proviso that a compromise should be made to meet the OAR dose tolerances (where a compromise may show a weakness in the treatment technique). Finally additional objectives were tuned to reduce normal tissue doses as much as possible without compromising the OAR dose tolerances or the PTV dose. In practice this approach resulted in relative weights in the range 1 - 5 for normal tissue objectives and 5 – 10 for OAR and PTV objectives.

The clinical impact of dose to normal tissues will depend on a number of factors including the volume of tissue irradiated (discussed in 2.5.2). The objective function can therefore be improved to better represent the true goals of the treatment. Radiobiological objectives designed

to represent the actual biological response of tissues to a particular dose distribution can be constructed. The use of biological objectives is an important area of research but, as the report of TG-166 states, due to their limitations reliance on biological objectives can be potentially dangerous (Allen Li et al., 2012). A more typical method is the use of dose-volume objectives. Rather than just using prescribed dose, objectives for a certain volume of the structure to receive a given dose can be defined. Biological objectives can then be used for evaluation of similar plans that both meet dose-volume objectives.

2.5. Clinical Evaluation

When comparing exIMRT with IMRT a method is required to determine whether or not the exIMRT plan is superior. The methods for comparing techniques therefore need to be defined.

2.5.1. Isodose

The first step is likely to be a qualitative analysis through visually assessing the three dimensional dose distribution. The isodose are lines joining points of equivalent dose and these can be viewed and assessed on screen. It is also possible to set nominal isodose aims e.g. keeping the 95% isodose close to the edge of the target. This can be taken a step further by using the conformity number (CN) (van't Riet et al., 1997) or more simply the conformity index (CI) defined as the ratio between the target volume and the volume irradiated to a certain dose level

2.5.2. Dose-volume data

For further quantitative analysis, dose-volume data are required. That is information on the dose received by particular volumes in the patient. The simplest example being the minimum, maximum and mean dose in a particular structure. However this information is not always useful. The minimum and maximum dose may be in a non-representatively small volume e.g. a single voxel. In addition, the calculated values will be subject to errors from a number of sources. For example, the way the structure is drawn and the way voxels are included in the structure can give different maximum and minimum doses. It may then be more useful to look at dose-volume information for example the minimum dose in 1% of the volume (ICRU83, 2010).

The use of dose-volume data will depend on the structure that is being investigated. When looking at the target volume, the focus should be in ensuring that the correct dose is delivered to the target with no significant hot or cold spots. We may then wish to look at the volume of PTV receiving 95% of the dose or the volume receiving 107% of the dose (ICRU50, 1993). When looking at OAR we will have to consider the organ type and its response to radiation. For example it is known that some organs respond in a serial way and some respond in a parallel way. For serial organs the maximum dose must be kept below a fixed values whereas for parallel organs it is the dose to a particular volume, or volume receiving above a certain dose, that is of interest (ICRU83, 2010). exIMRT plans will therefore be assessed using dose-volume objectives from UHCW clinical protocols as well as by simpler means.

As opposed to specific dose statistics dose-volume histograms (DVH) summarise the dose distribution over the entire 3 dimensional dose matrix in a graphical form. A DVH in its simplest form is a frequency distribution of dose values within a specified structure. Rather than displaying the frequency DVH are usually displayed as percentage volume against dose. Two types of DVH are in use, differential DVH and cumulative DVH. The most commonly used is cumulative DVH. With cumulative DVH the volume receiving *at least* the specified dose is plotted against dose. This method is analogous to the qualitative technique of covering the target with a specific isodose (Cheng and Das, 1999).

2.5.3. Equivalent uniform dose (EUD)

Consider a structure within the patient. Depending on the dose delivered to that region, there will be different biological effects. Assuming that the biological effects can be quantified on some one-dimensional scale, for example the grade of tumour control, there will be a number of dose distributions that give the same biological effect. The idea behind the EUD is to, for a given non-uniform dose distribution, find the uniform dose that gives the same biological effect. For the target EUD is the absorbed dose that, when homogeneously given to a tumour, yields the same mean cell kill as the given non-homogeneous irradiation. The concept of EUD is presented by Niemierko (Niemierko, 1997) who suggested that EUD could be defined as (Niemierko, 1999):

$$EUD = (\sum_{i=1}^{N} v_i d_i a^a)^{1/a} \quad (2.5)$$

where this is the same formulae as used in the LKB model for NTCP except that *a* corresponds to *1/n* in the LKB formulae (Appendix C). For a target volume, the logical choice would be an EUD objective with $a < 1$. The lower the value of *a*, the more effort will be given to avoiding cold spots. EUD could be of particular interest for exIMRT where it is expected that the target dose may not be homogeneous. For example, if an exIMRT plan reduces the OAR dose but exhibits a reduction in the target dose homogeneity this may still be preferred if the EUD for the target is unchanged.

2.5.4. Normal tissue complication probability (NTCP)

Either EUD or tumour control probability (TCP) and normal tissue control probability (NTCP) models can be used for biologically based plan evaluation. The report of TG-166 (Allen Li et al., 2012) suggests that EUD has the advantage of being less dependent on the chosen parameters when it comes to ranking treatment plans. However it would be useful to be able to have a feeling for the change in NTCP when evaluating the exIMRT technique.

NTCP is the probability that a given dose of radiation will cause an organ or structure to experience complications considering the specific biological cells of the organ or structure. The main NTCP models in common usage are the Lyman Kutcher Burman (LKB) model (Lyman, 1985, Kutcher et al., 1991) and the relative seriality models (Källman et al., 1992). Parameters for these model need to be derived from published clinical outcome data. Burman derived parameters for the LKB model from the Emami data for normal tissue response (Emami et al., 1991) to produce what is referred to as the Emami-Burman parameters (Burman et al., 1991). However in some cases more accurate values are available based on more up to date data including that presented by QUANTEC (Bentzen et al., 2010). Details of the models and parameters used in this research are presented in Appendix C.

2.5.5. Malignant induction probability (MIP)

Plans than have similar dose-volume data EUD and even NTCP may carry with them different risks of inducing secondary cancers. By reducing the low dose wash through exIMRT it is hoped

that this risk can be minimised. A method of ranking methods by their relative risk would therefore be desirable. Radiation therapy gives rise to premalignant initiated cells when DNA damage is miss-repaired, leading to mutations in the genetic code. The study of (Timlin et al., 2011, Timlin et al., 2015) introduced the concept of malignant induction probability (MIP) by considering the expected number of transformed cells in each voxel of the treatment volume. Two models based on linear and linear quadratic models of the probability of a cells being transformed were presented both giving similar results when it comes to ranking plans. Although the absolute MIP value was found to be dependent on the parameters the value of relative MIP (relMIP) was found to be a useful metric to rank plans regardless of parameter and model based uncertainties. The relMIP was used compare proton therapy with X-ray IMRT in (Timlin et al., 2015) but could equally be used for combined electron and X-ray IMRT. Details of the models and parameters used in this research are presented in Appendix C.

2.6. Discussion and conclusions

Existing studies demonstrate that combing X-ray IMRT and electron beams to improve depth modulation can reduce the dose distal to the target. However none of these studies have progressed to routine clinical practice. It is suggested then that further research into combined electron and X-ray IMRT is valid.

The study of (Das et al., 2004) demonstrates the theoretical benefits of combined electron and X-ray IMRT encouraging research into practical applications. The study of (Al-Yahya et al., 2005) builds on this work by using an add on electron MLC (eMLC). The use of eMLC is a viable option but introduces problems with integrating the election and X-ray components. The eMLC would either have to be removed or retracted between modalities potentially causing issues with matching of the electron and X-ray components. The PhD thesis of (Weinberg, 2007) proposes using X-ray MLC (xMLC) to avoid the issues around eMLC but the study was only partially successful. Weinberg demonstrated only some small improvements in dose distributions with a small additional contribution from the electron beam. It is suggested that these results could be improved with reduction of penumbra broadening of the electron component. The studies of (Surucu et al., 2010, Palma et al., 2012) both employ a reduced SSD to minimise penumbra

broadening but this would make integration of the electron and X-ray component difficult (discussed further in Chapter 5).

It is hypothesised that, rather than reduce SSD, scattering foils could be removed to reduce penumbra broadening of the electron field. This would have the added benefit of reducing X-ray contamination which is stated by (Henzen et al., 2014) as being potentially prohibitive. Scattering foil free delivery of electron beams with xMLC is a novel contribution of this research. In parallel to the work undertaken by the author over the last 5 years, scattering foil removal has been shown to be feasible by others for conventional electron beams and add on electron MLC to reduce X-ray contamination.

Only Weinberg and Palma et al. optimise the combined electron and X-ray dose distribution. However neither optimise the electron energy. Palma et al. goes some way to optimising the electron energy with range selection but this does not consider variations in penumbra broadening with energy (discussed further in Chapter 5). It is hypothesised that an iterative constrained optimisation of the photon intensity, the electron intensity, and the electron energy could maximise the potential of combined electron and X-ray IMRT.

BEAMnrc Monte Carlo modelling of radiation transport has been used for the electron component in a number of studies and shown to be accurate. However the scattering foil free electron beam line has not been modelled previously. This research will therefore use BEAMnrc to model the scattering foil free xMLC collimated beam.

A number of treatments sites have been considered for combined electron and X-ray IMRT but the greatest number of successful studies have been for breast treatments and for cancers in the head and neck. The research will therefore consider breast and head treatments as well as other sites for clinical evaluations. Clinical evaluation methods reviewed in this chapter will be used with the novel application of relMIP to combined electron and X-ray IMRT to quantify reduction of secondary cancer risk.

Chapter 3

Dosimetric characteristics of xMLC shaped scattering foil free electron beam

3.1. Introduction

This chapter presents an investigation into the feasibility of delivering electron beams shaped with X-ray photon MLC (xMLC) and jaws by way of measurement. It begins by addressing the fundamental problems associated with such a method. Following on from this the use of scattering foil free delivery as a novel way to minimise some of the problems is discussed and demonstrated. Finally questions raised about the practicality (dose rate) and safety (dose distal to the field) of xMLC delivery of electrons beams are addressed. In all cases a 10MeV electron energy has been used to demonstrate the principles which are likely to be applicable over the range of clinical energies.

3.2. SSD

Existing studies investigating electron beam shaping with xMLC suggest short source to surface distance (SSD) of 60 to 70 cm (Chapter 2). Although conceivable for MERT alone such short SSD would be very limiting if MERT were combined with X-ray IMRT. Short SSD dictates lateral or posterior beams only as anterior beams require the patient to be raised to an unsafe height. More importantly, matching with X-ray fields at an angle to the electron field would be limited by the X-ray field size. For an Elekta linac the half width of the maximum available X-ray field is 20cm. The distance from the source to the mechanical isocentre is 100cm. Hence the minimum SSD for an orthogonal electron beam would be 100-20 = 80 cm if the X-ray beam were to extend to the surface (see Figure 3.1). In practice, combining short SSD MERT fields with X-ray IMRT would

require separate isocentres. Using separate isocentres would introduce inaccuracies into the matching of the electron and X-ray components. There may be errors due to the positioning of the patient between isocentres as well as increased internal or external patient movement due to the extra time required. In order to attempt to reduce these errors image guidance would need to be repeated for both isocentres resulting in additional dose to the patient.

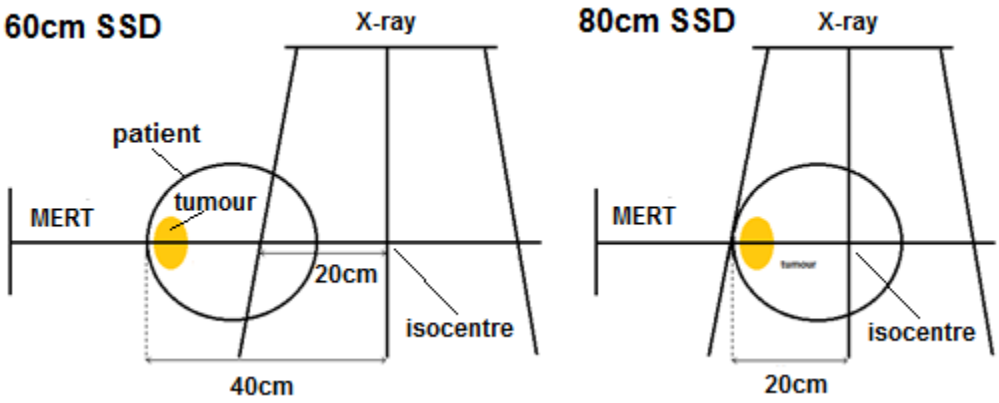

Figure 3.1 X-ray field orthogonal to MERT at 60cm SSD (left) and 80cm SSD (right), tumour not covered by maximum field size at 60cm SSD

To overcome practical issues associated with combining electron and photon in the same treatment, it is proposed to deliver electron beams through the xMLC at standard SSD of 80 to 90 cm.

3.3. Methods

Measurements with and without the scattering foil were made using an Elekta Synergy linear accelerator with MLCi head currently in clinical operation. The Elekta design uses a dual scattering foils design (Bjarngard et al., 1976). The primary thin tantalum (high-Z) foil scatters the initially narrow electron beam into an approximately Gaussian distribution. The secondary foil consists of a conical shaped copper or aluminium (low-Z) foil which is located downstream of the primary foil to flatten and broaden the beam. Removal of the scattering foils from the beamline can be achieved with only minor modification to the treatment machine. The primary scattering foil can simply be rotated out of the path of the beam as is the case in photon mode. As the linac is digitally controlled this can be done in service mode simply be editing the corresponding

machine item part. The secondary scattering foils sit on a carousel along with the X-ray flattening filter. There are five spaces in the carousel but for the linac investigated here not all spaces are used clinically. Unused spaces are covered with an aluminium blanking plate but removal of the blanking plate to leave an empty space is a relatively simple matter (see Figure 3.2). The carousel can then be rotated into the correct position by changing the appropriate machine item part as with the primary scattering foil. If this mode of operation were to be offered for clinical use by the manufacturers all that would be required is removal of the blanking plate and the addition of the scattering free foil mode to the software configuration of both the linac and the record and verify system.

The linac co-ordinate system of A to B and G to T is referred in the text and figures of this chapter. The system is independent of linac movement where A to B indicates left to right and G to T indicates the gun to target direction perpendicular to A to B. In this chapter an A to B measurement refers to a measurement across the MLC travel direction and G to T refers to a measurement in the perpendicular 'Y-jaw' travel direction as all measurement were performed with zero degrees gantry and collimator rotation.

A series of Measurements were made at 10MeV to characterise operation in scattering foil free mode, with additional measurements at 6MeV and 15MeV to provide a reference for Monte Carlo modelling at those energies (Chapter 5). A Sun Nuclear IC Profiler 2D Diode array was used to check beam stability and ensure beam symmetry. Measurements of depth dose and off axis profiles were made with a PTW 60012 electron diode in a PTW MP3 water tank. A PTW Advanced Markus chamber in WTe solid water at the geometric centre of the field at 90cm SSD was used to determine the variation in output with field size on the central axis and towards the edge of the available treatment area for the un-scattered beam line. Using xMLC to collimate the electron beams may result in an additional source of dose from electrons scattered in the linac head or in the air between the linac head and the patient. To determine whether this additional scatter dose is significant measurements were made in the patient plane at set distances from the field edge. A 10x10cm field was delivered and measurements were made using a 0.6cc farmer ionisation chamber with a 1.5cm thick Perspex build up cap. The chamber was positioned at distances up to 1m from the patient and charge recorded normalised to the reading at the centre of the open field.

Figure 3.2 Elekta scattering foil carousel with empty space

3.4. Electron beam delivery through xMLC

Measurements were carried out to examine electron beam delivery through the Elekta MLCi head xMLC at 95cm and 90cm SSD. The off axis profiles and depth doses were measured for a 10 MeV electron beam with applicator and for the same beam collimated with jaws and the 1cm wide MLC to 10cm and 2cm square to show the effects of penumbra broadening and increased photon contamination.

Off axis absorbed dose profiles measured at various depths in a water tank for a clinical (scattering foils in place) 10MeV 10x10cm electron beam with applicator are shown in Figure 3.3 along with the same 10MeV beam collimated with xMLC. It can be seen that collimating the electron beam with xMLC results in penumbra broadening, widening of the field size and loss of in field flatness.

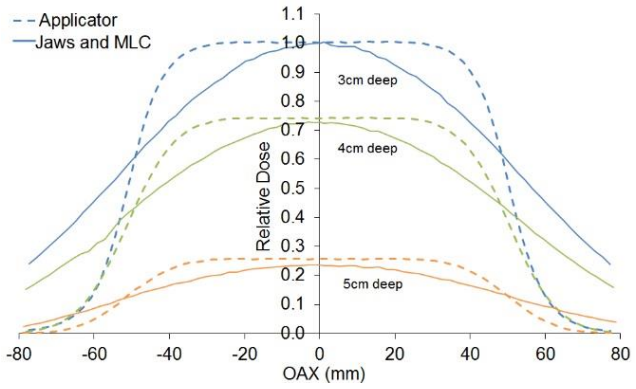

Figure 3.3 Measured off axis profiles in water for a 10MeV electron beam (scattering foils in place) at 95cm SSD, field defined by a 10x10cm applicator and by 10x10cm (set field size) Jaws and MLC (measurement in the MLC direction, Elekta MLCi 1cm wide leaves).

It may be possible to regain some in field flatness by intensity modulation with multiple small fields (Chapter 5). Moreover a flat field is not necessarily an advantage if intensity modulation to produce a non-uniform dose distribution is required. This is analogous to removal of the flattening filter for photon IMRT treatment which has now been generally accepted as best practice (Cashmore, 2008). Although it should be noted that as well as loss of flatness the lateral scatter of electrons results in an increase in dose outside the geometric field size for the electron field.

To apply intensity modulation to the electron field with xMLC multiple small fields or 'segments' will be required. This introduces another potential issue in that reducing the field size reduces the electron dose rate by reducing the contribution from electrons scattered onto the central axis. In order to give the correct dose the monitor units (MU) and therefore beam on time can be increased but this would increase treatment time, increase head leakage and importantly increase the relative contribution from contaminant X-ray photons.

Photon contamination can be determined from the tail of the measured depth curves. For a 10MeV 2cm square field at 90cm SSD the photon contamination is 7.3% of the maximum dose at 7cm deep (see Figure 3.9). This level of X-ray contamination could be significant as one of the aims of incorporating electron beams into the plan is to reduce the low dose wash.

In this work a new approach to reducing the two effects of increased penumbra broadening and increased X-ray contamination previously described above is proposed. The proposal is that the scattering foils are removed from the path of the electron beam. Removing the scattering foils will reduce the scattering angle of electrons leaving the linac head and remove a source of contaminant photons.

3.5. Scattering foil free electron beam

Scattering foils are designed to widen the electron beam that leaves the exit window to make it suitable for clinical use. By removing the scattering foils the width of the electron fluence and therefore the useful treatment area will be reduced. This electron fluence was measured as it leaves the linac head with EBT3 radiochromic film placed in air at 60 cm SSD (see Figure 3.4). This measurement shows that there is still significant scattering after removing the scattering foils. This scattering is likely to be from the Nickel exit window but will be investigated further through

Monte Carlo modelling (Chapter 4). The fluence distribution is approximately Gaussian with a FWHM of 12.8cm at 60cm SSD. This suggests a useful field diameter of around 12.8/60 * 90 ≈ 19cm at 90cm SSD.

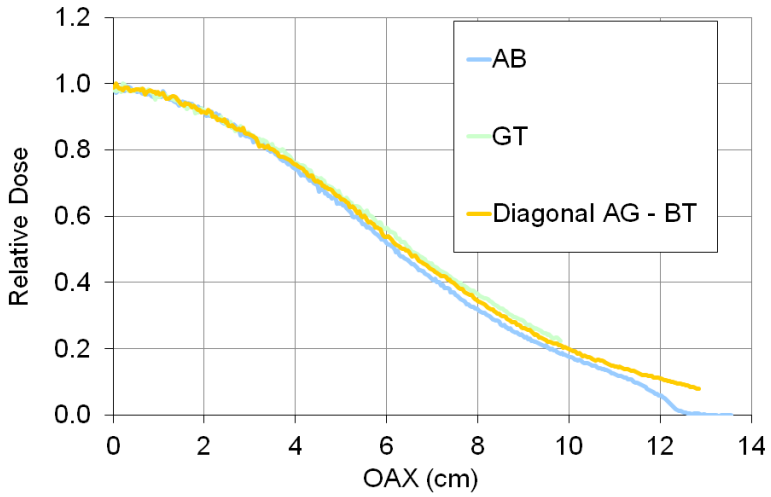

Figure 3.4 Measured electron fluence across half the field at 60cm SSD for a 10MeV field, scattering foils removed jaws and MLC set at 40x40cm in orthogonal planes and across the diagonal.

Although the linac is not designed to operate with the scattering foils removed, measurement with a Sun Nuclear IC Profiler 2D Diode array demonstrated that running in this mode is stable and that a homogenous electron beam can be produced. Symmetry in all directions to better than 1% was achieved with only minor adjustments to the beam steering currents set with the flattening foils in place (see Figure 3.5).

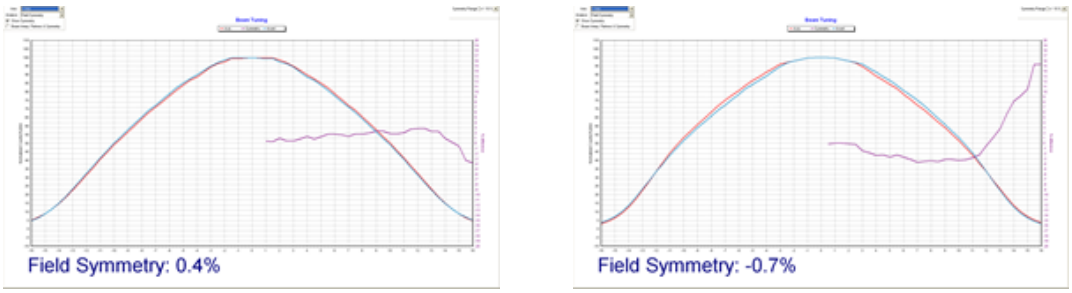

(a) (b)

Figure 3.5 Profiler measurements of field symmetry with scattering foils removed. Taken directly from Sun Nuclear Profiler software and showing measured profile (red), measured profile mirrored about the central axis (blue) and the % difference (purple), plotted against distance off axis (a) A-B and (b) G-T direction, 25x25cm set field size.

The dose deposited in the patient is related to the incident electron fluence but will be modified by the additional scatter in the air and in the patient. This is considered by measuring the dose with an ionisation chamber at depth in a water tank with the surface of the water at 90cm SSD. Measurement of the 10MeV beam with jaws and MLC at 40x40cm at 2cm deep, 90cm SSD confirm an approximately Gaussian dose distribution at depth with scattering foils removed (see Figure 3.6).

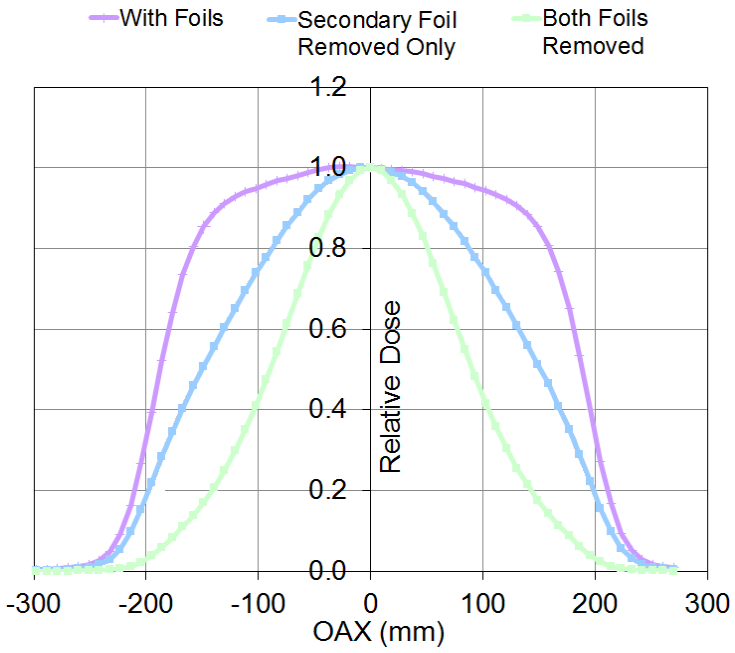

Figure 3.6 Measured off axis profiles in water for a 10MeV electron beam at 90cm SSD 2cm deep, 40x40cm Jaws and MLC (set field size). With and without the scattering foils across the A to B (similar profiles measured in the G to T and diagonal axis).

With both foils removed the FWHM of the distribution is 18cm, agreeing with the fluence measurements within 1cm. Perhaps then the useful treatment area could be defined as an 18cm diameter circle or, if 18cm is the diagonal of square, a 12.7cm square. Although this is a significant reduction in area compared to the 40x40cm square (maximum field size available with scattering foils in place) it is still a potentially useful size and comparable to that available for add on electron collimators developed by others. A larger area is available if just the secondary foils are removed. Removal of just the secondary foil is an attractive proposition as the shaping by the secondary foil is not required if the beam is intensity modulated. Perhaps some gains can be made by keeping the

primary foil to widen the beam but removing the secondary filter. This possibility will be investigated further below.

To investigate the potential advantages of delivery with scattering foils removed consider a 10x10cm field as a typical total treatment field size and a 2x2cm field as the component of a segmented field for MERT.

The 10x10 field at 90 cm SSD shows that for a larger field the penumbra width is reduced when removing both scattering foils (see Figure 3.7). Penumbra width defined as the distance between the 80% and 20% dose points is reduced from 43mm to 34mm in the A to B direction and from 33 to 29mm in the G to T direction.

Similarly widening of the field size is reduced with scattering foils removed. Field size defined as the 50% dose width has been compared to the ideal geometric width defined as the width of the light field on the water surface (for a 10cm wide field at 90cm SSD = 90/100x10 = 9cm). With foils in place the field size is extended by 16mm in the A-B direction compared to the ideal geometric field width. This is reduced to 4mm with scattering foils removed.

Removal of just the secondary foil appears to provide no advantage in terms of reducing the penumbra for 10x10cm field.

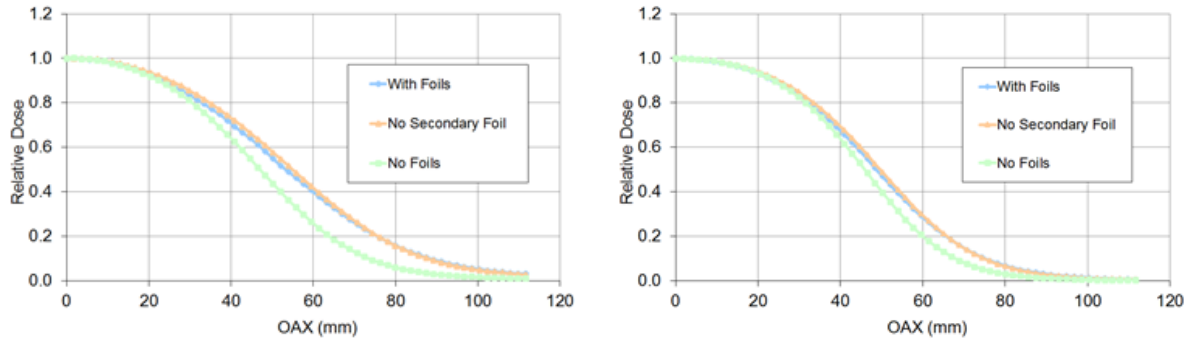

Figure 3.7 Measured off axis profiles in water for a 10MeV electron beam at 90cm SSD 2cm deep, 10x10cm Jaws and MLC (set field size). With and without the scattering foils across the A to B axis (left) and across the G to T axis (right).

For a 2x2 cm field penumbra broadening is relatively large and the field size is not maintained with or without scattering foils (see Figure 3.8). As discussed in Chapter 2 some studies suggest that one way to minimise penumbra broadening is to treat at reduced SSD. To investigate the SSD effect measurements were made at 90, 80, 70 and 60cm. For each SSD the set field size

was modified to give the same field size projected at the water surface as a 2x2cm set field size at 90cm SSD. Results are presented in Table 3.1. These results demonstrate a clear benefit to reducing SSD by reducing in air scatter and therefore field spread. From 90cm SSD to 60cm SSD the penumbra width is reduced by 11.7mm with scattering foils in place. However there is also a significant reduction in scattering with removal of the foils. At 80cm SSD the penumbra width is reduced from 18.3 to 14.3mm with scattering foils removed. This brings it closer to the measured penumbra with of 14.7mm at 70cm SSD. There is also a reduction in the benefit of reducing SSD with scattering foils removed as from 90cm SSD to 60cm SSD the penumbra width is reduced by 8.2mm. However the absolute penumbra is smaller at reduced SSD suggesting that SSD should be minimised where possible.

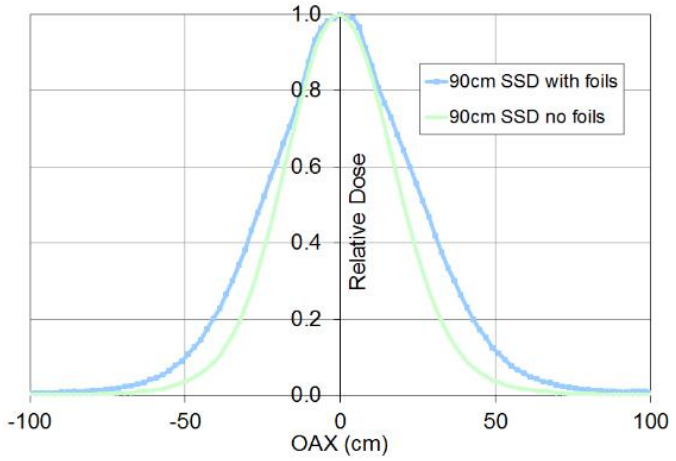

Figure 3.8 Measured off axis profiles in water for a 10MeV electron beam 2cm deep, 2x2cm Jaws and MLC (set field size) across the A to B axis. With and without the scattering foils at 90cm SSD.

Table 3.1 Reduction of penumbra width for a 2x2 field by reduction of SSD and by removal of scattering foils

SSD (cm)	With Scattering foils	No Scattering foils	
	80-20% Width (mm)		Reduction (mm)
90	23.2	18.6	4.6
80	18.3	14.7	3.6
70	14.5	12.6	1.9
60	11.5	10.4	1.1

X-ray contamination can be investigated by considering the tail of the depth dose curve. Measuring dose along the central axis will give the characteristic electron depth dose curve with electron dose stopping at the practical range of the electrons and leaving just the contribution from the more penetrating contaminant X-rays. For a 2x2 cm field removing the scattering foils reduces the dose at 10cm deep from 7.3% to 0.6% (see Figure 3.9). Removal of just the secondary foils has a reduced impact with the dose at 10cm deep remaining at 2.1%. Note that removal of both scattering foils does have the negative effect of a small reduction of the dose gradient between 90% and 70% dose.

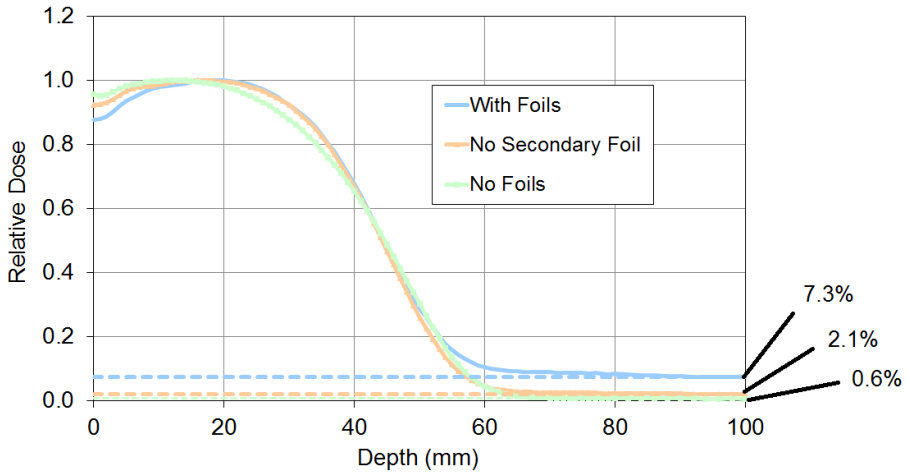

Figure 3.9 Measured percentage depth dose for a 10MeV electron field delivered through the jaws and MLC at 90cm SSD for a 2x2 cm field with and without scattering foils to show reduction in X-ray contamination

It has been suggested by (du Plessis et al., 2006) that the electron field should be defined by the MLC only, i.e. with backup jaws retracted, to avoid an additional source of scatter. However measurement of a 2x2cm profile with and without backup jaws demonstrated very little influence from the backup jaws for the Elekta linac investigated (see Figure 3.10). This is possibly due to the standard calibration procedure of setting the backup jaws 1mm behind the MLC.

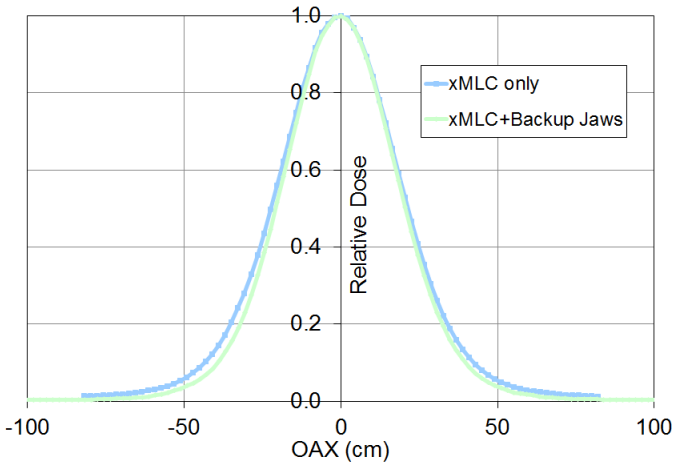

Figure 3.10 Measured off axis profiles in water for a 10MeV electron beam 2cm deep, 2x2cm Jaws and MLC (set field size) across the A to B axis. With and without backup jaws.

Unless otherwise stated all measurements above were made with a PTW 60012 electron diode detector and a PTW MP3 water tank. The electron diode is indicated for use with MeV electrons by the manufacturer and has been previously commissioned for use in the clinic. However to increase the confidence in results for dose delivery without scattering foils and small electron fields it has been compared to measurements using a PTW microDiamond detector. The microDiamond detector is a single crystal diamond detector utilising a diamond synthetically manufactured for reproducibility. Diamond detectors have been shown to demonstrate an improved response compared to silicon diodes including field size dependence, directional dependence and a response shift in very small fields (Laub and Crilly, 2014). If differences existed between microDiamond measurements and electron diode measurement this could indicate an inaccuracy that requires further investigation. In fact for the conditions used here there difference between the microDiamond and the electron diode data is <0.5% confirming the validity of the electron diode measurements.

3.6. Dose rate

A potential issue with the use of small electron fields collimated by the xMLC is the reduction in the effective dose rate, or ‘output’, seen as a reduction in the dose delivered per MU. The electron fluence at the surface of the patient on the central axis is a combination of electrons originating on the central axis and electrons scattered onto the central axis. Collimating the field

at the head rather than at the patient stops electrons high up that might otherwise scatter onto the central axis. This effect can be seen in Table 3.2. Measurements of dose rate have been made using an Advanced Markus Chamber at 2cm depth in solid water. For each field 100 MU was given and the recorded charge normalised to the recorded charge for a clinical 10MeV beam under reference conditions (1cGy/MU). With the scattering foils in place, it can be seen that collimating down to a 2x2cm field reduces the dose rate to 8%. However, with the scattering foils removed the dose remains at 40% of the clinical beam, a factor of 5 higher than the same beam delivered with scattering foils. This is partly because fewer electrons are absorbed by the scattering foils which results in an increase in the dose rate for a 10x10 applicator field when scattering foils are removed. It is also likely that fewer electrons originating on the central axis in the forward direction have been scattered away, reducing the effect of collimating down to the small field size.

Table 3.2 Dose rate relative to Clinical 10x10 10MeV beam, all at 2cm depth in WTe Solid Water measured with an Advanced Markus ionisation chamber

	Relative Dose Rate	
	With Scattering foils	No Scattering foils
10x10 Applicator 95cm SSD	1.00	2.29
10x10 xMLC 90cm SSD	0.87	2.44
2x2 xMLC 90cm SSD	0.08	0.40

The same method of measurement was used to determine how dose rate varied if small fields were delivered off the central axis. In section 3.5 it was determined that a useful treatment area would be around 180mm diameter or 127mm square. This suggests that individual small segments could be delivered with a field offset of 180/2 = 90mm, neglecting field width. To investigate the change in dose rate in this region, measurement were made for a 2x2cm field offset by 60 to 120mm in the B direction (see Figure 3.11). Over the full 120mm offset the dose rate remains at >10% of the clinical beam under reference conditions. This drop in dose rate does apply radially so that with an offset in both B and G of 80 mm the offset from the CAX along the diagonal equates to 113mm and the dose rate drops to 11% (not shown in Figure).

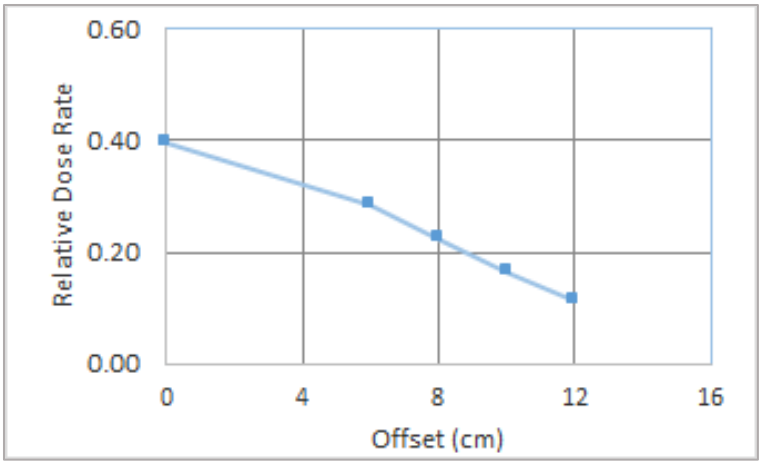

Figure 3.11 Variation of dose rate with field offset in the B direction for a 10MeV 2x2 xMLC scattering foil free electron beam at 90cm SSD relative to a clinical 10MeV 10x10 field delivered with an applicator at 95cm SSD

3.7. Peripheral doses

So far only the dose to the patient from the direct electron field has been considered. In general with any external beam radiotherapy technique there will also be photons and electrons that leak through the linac shielding or scatter in the head of the linac that reach the patient plane distal to the treatment field. This results in a low level of dose to the patient in areas other than the area being treated. This dose contribution should be minimal and is regulated to be <0.1% of the useful beam exposure at 1m. Using xMLC to collimate the electron beams may result in an additional source of dose from electrons scattered in the linac head or in the air between the linac head and the patients.

To determine whether this additional scatter dose is significant, measurements were made in the patient plane at set distances from the field edge. A 10x10cm field was delivered and measurements were made using a 0.6cc farmer ionisation chamber with a 1.5cm thick Perspex build up cap. The chamber was positioned at distances up to 1m from the patient and charge recorded normalised to the reading at the centre of the open field. Spot check measurements were also made with the build-up cap removed to account for dose from low energy scatter. For comparison, similar measurements were made for a 6MV 10x10cm field with and without a motorised heavy metal wedge (used for 3DCRT treatments) inserted.

It can be seen in Figure 3.12 dose drops of quickly for electrons delivered with xMLC. The relative dose is less than 0.1% at 1m and is actually lower than a for a 6MV wedged field (where the heavy metal wedge is a significant source of scatter).

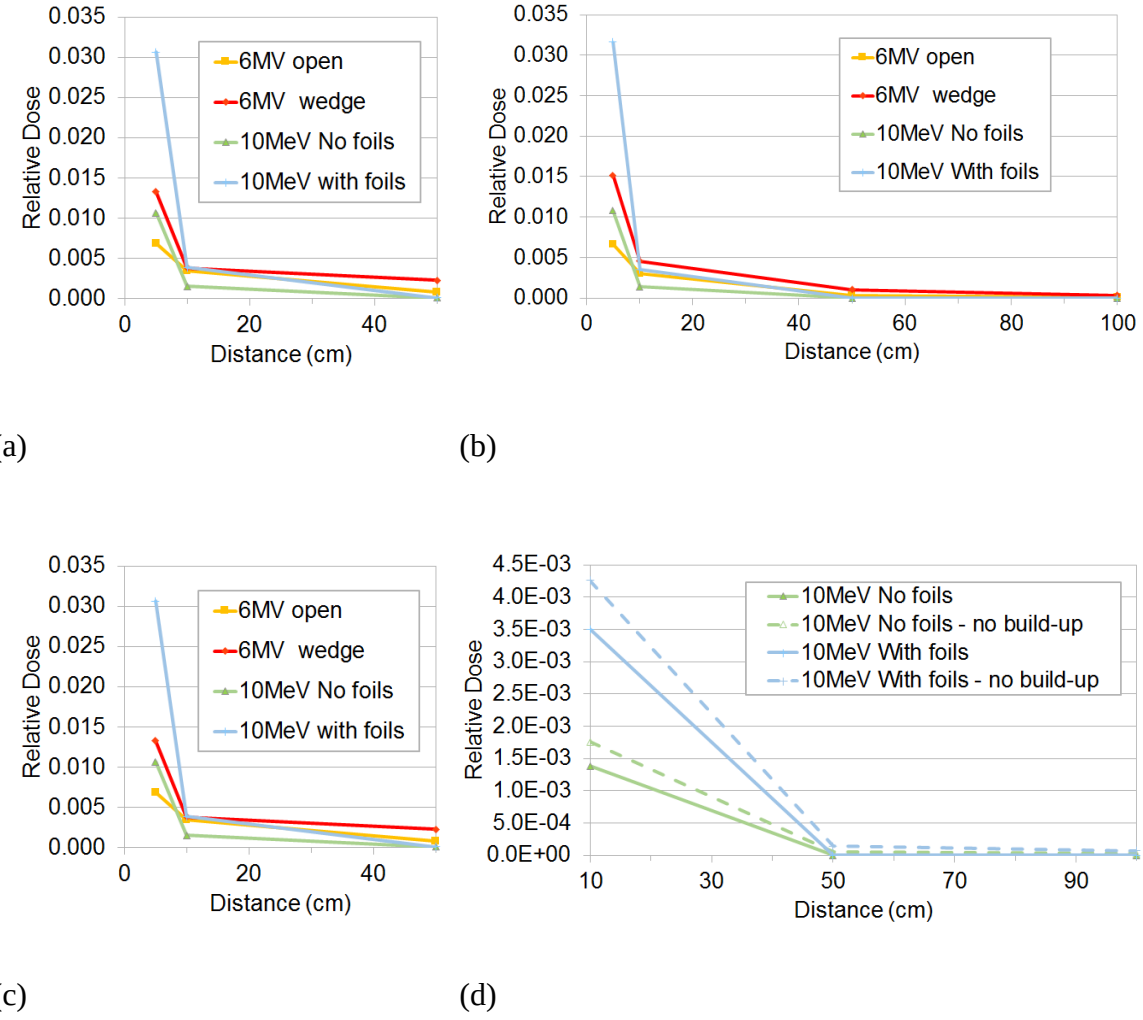

Figure 3.12 Dose distal to the field edge measured using a 0.6cc Farmer chamber and 6MV build up cap. Distance from the field edge towards G (a), towards T (b) and towards B(c). Detail with and without build up cap (d).

There is some reduction in dose away from the field edge when removing the scattering foils. At 5cm from the field edge in the A-B direction it is reduced from 3% to 1% (see subfigure (c)). At distance greater than 10cm from the field edge there is a small reduction in dose when removing the scattering foils (see subfigure (d)) but in all cases it is less than 0.01% at 50cm. This

includes dose measured with the build-up cap removed suggesting no high levels of low energy electrons are present.

3.8. Segment size

Previously, a 2cm electron segment size was assumed. This is the minimum field size suggested by Klein et al. in the context of MERT using xMLC at reduced SSD (Klein et al., 2008). Small fields are necessary to achieve the required resolution for intensity modulation. However, as the field size is reduced the extent of lateral scatter in the air and the patient does not reduce correspondingly such that the minimum effective field size is limited. The typical beamlet size of a few mm used for X-ray photon IMRT is therefore not practical. To investigate this effect small fields were measured with EBT3 radiochromic film at depth in WTe solid water (see Figure 3.13). The dose profiles for the scattering foil free 10MeV beam at 90cm SSD 2cm deep have been plotted for a 1x1cm, a 2x2cm and a 5x1cm field. Reducing the field size from 2cm to 1cm does not produce a smaller effective field size as expected (but has the negative effective of reducing effective dose rate). Increasing the length of the field to 5cm only increases scatter contribution, further increasing the width of the field.

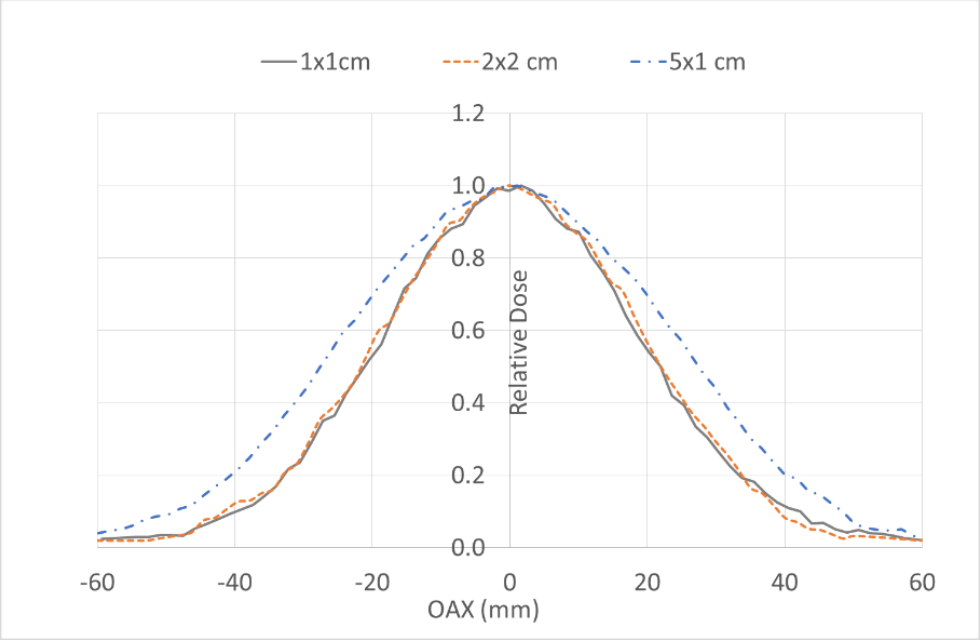

Figure 3.13 EDR2 radiochromic film measurements of 10MeV profiles at 90cm SSD and 2cm deep 1x1cm and 2x2cm profiles overly each other and 5x1cm (across the 1cm direction) is wider.

3.9. Discussion and conclusions

Shaping of the electron field with the xMLC is generally seen as an impractical proposition due to scatter in the linac head and in the air between the exit window and the patient. It has been shown in this chapter that some of the issues can be minimised by removing the scattering foils which is the primary source of scatter in the linac head. This in itself may at first seem impractical but it has been demonstrated that a stable symmetrical beam can be maintained with a reasonably sized effective treatment area of 18cm diameter. By removing the scattering foils penumbra broadening is significantly less. For a 10MeV field the 80-20% width is reduced by up to 9.6mm for a 10x10cm field and 4.6mm for a 2x2cm field. This reduction in penumbra broadening is not seen when only the secondary scattering foil is removed so for the technique to be effective both foils must be rotated out of the beam.

It has also been demonstrated that the issues of low dose rate and increased X-ray contamination associated with small fields can be avoided by removal of the scattering foils. Measured X-ray contamination is negligible with the scattering foils removed and the dose rate is over 20% of a standard clinical electron beam as long as segments are not offset beyond the 18cm diameter circular effective treatment area.

These results suggest that shaping the electron beam with xMLC is feasible but that the dose distributions produced are not ‘flat’ and significant lateral spread remains with scattering foils removed. What is required is to determine whether intensity modulation and combination with IMRT can produce useful dose distributions within these limitations. It is not practical to do this with direct measurement so first the electron beam will be modelled to allow calculated intensity modulated electron dose distributions to be produced.

Chapter 4

Monte Carlo modelling of an xMLC scattering foil free electron beam

4.1. Introduction

Historically one reason for a reluctance to implement complex electron treatments in the clinic has been the difficulty of calculating dose in the patient. Deterministic pencil beam models assume that the beam incident on the patient is actually a conglomeration of many smaller narrow pencil beams. This does not fully take into account the effects of inhomogeneities and lateral scatter. Consequently, in inhomogeneous media, pencil beam dose calculations have large errors for complex geometries. This issue is largely solved by using Monte Carlo based dose calculations (Lee et al., 2001).

Monte Carlo dose calculations use simulations of particle transport to build a true picture of the physical reality. The geometry of the system is defined along with a source of particles. Particles are created then travel a distance before interacting with matter based on random sampling from a probability distribution defined by the total interaction cross section. At this point, the particle may scatter into another energy or direction which is defined by the differential cross section. The same principle applies for if a new particle is produced. The process is continued until all particles are absorbed or leave the geometry. The dose delivered can be determined by making a tally of the energy absorbed in the area of interest. This value is the dose averaged over the number of initial source particles or 'histories', N. Mathematically, this averaging procedure is a Monte Carlo integration where the random points in the problem space are the random particle trajectories in the given geometry. According to the central limit theorem the dose calculated will approach the true value for large values of N. Calculated values will be subject to a statistical uncertainty that decreases as $N^{-1/2}$. If a high statistical precision is required calculation time may

be therefore be prohibitively long. Techniques that speed up Monte Carlo simulations without introducing a systematic error in the result are known as variance reduction techniques. With the application of variance reduction techniques and with improvements in high speed computing, Monte Carlo calculations have recently become a viable option for use in the clinic and are available as part of a number of commercial treatment planning systems.

As long as the model is specified correctly and with enough detail in the geometry Monte Carlo dose calculations of electron radiotherapy can be highly accurate (Lee et al 2001). Monte Carlo has been used in this study as the most accurate method of predicting not only dose in patient but also the interplay of scatter from the linac head when collimating with xMLC. Thus, any conclusions about the potential of modulated electron beams from this work will be based on data that reflects the clinical reality.

4.2. BEAMnrc scattering foil free model

BEAMnrc has been used to create a Monte Carlo model of the linac. BEAMnrc is a medical linac modelling tool which acts as a front end for creating the geometry to feed into radiation transport calculations by EGSnrc. There are a number of Monte Carlo codes available but, as well as having existing tools for the modelling of the medical linac, EGSnc is one of the most widely used Monte Carlo codes for simulating electron transport in medical applications and has been extensively validated against measurement (Rogers et al., 1995).

A three stage BEAMnrc model was used. Stage 1 models the passage of the electron beam through an Elekta linac head up to the collimators. The particles from the Stage 1 phase space file are then transported through Stage 2 which consists of an accurate model of the Elekta MLCi head collimating jaws and MLC. Stage 3 takes the particles from Stage 2 and transports them through the air gap between the bottom face of the MLC and patient, as well as in the patient phantom itself.

If modelling an unmodified linac Stage 1 could either include the scattering foil geometry explicitly or employ a virtual source model. Rather than simulate the passage of electrons through scattering foils directly a virtual source model considers the electrons as being created after the scattering foils with an energy and scattering angle as if they had passed through the scattering foils. In this work, however, the scattering foils are removed completely so there is no requirement

for the foils to be modelled. Therefore, the electron source simply becomes the direct parallel beam of electrons that exit the accelerating waveguide. The remaining components of scatter in the linac head do, however, have to be modelled, namely the ionisation chamber, the mirror and most importantly the exit widow. The exit window is designed to act as a barrier between the near vacuum of the accelerating waveguide and the open atmosphere of the linac head whilst providing minimum absorption of exiting electrons. On the Elekta linac the exit window consists of 0.125mm thick Nickel. In the absence of scattering foils the Nickel exit windows becomes the primary source of scatter and as such the density and thickness are critical.

Figure 4.1 shows the difference in scatter conditions with the nickel exit window only and with the primary scattering foil (a 0.07mm Tantalum disk) in place. There is still a significant amount of scatter just from the exit window. Removal of the primary scattering foils does reduce electron scatter as expected with a reduction in the average electron scattering angle from 8º to 6.5º.

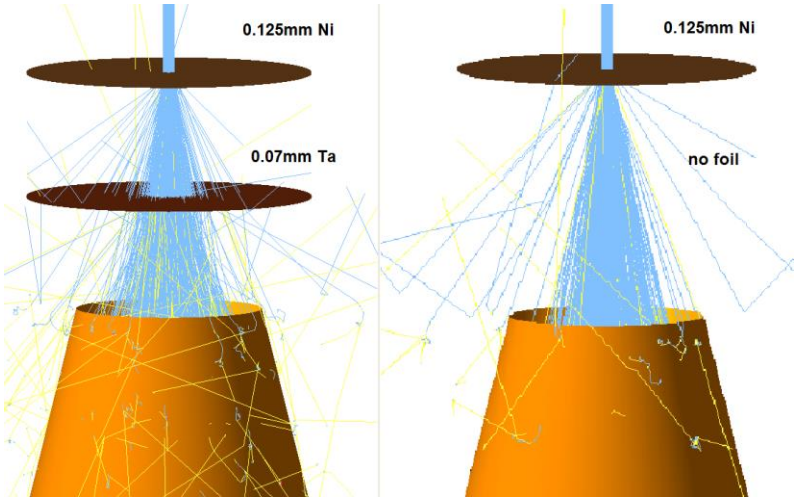

Figure 4.1 Monte Carlo Simulation of a 10MeV parallel electron beam incident on the nickel exit widow and a 0.07mm Tantalum primary scattering foil (left) and the exit window alone (right). Electrons tracks are shown in blue, contaminant X-ray photons in yellow as they enter the opening of the primary collimator. Disks represent the planes of the foils.

For each component of the Monte Carlo model every effort has been made to correctly reflect the geometry, materials and density of materials used in the linac design. Reference has been made to measurement of individual components and to the manufacturer's supplied technical drawings. The EGSnrc distributed ICRU521 materials (lower threshold energy for secondary

electron production than ICRU700) based on data from ICRU 44 (ICRU44, 1989) have been used except where new materials have been constructed to match Elekta specifications.

4.3. Monte Carlo transport parameters

In the process of slowing down within a system a typical fast electron path will involve 10^5 collisions most of which will involve only a slight change in direction and energy (Larsen, 1992). In the context of Monte Carlo modelling of radiation transport following each electron path directly from creation to absorption would require the tracking of a prohibitively large number of tracks. For this reason many track segments of the real electron path are grouped into a single step, a so called Condensed History (Berger, 1964). The cumulative effect of elastic and inelastic collisions during the step are taken into account by sampling energy and direction changes from the appropriate multiple scattering distributions at the end of the step. This approach is justified because the change in electron state in a single collision is usually small at high energies. The approach breaks down at lower energies and individual electron paths have to be followed. At high energies, the creation of secondary particles along the electron path is also required to be considered. EGSnrc uses the Class II Condensed history scheme where above set threshold energies bremsstrahlung processes that result in the creation of photons and inelastic collisions that set in motion atomic electrons are simulated explicitly and the secondary particles transported (Kawrakow, 2000).

There are some subtle variations to the condensed history approach available within EGSnrc which are controlled through user input parameters. Setting of the parameters that control the model incorrectly could potentially have a negative influence on accuracy of the simulation and therefore the calculated dose distribution. Each of these parameters along with the chosen value is described in the following subsections, followed by an associated sensitivity study.

4.3.1. Electron-step algorithm= PRESTA-II

The simplest possible approach one could take is to ignore deflections due to multiple elastic scattering during the condensed history step and to transport the electron on a straight line along the initial direction of motion. In order for this approach to be accurate the Condensed History

steps must be sufficiently short so that the straight line approach does not represent too severe an approximation. However, making the step lengths very short may cause the simulation to become extremely inefficient. EGSnrc employs electron-step algorithms that attempt to make corrections for deflections from the straight-line approach. The modified PRESTA-II algorithm is less efficient than PRESTA-I but better accounts for lateral deflections (deflections perpendicular to the initial direction of motion), and longitudinal straggling.

4.3.2. Spin effects= On

EGSnrc employs the screened Rutherford elastic scattering cross section. With spin effects turned on the correction for relativistic electron spin proposed by Mott is applied to the cross section. The effect of spin is significant below 1MeV for high-Z materials and below 100keV for low-Z materials. The physical effect of including spin is to make the effective range of electrons longer for low-Z materials and shorter for high-Z.

4.3.3. XIMAX = 0.5.

This value defines the maximum path length size before a new path is generated. It is equal to the first Goudsmit-Saunderson (GS) moment per step and is roughly half the multiple scattering angle squared.

4.3.4. ESTEPE = 0.25

Fractional energy loss per step is restricted to 25%. This is the Default value in EGSnrc. Smaller values can be used for high precision work but increase computation time.

4.3.5. Boundary crossing algorithm= PRESTA-I

One problem with the condensed history approach is that part of the electron path may be between two materials. The true electron trajectory would then be different to that simulated leading to interface artefacts. The PRESTA boundary crossing algorithm reduces the step size close to the interface between materials. No electron can take a path that is greater than the perpendicular

distance to the next boundary, unless that distance becomes less than a set value. The alternative is to use EXACT. EXACT reverts to single elastic scattering mode at the boundary between structures making the simulation less efficient.

4.3.6. Skin depth for BCA= default

This value sets the maximum perpendicular distance required by the PRESTA boundary crossing algorithm or the distance at which the simulation goes into single elastic scattering mode for the EXACT algorithm. The default is to allow the algorithm to calculate a value based on the scattering power at the electron cut of energy ECUT.

4.3.7. Global ECUT= 0.7, Global PCUT= 0.01, Global SMAX= 5

These are Global limits on the electron and photon cut off energy and step size for all calculations. Photon cut off energy has been set relatively low at 0.01 MeV (10keV) due to the need to model the effect of any low energy head scatter component on the surface dose. The electron cut off has been set at a kinetic energy of 0.7 – 0.511 = 0.189 MeV.

4.3.8. Sensitivity study

Confidence that the above parameters are appropriate was achieved through a sensitivity study. The depth dose for a 10MeV 2x2 cm field at 90cm SSD was calculated in water with different Monte Carlo transport parameters to determine the sensitivity of the accuracy and speed of the calculation to these values. The effect on simulation time and the change in the dose at a depth of 4cm, D_{4cm}, (close to R_{50} for this energy) are summarised in (see Table 4.1).

Table 4.1 Sensitivity of calculated dose and calculation time to Monte Carlo transport parameters

	Change in dose at 4cm deep	CPU time for 1E7 histories	effect on CPU time
All parameters as 4.3.1 to 4.3.7	-	418.9	-
Spin = off	-6.5%	392.3	-6.3%
XIMAX = 0.1	0.0%	487.8	16.5%
XIMAX = 1.0	0.0%	435.0	3.9%
ESTEPE = 0.05	-2.0%	520.9	24.4%
ESTEPE = 1.0	0.0%	456.3	8.9%
ECUT = 0.511	0.0%	449.0	7.2%
ECUT = 3.0	15.3%	126.9	-69.7%
PCUT =1.0	-2.7%	390.0	-6.9%
PRESTA-I electron step algorithm	-0.6%	356.7	-14.8%

With spin turned off as expected the effective range of the electrons is reduced resulting in a shift in the depth dose curve and a reduction in D_{4cm} of 6%. Variations in XIMAX or ESTEPE do not have enough of a macroscopic effect to alter the calculated dose distribution and do not have a large effect on calculation time. Reduction of ECUT down to the rest mass energy makes no change to the dose distribution with a small increase in CPU time. Conversely increasing ECUT to 3 MeV discounts enough electrons to increase the average beam energy and significantly affect the calculated depth dose. The D_{4cm} is increased by 15% compared to the reference value. Although calculation time is reduced this is clearly not acceptable. Increasing PCUT makes a small reduction in calculation time but with a small associated change in depth dose. Using the old PRESTA-I electron step algorithm reduces calculation time slightly and in this situation there is only a small change in calculated dose. However, it is known to be less accurate in some situations so it is not recommended for use.

Boundary crossing parameters only affect the dose at the junction between materials. To test them the dose was re-calculated in a phantom consisting of 1.6cm layers of water/air/water/bone/water. Results are summarised in Table 4.2 and Figure 4.2. Changing from

the PRESTA boundary crossing algorithm to the potentially more accurate EXACT algorithm had no effect on the calculated depth dose within 1SD but increased calculation time by 200%. Similarly setting the skin depth to a fixed small value (0.01mm) had no discernible effect on the depth dose but increased calculation time by 500%.

Table 4.2 Sensitivity of calculation time to Boundary Crossing algorithm

Boundary Crossing Algorithm	CPU time for 1E7 histories	effect on CPU time
PRESTA	416.6	-
EXACT	1279.3	207.1%
PRESTA Skin Depth = 0.001	2569.5	516.8%

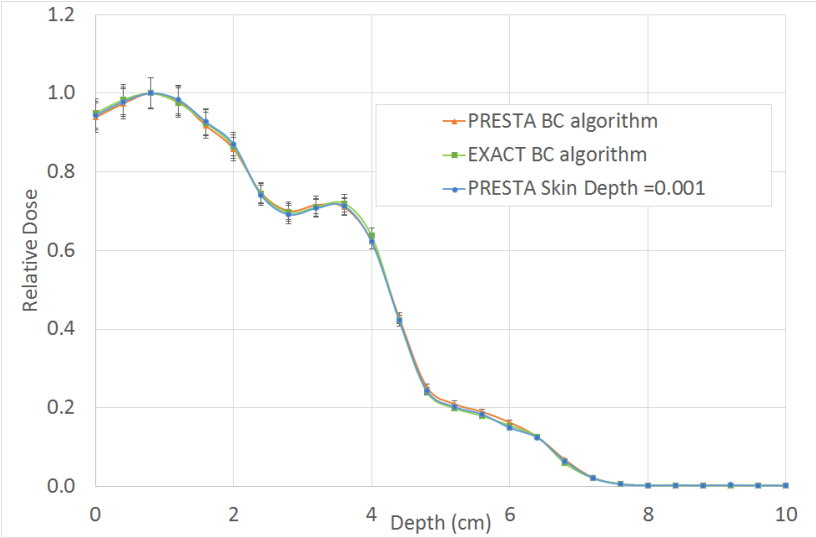

Figure 4.2 10MeV 2x2cm Monte Carlo calculated depth dose in a water/air/water/bone/water phantom with different boundary crossing algorithms

4.4. Parallel processing

The nature of the Monte Carlo dose calculation lends itself to the use of parallel processing as a method of reducing calculation time. Multiple sets of histories can be run separately as batches (with different random number seeds) and then combined at the end of the run. This is not a true parallel approach where processors communicate with each other but allows any single calculation

to spread over as many processors as are available (as long as each batch has 100+ histories, not an issue when ~10^6 histories are used). Batches have been run on either an Intel® Core™ i5-2450M CPU @2.5 GHz with two cores and hyper-threading allowing 4 batches to be run simultaneously with only minimal reduction in the speed of each batch or on the Coventry University high performance computing cluster Zeus with up to 144 nodes of Intel® Xeon® E5-4620CPU processors 8 cores per node allowing >100 batches to be run simultaneously in single submission depending on availability.

4.5. Tuning the beam model

The beam model was tuned in order to agree with measurements for the 10MeV beam investigated in Chapter 3. The primary electron source was modelled as a 1mm diameter disk of parallel electrons incident on the nickel window. The energy spectrum of the incident electrons was approximated to a Gaussian function. This creates the following four parameters that need to be iteratively adjusted until dose predictions agree with measurement.

1. Thickness of exit window
2. Mean energy of incident electron beam
3. Energy spread of incident electron beam (FWHM of Gaussian)

The simulations were run to a variance of better than 1% and the parameters varied in order to improve agreement with measurement for a 10x10cm field at 90cm SSD (see Figure 4.3 and Table 4.3).

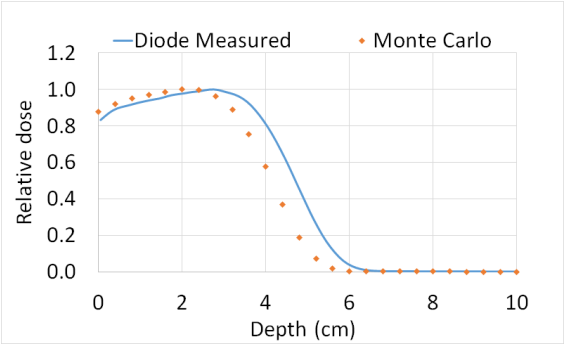

(a) 10MeV

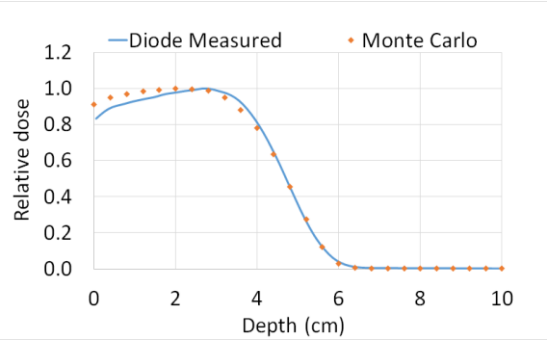

(b) Increase energy

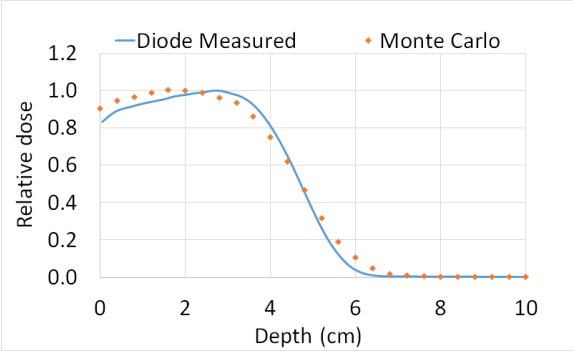

(c) broad spread of energies

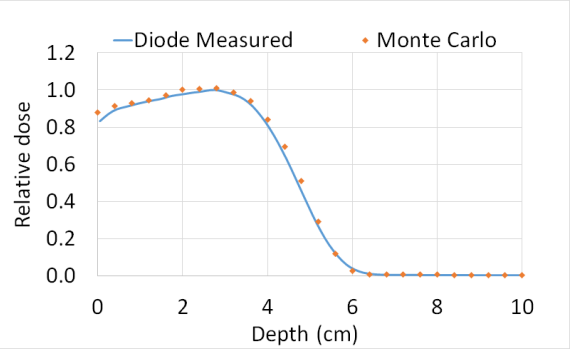

(d) monoenergetic

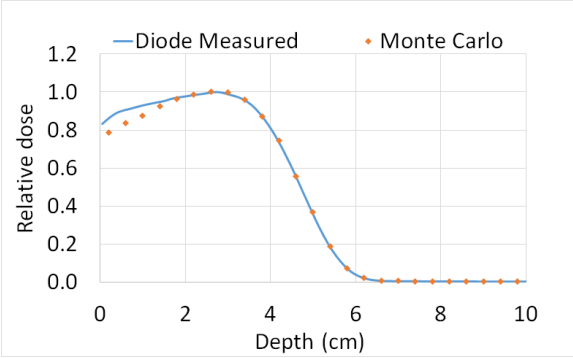

(e) correct material 0.15mm thick

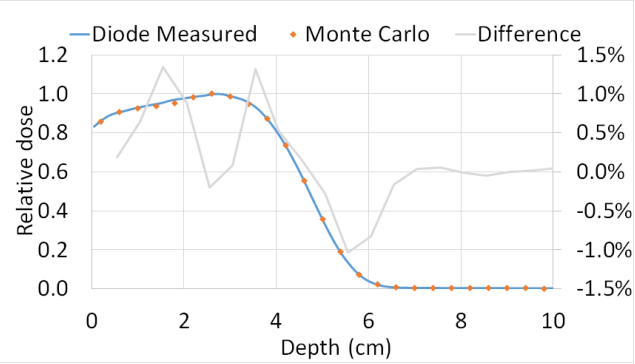

(f) final model (0.11mm thick)

Figure 4.3 10MeV Energy tuning using 10x10cm field depth dose curve at 90cm SSD. See Table 4.3 for corresponding modelling parameters.

Table 4.3 Modelling parameters for energy tuning as displayed in Figure 4.3

		Mean Energy (MeV)	FWHM (MeV)	Window Material	Window Thickness (mm)
(a)	Initial guess	10	1.5	Aluminium	0.1
(b)	Increase energy	12	1.5	Aluminium	0.1
(c)	Increase energy spread	12	3.5	Aluminium	0.1
(d)	Decrease energy spread	12	monoenergetic	Aluminium	0.1
(e)	Correct window material and optimised energy	11.7	1.2	Nickel	0.15
(f)	Optimised window thickness and energy	11.7	1.2	Nickel	0.11

With an initial guess of 10MeV mean energy and 1.5MeV FWHM and a 0.1mm aluminium exit window the penetration of the calculated depth dose falls short of the measured data (see subfigure (a)). Increasing the mean energy to 12 MeV improves the comparison but there is an overestimate of dose in the first 2cm (see subfigure (b)). Increasing the spread of energies correspondingly broadens the depth dose (see subfigure (c)) whereas a monoenergetic beam is closer to measurement (see subfigure (d)).

The Elekta technical specification for the SL series linac exit window is 99.9% purity Nickel 8.9g/cm^3 0.125mm thick. Using the correct specification for the exit window the energy was tuned to provide the beast fit to measurement. Small changes in the thickness of the window were then made to find the best fit to measurement (see subfigure (e) and (f)). Optimum agreement was found with a 0.11mm thick 8.9g/cm^3 Nickel window with Gaussian distribution with 11.7MeV mean energy and 1.2MeV FWHM. The window thickness is 0.015mm off the manufactures specification which could be due to manufacturing tolerances and impurities in the physical window but is more likely to be compensating for small inaccuracies in the electron source model.

4.6. Small fields

In Chapter 2, an electron segment size of 2x2cm was chosen. The Monte Carlo model was therefore validated for a 2x2cm field. The model was used to calculate the dose distribution for a 2x2cm field on the central axis, collimated with Jaws and MLC and this was compared to measurement. As the dose profiles exhibit a high dose gradient the gamma index analysis (Low et al., 1998) was used to compare data. A gamma analysis criteria of 1% global dose difference

(relative to maximum dose) and 1mm distance to agreement were used. Good agreement was seen between predicted and measured dose without further modification of the beam model tuned to the 10x10cm data (see Figure 4.4). Gamma index was less than 1 for most points and less than 1.2 for all (see Figure 4.4 sub-figure (b) and (c)).

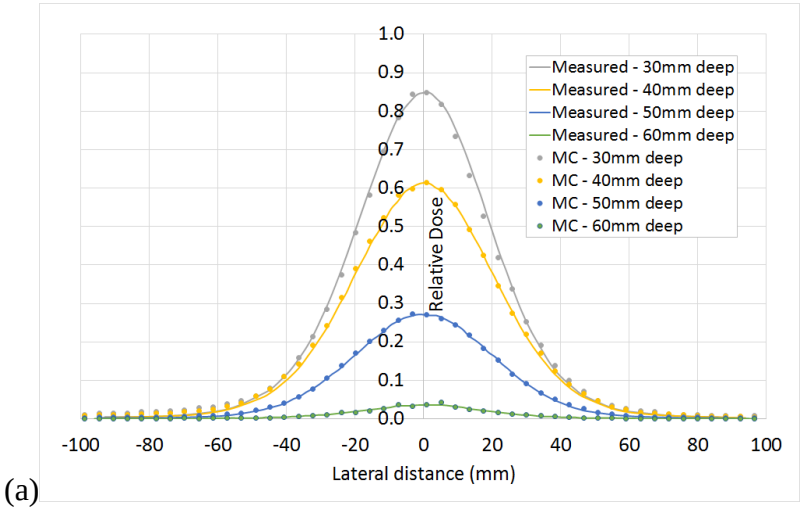

(a)

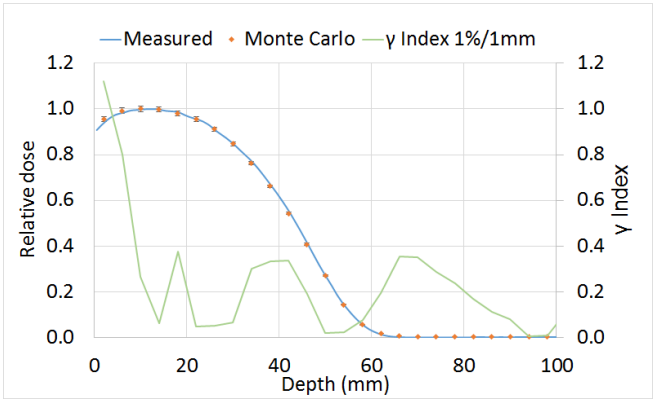

(b)

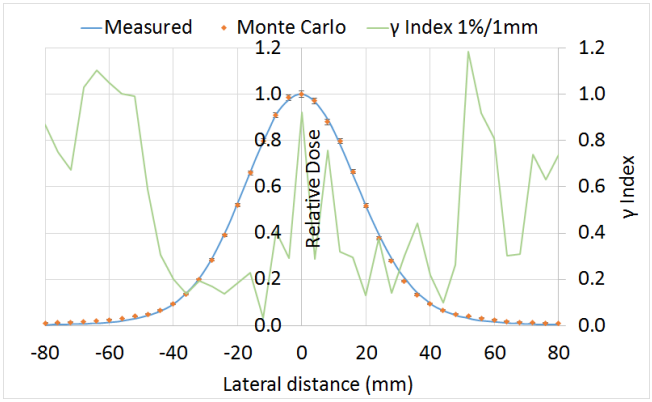

(c)

Figure 4.4 Comparison of measured and Monte Carlo calculated dose for a 2x2cm field at 90cm SSD, (a) profiles at 4 depths, (b) detail of depth dose and (c) detail of profile at 3cm deep both with error bars from Monte Carlo variance and gamma index overlaid in green.

Although not all potential segments position were validated a single offset segment was investigated by calculating the dose for a field offset from the central axis by 6cm and comparing to measurement. Similarly good agreement was seen for the offset field.

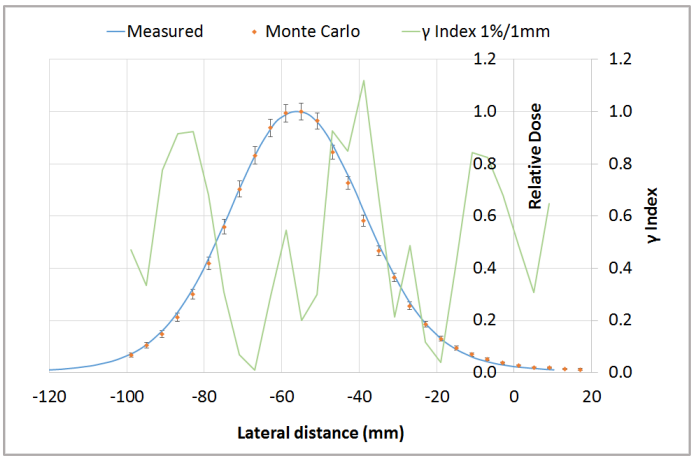

Figure 4.5 Comparison of measured and Monte Carlo calculated dose for a 2x2cm field at 90cm SSD 3cm deep offset from the central axis by 6cm in the A-B direction (offset defined at 100cm SSD). Error bars from Monte Carlo variance and gamma index overlaid in green.

4.7. SSD

Variations in SSD will result in dosimetric effects due to changes in the volume of air between the linac and the patient as well the divergence of the electron beam. Air is correctly accounted for in the Monte Carlo model as ICRU air with a density of 1.20E-3 g/cm^3. By changing the distance between the phase space file and the phantom surface, the SSD and the volume of air the electron beam passes through should change correspondingly. This was tested by recalculating the 90cm SSD 10MeV data with the phase space source moved to simulate 80cm SSD.

Good agreement was seen between Monte Carlo and the measured data at 80cm SSD suggesting that the corresponding variation in scatter of the beam are correctly modelled (see Figure 4.6)

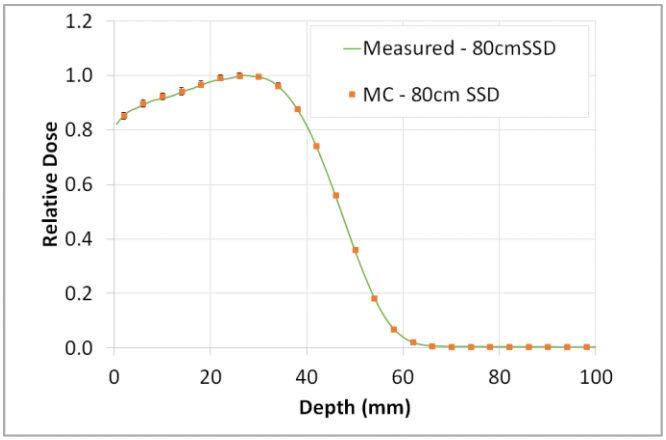

Figure 4.6 Comparison of measured and Monte Carlo calculated depth dose curves for a 10x10cm field at 80cm SSD.

4.8. Energy

Additional energy modes for use with treatment planning studies have been created by modifying the validated 10MeV beam model. A total of three energies have been chosen from the clinical energies available at UHCW. Energies between 4MeV and 15MeV are available but 4MeV is likely to be too low to be of use. A 6MeV and 15MeV model have been created alongside 10MeV providing a range in half value depth (R_{50}) of between 2.8 and 6.6cm. Energies have been modelled by shifting the mean energy of the source energy spectrum and altering the FWHM to match measured 10x10cm percentage depth dose at 90cm SSD with scattering foils removed collimated by MLC and jaws (see Figure 4.7).

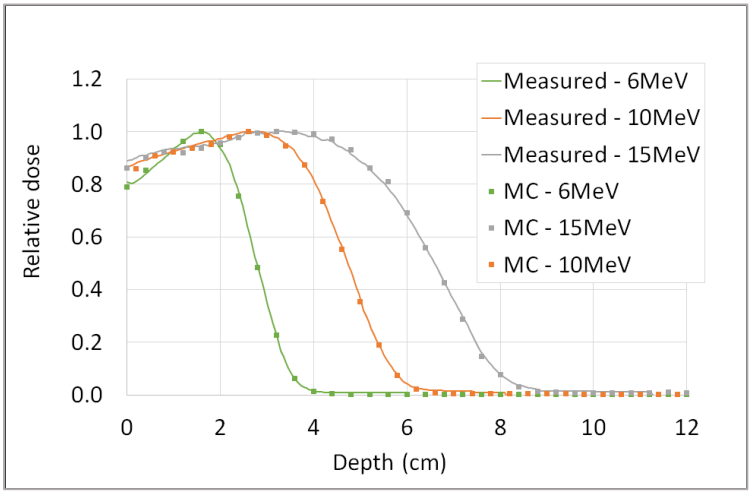

Figure 4.7 comparison of measured and Monte Carlo calculated dose for a 10x10cm field at 90cm SSD 6MeV, 10MeV and 15MeV.

4.9. CT calibration

In Chapter 5, dose will be calculated in geometries of unity density but for the clinical evaluation of Chapter 6 dose will be calculated using geometries generated from patient CT (X-ray computed tomography) data. When a CT scan is taken X-ray images from multiple angles are back projected to build a cross sectional picture of the inside of the patient in that position. Cross sections at multiple positions are taken to form the CT data set which can then be reconstructed into a three dimension image of the patient. For each voxel of the image a grey scale value equal to the Hounsfield unit (HU) is calculated describing the attenuation of X-rays relative to water at that point in the patient. For deterministic dose calculations all that is required is to convert this HU to the electron density of the material. For water like materials there is a linear relationship between electron density and HU. When bone like materials are included there is an increase in attenuation due to the photoelectric effect and the relationship becomes two hinged straight lines. This relationship can be defined by scanning materials of known electron density and building an electron density calibration curve.

For the Monte Carlo dose calculation material composition as well as the physical density are required to determine the correct interaction cross sections. The Monte Carlo dose calculation therefore requires a calibration between HU unit material and density. This calibration has been achieved using the DOSXYZnrc CTcreate utility with a ramp function as described by (Kawrakow et al., 1996). The ramp function has been modified for the CT scanner used for patient scans via the electron density calibration phantom dataset (see Figure 4.8).

The HU for air is by definition -1000. However, many CT image voxels in air will have a HU value that is higher or lower than -1000 due to image noise and non-uniformity. For the purposes of this study it is important that voxels are recognised as air and not defaulted to vacuum or assigned to lung material in error. To encompass all voxels with a value of -1000 ±10% the HU range for ICRUair was set at -1100 to -900. The density of ICRUair was set to 1.19E-3 g/cm^3 at -1100 HU and 1.21E-3 g/cm^3 at -900 HU to result in an interpolated density of 1.20E-3 g/cm^3 at -1000 HU. The small (less than 1%) variation in air density with HU was included as the CTcreate utility cannot perform the interpolation when identical HU values are used.

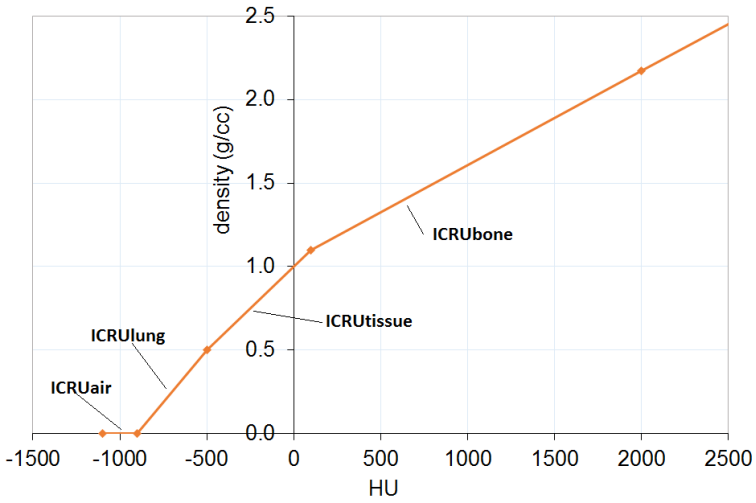

Figure 4.8 CT calibration curve for Monte Carlo dose calculations

4.10. Conclusions

This chapter has described the development of the electron Monte Carlo beam model for use in the studies in Chapter 5 and Chapter 6. In doing so, it has been shown that small scattering foil free electron segments collimated with jaws and MLC at 90cm SSD can be accurately calculated with Monte Carlo dose calculation. Note, however, that creating a clinical beam model would require additional work to validated dose calculations in inhomogeneous media and with variations in obliquity as well as calibration of output (IAEA, 2004, Hu et al., 2008, Smilowitz et al., 2015).

Chapter 5

Optimisation

5.1. Introduction

Having determined that the delivery of xMLC shaped scattering foil free electron segments is feasible (Chapter 3), this chapter exploits the accurate dose calculation algorithm developed in Chapter 4 to optimise the combined electron and X-ray photon (exIMRT) spatial dose distribution. The chapter starts with a description of the problem formulation including the optimisation methods investigated. This is followed by simulation studies to investigate the interaction of electron segments. These studies include investigation of the most appropriate dimension and separation of segments to deduce the number of free variables in the optimisation problem. This is followed by a comparison between both deterministic and heuristic search strategies. The overall optimisation approach developed in this work is then presented and its performance evaluated on appropriate test cases.

In a real situation such as the optimisation of radiotherapy dose distributions, the solution will be only as good as the formulation of the optimisation problem. Although the development of the optimisation approach is presented as a linear narrative in this chapter, some iteration was required due to the interdependence between defining an effective objective function and identifying a suitable solver.

5.2. Problem formulation

To be in a position to solve the problem of optimising the exIMRT dose distribution it is necessary to first ensure that the problem is well defined and understood before formulating it in such a way as to be able to use computational techniques to solve it.

5.2.1. Limitations and assumptions

As detailed in Chapter 2 current solutions to the optimisation of IMRT dose distributions can generally be split into two distinct methodologies, sequential optimisation and direct aperture optimisation (DAO). For this study beamlet based optimisation equivalent to the first stage of sequential optimisation is used. It is noted that the required conversion of the idealised X-ray intensity map resulting from the beamlet weight optimisation into a deliverable segmented field is not implemented. This approximation will however be considered when comparing calculated dose distributions with 'segmented' plans from commercial treatment planning systems (Chapter 6). Such limitation does not however apply fully to the electron components. Indeed, whilst the overall electron segmentation has not been implemented, each 2x2cm segment, that, when combined together, form the overall electron component, is practically deliverable.

Automated selection of beam angles is feasible (Chapter 2) but is not in the scope of this work. Similar to standard current clinical practice, beam angles have been optimised through trial and error guided by the experience of the investigator.

The only constraint imposed is that the beamlet weights must be positive. The requirements in terms of goals are expressed within the objectives such that the cost resulting from an objective met would be minimum.

5.2.2. Constrained minimisation problem

The optimisation problem can be formulated as:

$$\min_{x} F(x) \tag{5.1}$$

$$subject\ to: x \geq 0$$

where x is a vector of the electron segment weights and the X-ray beamlet weights that form the problem variables for the cost function $F(x)$.

To complete the problem formulation a set of dose objectives need to be defined and the cost function must be formulated in such a way to enable the dose objectives to be met. In this work, consideration is given to the so called weighted sum approach using quadratic cost function of the form given in equation 5.2:

$$minF(x) = min \sum_{k=1}^{K} \sum_{o=1}^{O_k} w_{k,o} f_{k,o}(d_k(x)) \tag{5.2}$$

where, k =1 to K represents the set of structures defined by the user; o=1 to O_k represents the number of objectives per structure k and $d_k(x)$=A_k x is the calculated dose where A_k is the influence matrix for each structure and x is a vector containing the electron segment weights and X-ray photon beamlet weights. For each structure k, one or more objectives $f_{k,o}\left(d_k(x)\right)$ are defined to contribute to the total objective function. A user input weighting, $w_{k,o}$, is defined for each objective. The weighting is adjusted, based on clinical requirements, to tune the overall cost function. Such formulation is applicable to the MERT, IMRT and exIMRT problems detailed in the following sections.

Although methods for solving IMRT optimisation problems are well documented (see Chapter 2) the addition of electrons to the IMRT plan introduces an additional level of complexity. The dependence of the dose distribution on the modality and energy of the beam as well as the intensity may lead to a non-convex problem with local minima. Different approaches to optimisation of the exIMRT problem have therefore been considered.

5.3. Methods

5.3.1. Radiotherapy treatment planning environment

The CERR environment (Deasy et al., 2003) was used as a framework for this study. CERR (Computational Environment for Radiotherapy Research) is a software platform created by Washington University St-Louis for developing and sharing research in radiotherapy treatment planning. CERR is able to display medical images, display and manipulate calculated dose, calculate dose metrics and calculate X-ray dose for IMRT research. Using a platform such as CERR removes the need to reproduce these tools as part of this study. CERR is written in MATLAB allowing efficient integration with MATLAB's optimisation toolboxes as well as allowing additional functionality to be added simply by creating a new function in MATLAB.

The photon dose component of the exIMRT beam has been calculated using the QIB pencil beam algorithm using the method of Ahnesjö (Ahnesjö et al., 1992). This dose calculations forms part of CERR and has been validated and used in a number of studies including (Sayre and Ruan, 2013, Craft et al., 2014, Salari and Unkelbach, 2013, Rocha et al., 2012, Unkelbach et al., 2014). There are limitation to the accuracy of the QIB dose calculation and these are discussed in Chapter 6. A nominal 6MV energy X-ray dose calculation has been used with 4mm square beamlets. CERR was run on an Intel Core i5-2450M CPU.

5.3.2. Optimisation solvers

A simple approach to optimising the dose distribution is to select segment weights to minimise the difference between the calculated and desired dose. This approach has been taken from the CERR optimisation example (Deasy, 2005) and used initially as a way to investigate the combining of multiple electron segments. It was later incorporated into the final two stage algorithm (see Section 5.5.4). A description of this approach follows.

The desired dose D_k^{aim} and a weighting w_k is defined for each structure. The difference between the desired dose and the calculated dose $d_{k,n}(x)$ is determined for each voxel n of each structure k. The square of this value is summed over all N_k voxels of each structure to use as the objective $f(x)$ in equation 5.2. The problem becomes one of finding a solution for x to minimise this function:

$$f_k(d(x)) = \sum_{n=1}^{N_k} \left(d_{k,n}(x) - {D_k}^{aim}\right)^2 \tag{5.3}$$

As this is a quadratic objective with linear constraints ($x \geq 0$), $f(x)$ can be expressed in matrix notation and the problem re-written as:

$$f(x) = \frac{1}{2}x^T Hx + f^T \tag{5.4}$$

$$H = wA^T A$$

$$f = -wD^{aim} A$$

where x is a vector containing the electron segment weights, w is the weighting factor, D^{aim} is the desired dose and A is the influence matrix. Such equation can be solved by quadratic programming using the MATLAB quadprog trust-region-reflective solver (Coleman and Li, 2006).

Alternative solutions to minimising the more complex weighted sum cost functions have been investigated as part of this study. Methods that use the gradient of the function to define the search direction are more efficient at finding the optimal solution than line search or trust region methods. As a bounded non-linear multivariable problem the natural choice from the MATLAB optimisation toolbox is the fmincon gradient-based optimisation with either the interior-point or sequential-quadratic programming (SQP) solvers. The interior point algorithm (Karmarkar, 1984) uses a barrier function to define a feasible region and reaches a solution by traversing the interior of a this feasible region. The SQP solver expands the problem to a sequence of optimisation sub problems, each of which optimises a quadratic model of the objective subject to a linearisation of the constraints.

A set of solvers that do not rely on the quadratic formulation of the objectives was also investigated. Whilst any type of objective formulation could be adopted, for the purpose of comparison the same quadratic cost function was used with all the solvers investigated.

The simplex search algorithm (Nelder and Mead, 1965) implemented in the 'fminsearch' function is a direct search method that does not use numerical or analytic gradients.

Three algorithms inspired by nature were also investigated, namely genetic algorithm, particle swarm optimisation (PSO) and firefly optimisation.

Genetic algorithms are metaheuristic algorithms inspired by the process of natural selection. Populations of candidate solutions undergo random mutations and crossover between populations. During each successive generation, a proportion of the existing population is selected to breed a new generation.

PSO attempts to solve the problem by moving populations of candidate solution, dubbed particles, around the search space. Each particle movement is governed by its local best known position but also the best know position found by other particles.

The Firefly algorithm is a modification of the PSO algorithm where the attractiveness of two particles is now proportional to the distance between them. Details of the metaheuristic algorithms investigated and the parameter used are given in Appendix A.

5.3.3. Common set up for optimisation solvers

The common algorithms parameters defined to help the comparison between algorithms were: normalisation of problem, starting value of x, normalisation of the cost function value, termination tolerance on change in function value, termination tolerance on step size and maximum number of iterations or maximum number of function evaluation. Given incorrect parameters the function might either give an inaccurate result or fail to recognise when it has converged. The problem was normalised by dividing the prescribed dose by the median dose of a single segment/beamlet and the total number of segments/beamlets. Given this normalisation an appropriate starting value for x is: x=1. Using this starting value the optimisation function was evaluated and normalised to give a value of $F(x)$=10 for x=1. The termination tolerance on the change in function $F(x)$ (TolFun) and the termination tolerance on step size (TolX) were set at 1.0e-08 and 1.0e-10 respectively. For functions that fail to converge within these criteria a maximum number of function evaluation of 80000 was set. A value of 80000 was chosen based on the number of function evaluations the simplex search method required to begin to approach a minimum and terminate on TolFun. If solvers did not approach a minimum value in the same time as the simplex search method then it was decided to discount them as being too inefficient. The actual time taken for optimisation depends slightly on the algorithm but 80000 iterations for this problem corresponds to approximately 6 hrs running time.

5.3.4. Phantoms used to evaluate the approach

Two different software phantoms with unit density were created to evaluate the principle prior to validating the approach using clinical case studies.

The first software phantom was a 20cm cube developed to evaluate the electron only (MERT) optimisation, (see section 5.4). It included the following target shapes:

- A slab placed close to the depth of maximum dose at 2cm deep to evaluate the impact of the electron segment location and size as well as gaps between segments on field penumbra and flatness.
- A stepped target to assess the capability of the algorithms to realise depth modulation for a simple plan geometry. Three steps were selected to correspond to the 90% dose level for 6, 10 and 15MeV respectively.
- A slab at depth modified to create shapes similar to those described in TR430 (IAEA, 2004). An asymmetric oval, a 'C' shape and a triangle, all approximately 7.5 by 7.5cm, were designed to evaluate the ability to modulate the intensity in two dimensions.

The second phantom was a 20 cm diameter cylinder created to develop and test the combined electron and photon exIMRT method, (see section 5.5). The target and OAR geometry aimed to approximate to a clinical situation (see Figure 5.1). The phantom includes a concave PTV which follows the cylinder outline with 5mm between the PTV and the surface. The PTV wraps around a 2 cm diameter OAR, denoted OAR_{high}. Two additional OARs, denoted OAR_{med} and OAR_{low} are located at increasing depth in the patient, each separated by 2cm. The PTV and OARs were designed to evaluate the ability of the procedure to produce conformal treatments. A large volume structure, labelled 'distal', was realised to monitor the low dose wash away from the PTV.

The PTV has been edited back from the surface of the phantom to leave a 5mm gap between the surface and the PTV. As explained in Chapter 1 both the X-ray dose distribution, and to a much lesser extent the electron dose distribution, exhibit a region of build-up at the surface of the patient. If the PTV were to extend to the surface this could cause problems. First, because it is difficult to achieve the required dose in the region close to the surface the optimiser might fail to converge. Second, in attempting to optimise the dose distribution in the region close to the surface the algorithm might create peaks in the X-ray dose fluence to push the dose up in this region (ICRU83, 2010). The PTV exists to ensure dose coverage of the CTV in the presence of set up errors and patient movement. A high skin dose may therefore not actually be required. Peaks in the fluence distribution may also result in hot spots in the dose distribution when movement is taken into

account. One option is to simply edit the PTV away from the surface of the patient by a few mm (James et al., 2008) and this is the approach simulated here.

It should be noted that editing the PTV in a clinical situation does reduce the robustness of the plan to set up errors and patient movement. In a clinical situation if the PTV extends close to or beyond the surface, but a high skin dose is undesirable, then virtual bolus can be used to provide a so called 'flash margin'. The virtual bolus is added in the planning system for the process of optimisation but then removed for the final dose calculation. Alternatively if the CTV itself extends close to the surface of the patient then a layer of real bolus can be used to provide build-up. It is possible that the higher surface dose of the exIMRT electron component could be used to negate the need for bolus in some situations. However comparisons of surface dose have not been included in this study as the accuracy of the X-ray dose calculation in the build-up region has not been verified and it is recognised that most dose calculation algorithms cannot accurately calculate dose in the build-up region (ICRU83, 2010).

A prescribed dose of 60 Gy and a maximum OAR_{high} dose of 45 Gy were chosen to mimic a typical PTV/OAR relationship. Specific dose objectives were defined as shown in Figure 5.1. A PTV target of at least 95% of the volume to 95% of the prescribed dose and less than 5% of the volume to 105% of the prescribed dose was used as simplistic analogy to clinical dose volume objectives. Clinically these target dose objectives are occasionally used exclusively (for example breast radiotherapy) but are typically used in combination with the ICRU83 (ICRU83, 2010) recommended values for reporting near-minimum, $D_{98\%}$, and near-maximum, $D_{2\%,}$ or similar. For example dose objectives of 98% of the volume to >90% dose and <2% of the volume to >107% dose as well as 95% volume to >95% dose and <5% volume to >105%. Although it is convenient to use a single minimum and maximum dose constraint in order to develop the technique, it should be noted that as a result there may me small areas of the target with clinically unacceptable dose coverage or small unacceptable hot spots. Clinically approved dose objectives, in use at UHCW, have been used for the treatment plan comparisons of Chapter 6.

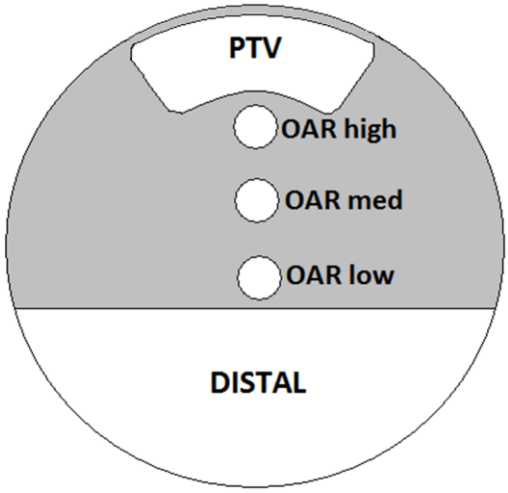

Dose objectives
PTV
>95% volume to 57Gy 50% volume to 60Gy <5% volume to 63Gy
OAR_{high} <45Gy
OAR_{med}, OAR_{low} & DISTAL as low as possible

Figure 5.1 Cylindrical software phantom to test exIMRT optimisation

5.4. MERT

5.4.1. MERT Introduction

Although optimisation of photon IMRT is well established the optimisation of electron beams is not and the optimisation of the combined exIMRT dose distribution even less so. This section will address optimisation of the electron (MERT) dose component and examine what is achievable using the xMLC collimated scattering foil free electron segments before moving onto exIMRT in the next section.

5.4.2. Electron matrix resolution

This study adopts the 2x2cm electron segment size that was chosen based on measurement in Chapter 2 and calculated using Monte Carlo in Chapter 3. Ideally, the location of each 2x2 cm field on the position matrix would not be constrained such that the spacing and overlap of segments formed part of the optimisation. However, this is computationally difficult and it would be much simpler to have the segments arranged on a predefined position matrix. For this study a fixed position matrix has been used but the resolution of this matrix has been considered. With a regular 2cm square matrix each segment is abutting to the next. Increasing the matrix resolution would allow more control over the overlap of segments and the gaps between segments to create a 'feathering' effect. This is analogous to Gaussian edge feathering for abutting open electron fields

of dissimilar energy which has been shown to improve uniformity of dose in the PTV by up to 33% (Eley et al., 2011). Increasing the matrix resolution would however have the negative effect of increasing the number of variables and therefore computation time. For each energy, a 10x10cm field with 2cm spacing would consist of 25 electron segments but reducing the spacing to 0.5cm would increase the number of electron segments to 400.

Determining the optimum resolution of this position matrix is perhaps not trivial. For X-ray photon IMRT it is assumed that the dose contribution outside the edge of the beamlet is small and beamlets are arranged abutting each other on a regular matrix. However, for electron segments the geometric field size is not maintained and the dose contribution from beyond the shadow of the jaw opening is just as important as that inside. This is demonstrated with two 10MeV 2x2cm segments in Figure 5.2. Two segments side by side create a single larger Gaussian dose distribution with a match plane that happens to fall at the 85% isodose at 2cm deep (see sub-figure (a)). In fact in this situation a more uniform distribution could be obtained with a 1cm or even 2cm gap between segments (see sub-figures (b) and (c)). An alternative could be to separate the segments and attempt to match each segment according to the fifty percent isodose (see sub-figure (d)). However, this does not appear to hold any intrinsic advantage.

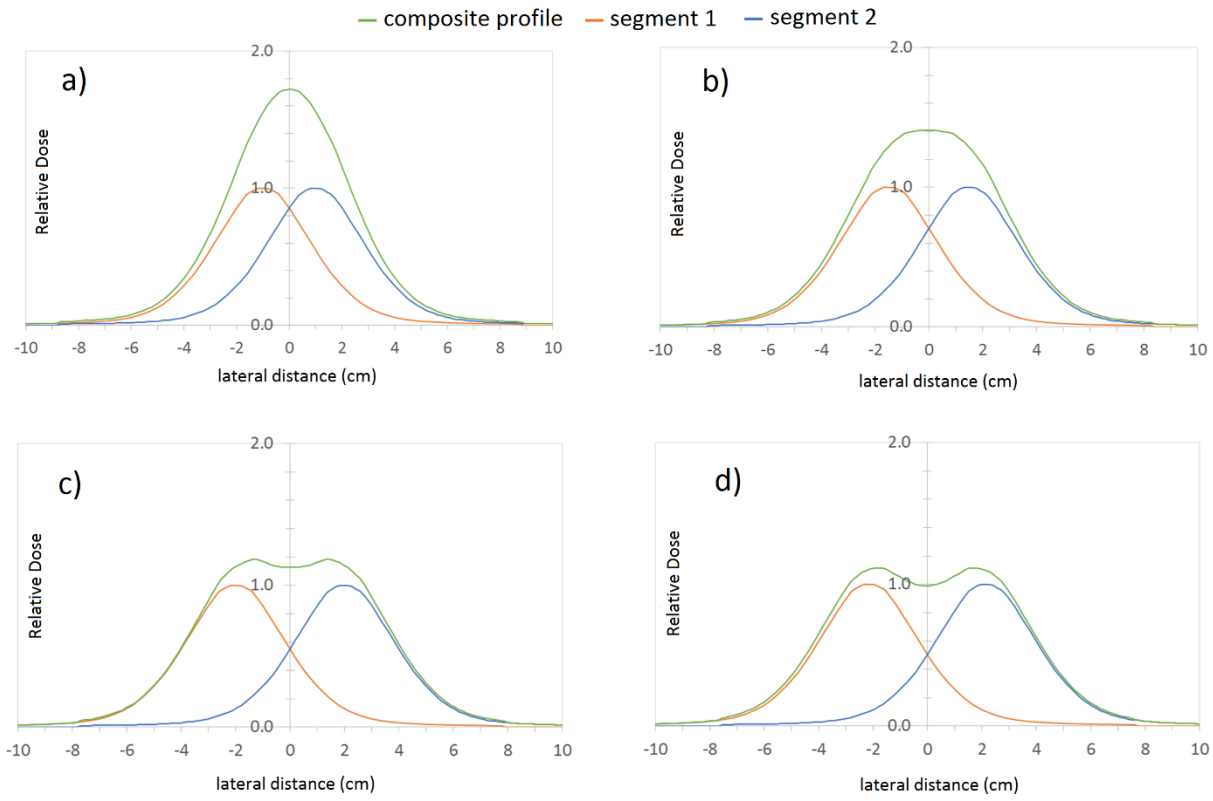

Figure 5.2 Matching of two 90cm SSD 10MeV 2cm segments at 2cm deep a) no gap, b) 1cm gap, c) 2cm gap and d) matched to 50% isodose (gap size defined at isocentre).

There are advantages to reducing the size of the position matrix to allow a finer resolution. A smaller position matrix would allow for more precise positioning of the effective field edges. In the example of two 10MeV 2x2cm fields there is a difference in the 50% widths between having no gap between segments and a 2cm gap between segments of 14 mm (see Figure 5.3). This could lead to an error of up to ±7mm if the PTV edge lies between these two points. With a 1 cm resolution a 1cm gap is possible which would reduce the potential error to ±3.5mm in this case at this particular depth.

This demonstration with just two electron segments suggests that there are potential advantages to increasing the resolution of the 2x2cm electron segment position matrix by reducing the spacing of segments. Intensity and energy modulation of the electron field will therefore be tested with 0.5mm and 1cm spacing alongside 2cm spacing to allow greater control over gaps and positioning of the field edge.

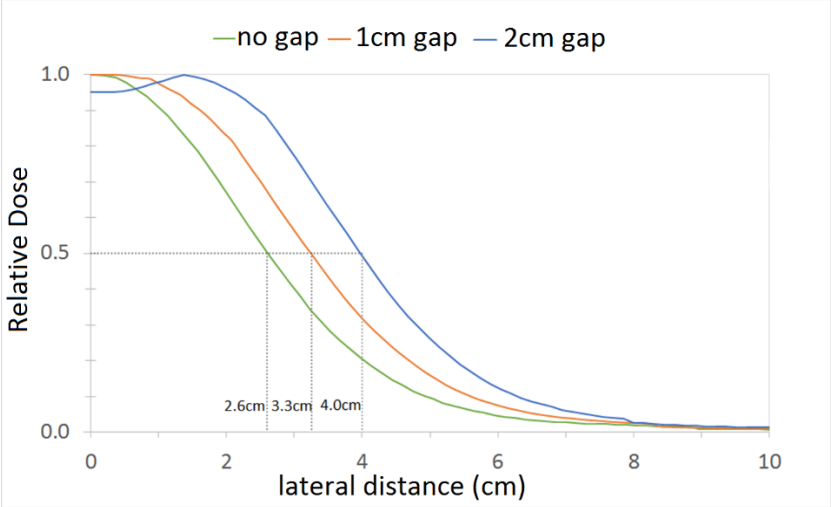

Figure 5.3 Matching of two 90cm SSD 10MeV 2cm beamlets at 2cm deep. Field edge position with gap (gap size defined at isocentre).

5.4.3. Electron intensity modulation

Intensity modulation of the electron field will be achieved through optimisation of the electron segment weights. One of the greatest challenges of combining multiple electron fields is to do so without creating hot and cold spots. This section will start by attempting to create a uniform field through modulation.

The achievable uniformity of a 10x10cm 10MeV field was determined by optimising dose to a slab placed close to the depth of maximum dose at 2cm deep. The profiles for the composite optimised fields have been evaluated for flatness, defined as the ratio of the maximum and minimum dose in the central 8cm of the 10cm wide field (IEC, 1989). Maximum and minimum dose have been used rather than reference to the central axis as this may not be relevant for the modulated field.

By modulating the weights of a 5x5 matrix of 2x2cm segments for 10MeV at 2 cm deep a uniform field in the high dose region can be achieved (see Figure 5.4 and Table 5.1). Within the central 8cm of the field, the flatness of the optimised profile is similar to a clinical electron field delivered with a 10x10cm applicator at the surface. Compared to the non-optimised field (all weights =1) the flatness is improved from a value of 1.46 to 1.11. As expected there is an increase in dose outside the field edge with penumbra width increasing by 1.7cm.

Due to the dependence of lateral scatter on energy there is a reduced penumbra width at 15MeV and an increase at 6MeV when compared to 10MeV. However, the achievable flatness within the 8 cm area is similar for all energies (1.09, 1.11 and 1.11 for 6MeV, 10MeV and 15MeV respectively).

There is an improvement in both flatness and penumbra width moving from 90cm SSD to 80cm SSD demonstrating that minimising SSD where possible is advantageous.

Using an increased resolution position matrix creates only a small improvement in field flatness for 10MeV at depth with 1.08 and 1.11 flatness for a 0.5cm spacing and a 2cm spacing respectively.

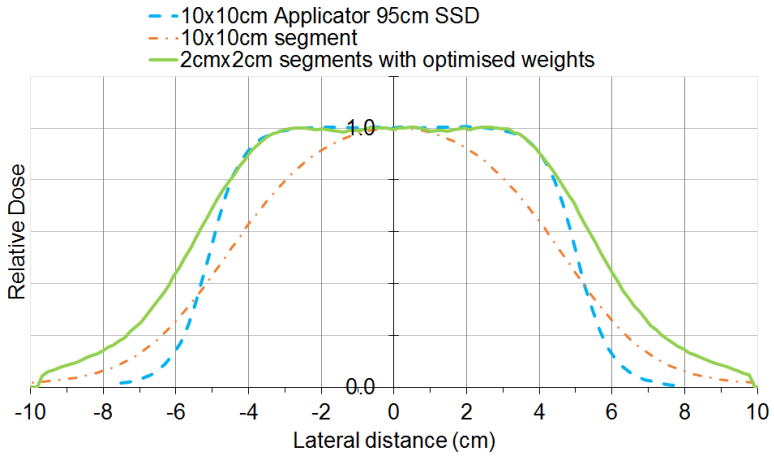

Figure 5.4 Intensity modulation to create a flat dose distribution. Calculated profile for a 5x5 matrix of 2cm electron segments optimised for uniformity at 2cm depth 90cm SSD 10MeV electron beam compared to measured 10MeV 10x10 field collimated with jaws and MLC and a measured clinical 10MeV field collimated with a 10x10cm applicator at the water surface also at 2cm deep

The profile for individual segments as well as the combined dose profile is given in Figure 5.5 for 6, 10 and 15MeV. Examining the optimised segments weights for 10MeV reveals that at some points the optimiser will choose to leave a gap between segments. This can be seen in subfigure (b) where only three out of the 5 segments across the midline contribute to the composite dose. As penumbra width will depend on energy so will the matching of segments. In subfigure (a) the central segment weight is reduced for 6 MeV compared to 10 MeV and in subfigure (c) there is a small contribution from all 5 segments for 15 MeV.

Table 5.1 Calculated field penumbra width and flatness for a modulated and un-modulated electron beam at 2cm deep (2cm segment spacing unless stated)

	Energy	SSD	80-20% width (cm)	Flatness (max/min)
10x10 Applicator	10MeV	95	1.18	1.08
10x10 MLC		90	3.38	1.55
Composite 2x2cm (all weights=1)		90	3.30	1.46
Composite 2x2cm Optimised		90	2.83	1.11
Composite 2x2cm Optimised – 1cm spacing		90	2.79	1.09
Composite 2x2cm Optimised – 0.5cm spacing		90	2.79	1.08
Composite 2x2cm Optimised		80	2.48	1.06
Composite 2x2cm Optimised	6MeV	90	3.47	1.09
Composite 2x2cm Optimised	15MeV	90	2.26	1.11

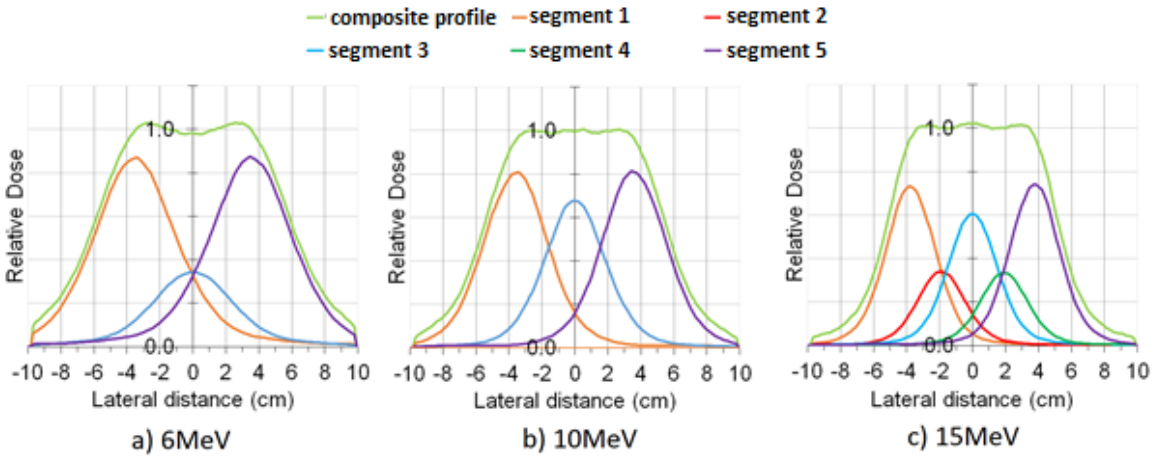

Figure 5.5 The effect of energy on the segment weighting required to produce a flat field. Composite profiles and the constituent segments for a) 6MeV, b) 10MeV, and c) 15MeV at 90cm SSD 1.5cm, 2cm and 3.0cm deep respectively. The optimisation leads to segment 2 and 4 having zero weighting for 6MeV and 10MeV. Composite profile is for a 2d matrix so also includes a contribution from segments not in this plane.

Intensity modulation to conform dose in two dimensions was tested by optimising dose to the structures defined in section 5.3.4. 10MeV electron segments were optimised to conform dose to the three distinct shapes, namely the asymmetric oval, the 'C' shape and the triangle. Conformity of the dose distributions is limited by the penumbra width of the electron segments but target

coverage to 95% of the volume with the 95% isodose was achievable with some shaping of the surrounding isodose distributions with the highest dose limited to 110% (see Figure 5.6).

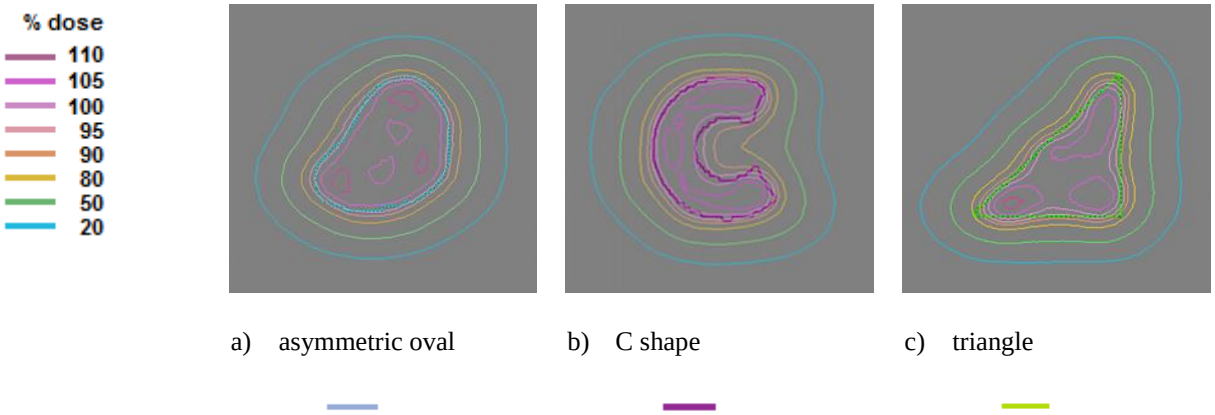

Figure 5.6 Intensity modulation of segments to conform dose to 2D shapes as seen from the beams eye view. 90cm SSD 10MeV 2cm deep.

5.4.4. Electron energy modulation

The use of multiple energies is potentially advantageous as this will allow true depth modulation. However combining multiple energies is problematic due to the matching of dissimilar penumbra widths (see Chapter 2).

Some improvement to dose distributions with multiple energies can be made with the use of gaps as described in 5.4.2 and by weighting of energies relative to each other. In Figure 5.7 it is shown how by abutting a 6 MeV field to a 15 MeV field increases the maximum dose to 140% of the 15 MeV only value due to the overlap of the larger penumbra width. Removing one 6 MeV segment to create a 2cm gap reduces the maximum dose back to 100% but reduces dose on the 6 MeV side of the distribution. The situation can be improved by manually increasing the weight of the remaining 6 MeV segment by a factor of 1.08 to improve the uniformity of dose distribution whilst limiting the maximum dose to 110%.

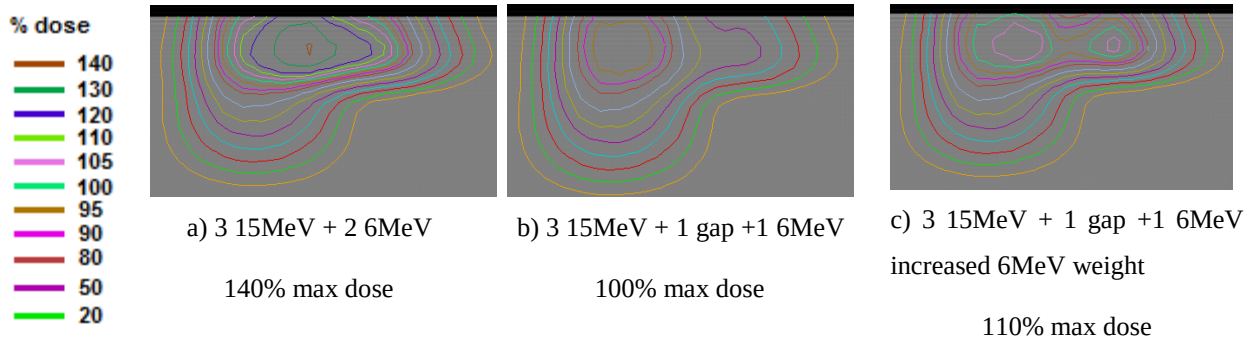

Figure 5.7 Isodose lines for abutting segments of dissimilar energy without optimisation. Without a gap, with a 2cm gap and with a 2cm gap and manual increase of the 6MeV segment weight.

There are two options, defined in this work as 'range selection' and 'free optimisation' to automatically optimise the electron energy. Range selection determines the energy at each position based on the depth of the target and the electron energy range. Free optimisation enables the optimiser to choose the energy based on the cost function to be minimised.

To test the electron energy optimisation methods, segments were optimised to conform dose to a stepped PTV while minimising dose to a similarly stepped OAR. For range selection the energy at each step was limited to the energy corresponding to 90% dose at the PTV depth (where the step depths are set such that this is the case for three energies used). For free optimisation 6, 10 and 15MeV segments were allowed at all positions and no preference was built into the optimisation. The results for both range selection and free optimisation are shown in Figure 5.8 and Table 5.2.

The resulting electron weights are shown as a relative intensity map in Figure 5.9. As expected the optimum solution for both range selection and free optimisation contains gaps between the segments. In particular the column of 6 MeV segments abutting to 10 MeV segments has zero weight with both methods. Free optimisation produces a much more uniform dose distribution within the PTV. This is achieved partly by mixing of enegies (energy modulation) and partly by choosing 15 MeV over 10 MeV in much of central part of the PTV. This does have the negative effect of increasing OAR dose for free optimisation compared to range selection. In a clinical situation the improved target dose uniformity would be adventageouse as long as the clinical OAR dose objectives were met. Free optimisation will therefore be used for the exIMRT study.

As in 5.5.3 there is little or no improvement in either uniformity or OAR dose by increasing the resolution of the position matrix. Compared to a 2cm spacing, with a 0.5mm spacing maximum dose is reduced from 111.7 to 110.2 % of the mean dose and minimum dose is increased from 72.0% to 72.6% of the mean dose. This suggests that the benfits of increased resolution for segmented electron fields is small compared to the application of feathering to the edge of open electron fields. Increased resolution therefore unnecessarily increases calculation time for the optimisation procedure so will not be used for the exIMRT study.

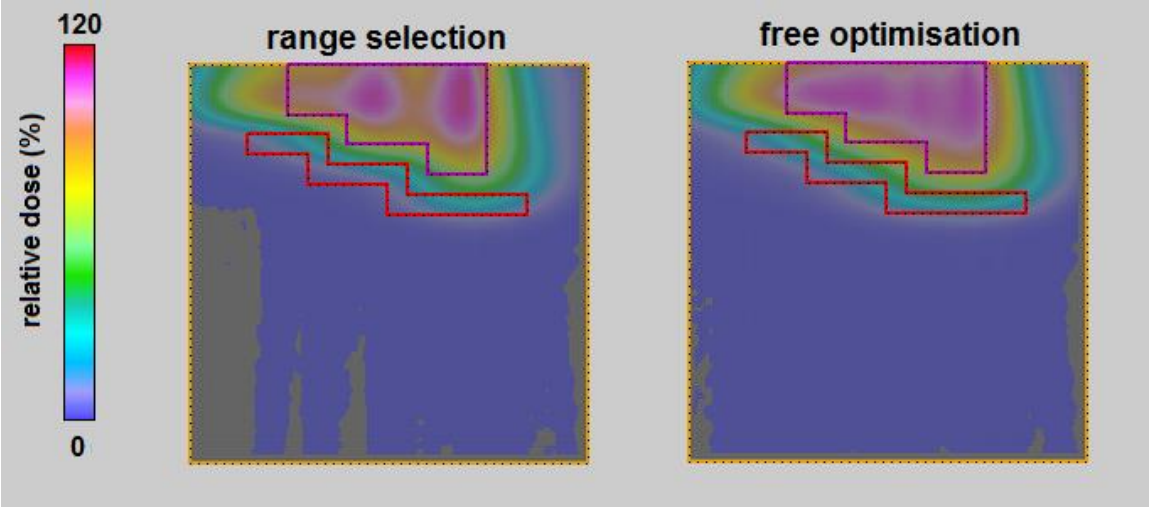

Figure 5.8 Dose distribution for a stepped PTV used to demonstrate energy modulation of the MERT beam. Energy fixed at 6, 10 then 15 MeV across the PTV (range selection) or left to the optimiser to choose between the three energies (free optimisation).

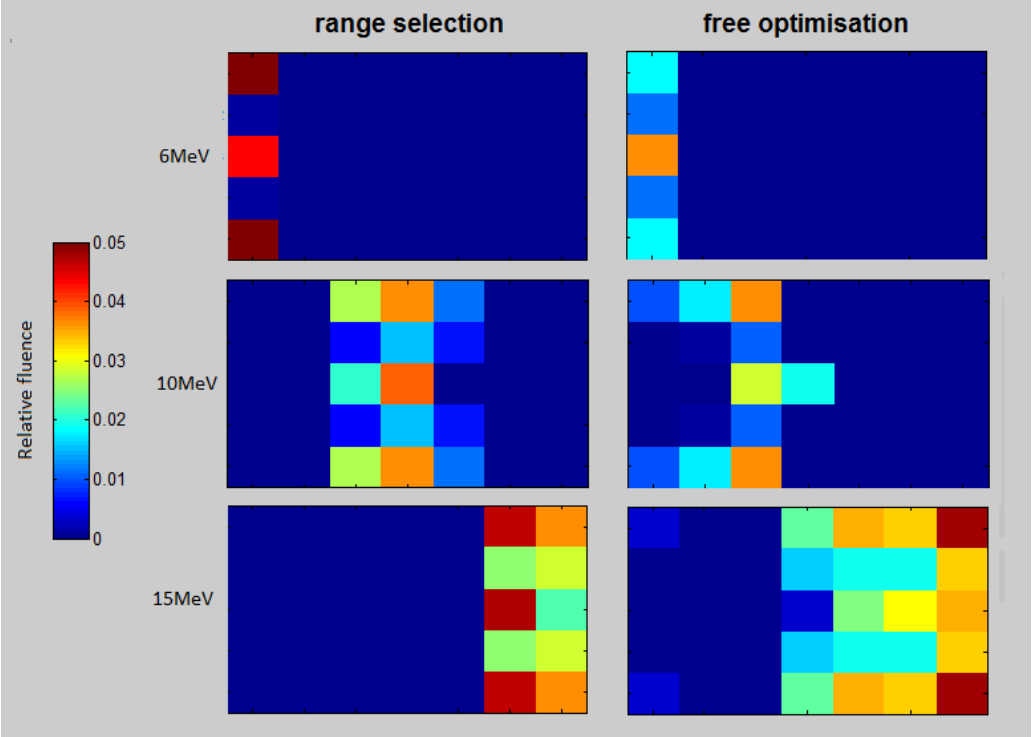

Figure 5.9 Fluence maps for a stepped PTV used to demonstrate energy modulation of the MERT beam. Energy fixed at 6, 10 then 15 MeV across the PTV (range selection) or left to the optimiser to choose between the three energies (free optimisation).

Table 5.2 Dose data for a stepped PTV used to demonstrate energy modulation of the MERT beam. 5x7 matrices of 2cm square segments with 0.5, 1cm or 2cm segment spacing. Dose normalised to mean dose to PTV.

			PTV			OAR	
Method	spacing (cm)	Number of variables	PTV mean (%)	max (%)	D_{min} (%)	max (%)	mean (%)
range selection	2	35	100.0	121.2	59.0	53.2	19.2
free optimisation	2	105	100.0	111.7	72.0	66.6	33.6
free optimisation	1	105	100.0	110.5	72.6	66.5	33.9
free optimisation	0.5	105	100.0	110.2	72.8	66.5	33.9

5.5. exIMRT

5.5.1. exIMRT Introduction

Having investigated the optimisation of the MERT field, this section is concerned with incorporating this work into the optimisation of the combined electron and photon dose distribution. The approach used in this study is intended to test the hypothesis that MERT can be

improved by combining it with photon IMRT to produce exIMRT. That is that the photon IMRT component is used to 'fill in the gaps' in the desired dose distribution not covered by the electron dose distribution. This is illustrated in Figure 5.10 where the IMRT X-ray beam has been used to sharpen the penumbra of the electron field producing a combined dose distribution that is similar to a 6MV X-ray only field at 1.5cm deep but with a reduced dose to the central axis at 10 cm depth.

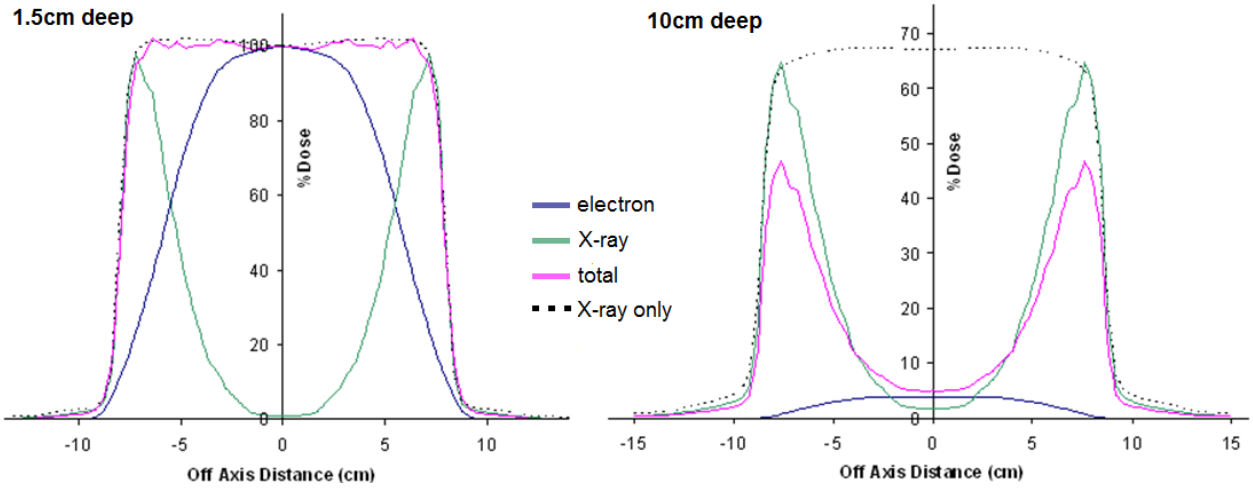

Figure 5.10 Illustrative dose distributions calculated with XiO treatment planning system pencil beam model for overlaid 6MV X-rays and 15MeV electrons. 6MV X-ray beam intensity modulated to offset the wide penumbra of the electron beam and produce a uniform dose distribution at 1.5cm deep. At 10cm combined electron and X-ray dose has dropped to less than 5% on the central axis but the X-ray only dose is 68%.

To this end a two stage optimisation process has been developed. In the first stage the electron dose distribution is optimised and the photon dose distribution used to fill in the gaps. Some overlap of the exit dose from the photon beams with the electron beams is inevitable so the electron dose is reduced by a user input weighting and a 2nd stage used where the electron and photon weights are optimised as one. The development of this two stage approach is described in the following sections.

All calculations were performed for the 20cm cylindrical exIMRT phantom described in 5.3.4.

5.5.2. Treatment plan set up for the cylindrical phantom

An X-ray IMRT only treatment plan was set up with 5 fields equally spaced starting from gantry zero. The isocentre was placed in the centre of the PTV and X-ray beamlets calculated with 4mm width to an 8mm margin around the PTV. This resulted in a total of 388 beamlets each weighted independently to produce an optimisation problem with 388 variables.

A separate exIMRT plan was created with an anterior MERT field added to the IMRT plan with overlapping 6, 10 and 15 MeV segments. The isocentre was moved to the centre of the phantom to provide some reduction in SSD for the electron beam. As there is a significant dose contribution from the anterior electron component it is possible to use more oblique photon fields to avoid OAR with the exIMRT plan. Hence, for the exIMRT plan, gantry angles were altered from the equispaced 5 field arrangement to oblique fields (62, 104, 256 and 298 degrees) retaining the anterior (0 degree) X-ray beam coincident with the electron beam. For each electron energy a 7x5 matrix of electron segments was used (chosen to cover the PTV). There is a slight reduction in X-ray beamlets due to the change in beams eye view compared to the IMRT problem giving a total of 507 variables for the exIMRT problem.

5.5.3. Optimisation solvers

For this study to be successful the exIMRT inverse planning process should be sufficiently efficient to allow the creation and modification of treatment plans in real time. The optimisation algorithm should therefore take minutes/hours rather than days. However, it is also important that the best possible, and ideally the globally optimal, exIMRT solution be found. If the algorithm becomes trapped in a local minimum then the solution might give a false representation of the benefits of exIMRT as compared to IMRT.

For simplicity the selection of an optimisation solver was first evaluated using an X-ray only IMRT problem and a simple cost function using minimum and maximum dose objectives, (equation 5.5).

$$f_k\big(d(x)\big) = \sum_{n=1}^{N_k} \big(d_{k,n}(x) - {D_k}^{max}\big)^2 . C\big(d_{k,n}(x) - {D_k}^{max}\big) + \sum_{n=1}^{N_k} \big(d_{k,n}(x) - {D_k}^{min}\big)^2 . C\left({D_k}^{min} - d_{k,n}(x)\right) \tag{5.5}$$

where $d_{k,n}(x)$ is the calculated dose determined for each of the *n* to N_k voxels contained by each structure *k*, *C(y)* =1 for *y*>0 and *C(y)* = 0 for y ≤0 and suitable values of maximum, ${D_k}^{max}$, and minimum, ${D_k}^{min}$, objective values based on the dose objectives were used. Using this optimisation function different optimisation solvers were tested against each other for accuracy and efficiency. First, the MATLAB fminsearch solver was used as a baseline for comparison with other methods before investigating the solvers described in 5.3.2.

Results of optimisations with each of these solvers are presented in Figure 5.11. As might be expected fminsearch iterates towards a solution but does so over the maximum set of function counts. The most efficient fmincon option for the IMRT problem was the interior-point algorithm with the 'l-bfgs' (limited memory Broyden–Fletcher–Goldfarb–Shanno) large scale quasi-Newton Hessian approximation. This produced an acceptable (within dose objectives) solution in less than 8000 iterations. A factor of 10 improvement over the fminsearch simplex search method. The performance of the SQP algorithm was disappointing. Some commercial treatment planning systems use solvers based on the SQP method (Chapter 2) but the MATLAB implementation of the algorithm was not suitable for this problem.

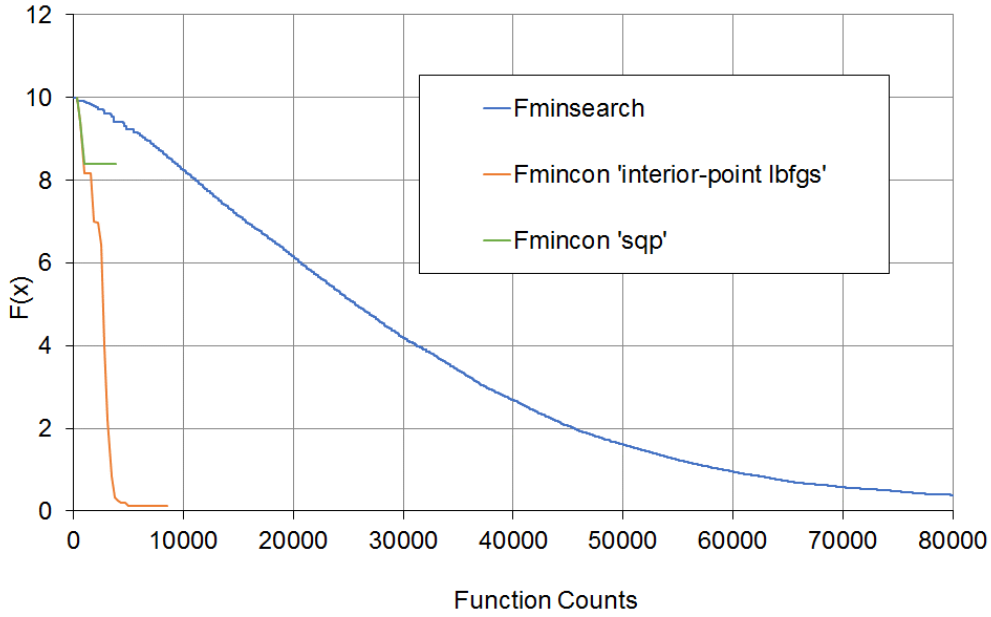

Figure 5.11 Plot of cost function value *F(x)* against function counts for an IMRT problem with the MATLAB fminsearch simplex search and fmincon interior-point and SQP algorithms

For the exIMRT problem the dependence of the dose distribution on the modality and energy of the beam as well as the intensity may lead to a non-convex problem with local minima. There may then be advantages to using a heuristic or metaheuristic algorithm designed to find an approximate global solution avoiding getting stuck in local minima.

Before application of the metaheuristic algorithms to the IMRT problem they were first tuned and tested with known optimisation problems. First the optimisation algorithms were used to calculate effective gains for a proportional–integral–derivative (PID) controller. Application to such a simple systems serves as a proof of concept exercise and provides an opportunity to effectively program and structure the algorithm for later use. The algorithms were then applied to three mathematical functions that exhibit multiple local optima, the Griewank function, the Ackley function and the Rosenbrock function. These are well known structure optimisation function problems taken from published comparisons of optimisation methods (Karaboga and Basturk, 2007). The Griewank and the Ackely functions create a series of spaced out local optima that some optimisation programs could become trapped inside. For the Ackely function each local optima has a steeper gradient than the global optima such that an algorithm that uses the gradient to calculate its variables will become trapped in a local optima. The Rosenbrock function is perhaps most similar to the IMRT problem with a global minimum inside a long, narrow, parabolic

spaced flat valley. All three functions have a global minimum of zero. The ability of each metaheuristic algorithm to approach a solution of zero provides an effective benchmark for the algorithms to assess their performance. Each of the algorithms was tuned until the best results with each of the test functions was achieved. A description of these tests in presented in Appendix A and a summary of the results is presented in Table 5.3.

Table 5.3 Results of errors for three optimisation algorithms and three test functions with 30 variables

Function	GA	PSO	Firefly
Griewank function	1.23	1.11 E-02	2.87E-09
Ackley function	1.09	1.49 E-06	3.01 E-12
Rosenbrock function	166.28	402.54	2.20 E-01

For all three test functions the GA iterates to an approximate solution but does not begin to approach the global minimum. The GA solution is significantly higher than the PSO and the Firefly algorithm solutions for both the Griewank and Ackley functions. For the Rosenbrock function the GA algorithm gives an improved result compared to PSO, however neither algorithms are approaching the global minimum of zero. The Firefly modification to the PSO algorithm gives improved results for all three test functions and a lower value than the GA for the Rosenbrock function. This suggest that modifying the attractiveness of particles according to the distance between them allows the Firefly algorithm to search multiple local minimum and better find a global solution than either the fixed attractiveness of the PSO algorithm or the unguided mutation of the GA.

The tuned metaheuristic algorithms were then applied to the five-field X-ray only IMRT problem. As with the test functions, the best performing metaheuristic algorithms tested was the Firefly algorithm, (see Figure 5.12). The metaheuristic algorithms require an increased number of function evaluations compared to gradient based optimisation due to the random element of their search. However the Firefly algorithm drops to 0.3 after just 40000 function evaluations whereas the GA and PSO algorithms remain a factor of 10 higher after 80000 function evaluations. These results were used to justify the adoption of the Firefly algorithm for the exIMRT optimisation problem.

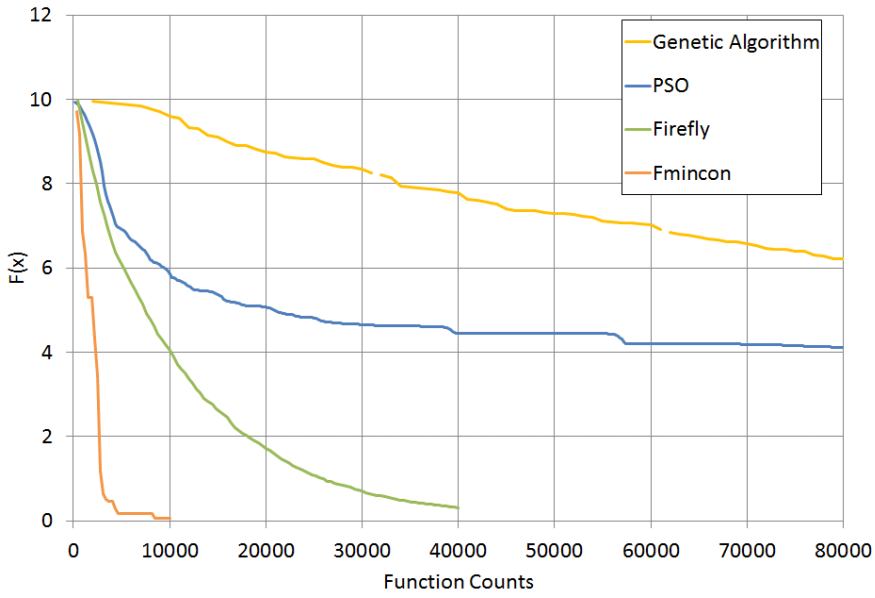

Figure 5.12 Plot of cost function value *F(x)* against function counts for an IMRT problem with genetic algorithm, particle swarm optimisation (PSO), Firefly and MATLAB fmincon interior-point algorithms.

5.5.4. exIMRT optimisation

The two best performing algorithms tested on the IMRT problem, namely Firefly and fmincon interior point algorithm were subsequently selected for the exIMRT problem. The original cost function described in equation 5.5 was modified to include dose objectives in terms of PTV coverage and dose homogeneity as well as OAR specific dose limits. To force the algorithm to conform the target dose to the PTV an artificial OAR, referred to as a 'Helper' structure, was wrapped around the PTV. The objectives definitions together with the importance factors allocated to each objective are given in Table 5.4. Note that the sum of the square of dose differences has been divided by the total number of voxels in that structure and by the square of the aim value. Normalising in this way removes any dependence of the objective function on either the size of the structure or the magnitude of the aim value.

To provide a comparison with the exIMRT problem the X-ray IMRT optimisation problem was re-optimised using the objectives described in Table 5.4. These objectives include a target for D_{OARmed}^{max} that was set at a relatively low value based on preliminary work with exIMRT. For the IMRT problem a value of *F(x)*= 1.54E-4 was achieved, 65% of which was from the D_{OARmed}^{max} component.

With the exIMRT problem the fmincon interior-point algorithm iterates to a solution in a similar number of function evaluation to the IMRT problem (see Figure 5.13). The Firefly algorithm reduces the optimisation function with each step but does not reach a solution close to the fmincon interior-point algorithm after 80000 iterations.

Although reduced from 10 to 7.09E-03, the final solution of the fmincon optimisation is higher than the IMRT solution and dose objectives are not met.

One option to attempt to improve the solution is to perform a 'warm start' by seeding the optimisation algorithm with known good solutions. Attempting multiple warm starts from the last position with the fmincon interior-point algorithm did not yield any significant improvement. If we hypothesise that the Firefly algorithm is tending towards a global solution then perhaps it is this solution that should be used for the warm start. Using the Firefly final position as a warm start for the fmincon interior point algorithm provides a large improvement over the Firefly algorithm alone and a slightly improved result over fmincon interior point algorithm alone. However it is still not an acceptable solution.

Table 5.4 Objectives contributing to the cost function. Where $C(y)$ =1 for y>0 and $C(y)$ = 0 for y ≤0, $\boldsymbol{N_{<\mathrm{D}_{PTV}^{min}}}$ is the number of voxels with value less than $\boldsymbol{D_{PTV}^{min}}$, $\boldsymbol{N_{>\mathrm{D}_{PTV}^{max}}}$ is the number of voxels with value greater than $\boldsymbol{D_{PTV}^{max}}$ and all other variables are defined in the text or assigned a target value in the table.

Structure	dose objective	objective function	objective value	w_k
PTV	$D_{50\%}$= 60Gy	$\frac{\sum_{n=1}^{N_{PTV}}(d_{PTV,n}(x)-D_{PTV}^{aim})^2}{D_{PTV}^{aim\,2}.N_{PTV}}$	$D_{PTV}^{aim}=60Gy$	10
	V_{57Gy} >5%	$\left(\left(N_{<\mathrm{D}_{PTV}^{min}}/N_{PTV}\right)-V^{min}\right)^2$	$D_{PTV}^{min}=57Gy$ $V^{min}=4\%$	10
	V_{63Gy}<5%	$\left(\left(N_{>\mathrm{D}_{PTV}^{max}}/N_{PTV}\right)-V^{max}\right)^2$	$D_{PTV}^{max}=63Gy$ $V^{max}=4\%$	7
OARhigh	$D^{max}<45$	$\frac{\sum_{n=1}^{N_k}(d_{k,n}(x)-D_k^{max})^2.C(d_{k,n}(x)-D_k^{max})}{D_k^{max2}.N_k}$	$D_k^{max}=D_{OARhigh}^{max}=43$	5
OARmed	As low as possible		$D_k^{max}=D_{OARmed}^{max}=3$	1
Helper	Drop off in dose at edge of PTV		$D_k^{max}=D_{help}^{max}=56$	1
Total – PTV	No hot spots		$D_k^{max}=D_{total}^{max}=60$	1

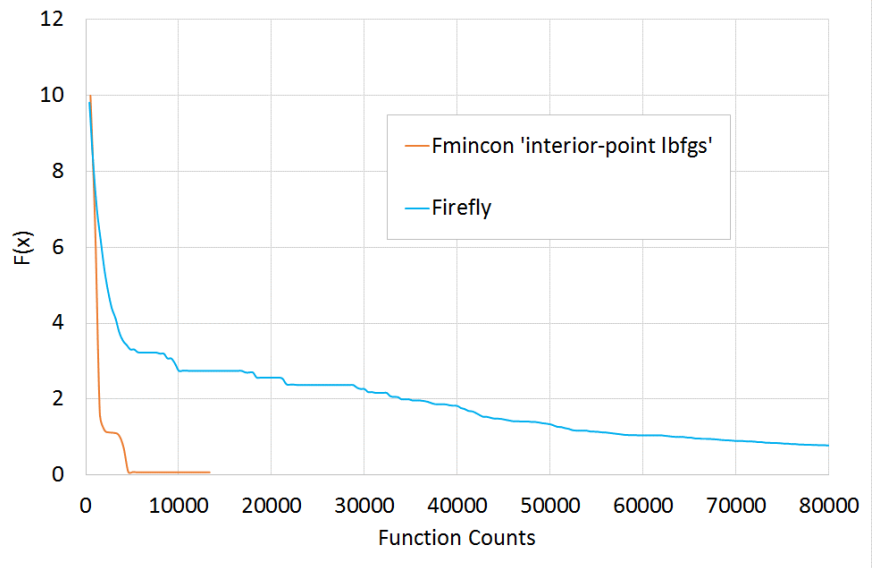

Figure 5.13 Plot of cost function value *F(x)* against function counts for an exIMRT problem with Firefly and MATLAB fmincon interior-point algorithms.

Results of the fmincon and Firefly+fmincon optimisations are presented in Table 5.5. Note that the two methods give similar values for the optimisation function but very different solutions. The difference in the solutions is illustrated by the mean dose to the PTV from the electron contribution as a ratio of the mean dose to PTV from the combined electron and X-ray photon dose. The Firefly+fmincon method produce a solution with 31% electron dose whereas the electron contribution is just 14% with fmincon alone.

Given enough time for the Firefly optimisation to converge, it is possible that a two stage 'metaheuristic+gradient' method would iterate towards the global solution with an optimal combination of photon and electron dose. This is a possible area for future research, however for this study an alternative approach was developed. The approach developed in this work was to allow the user to control the fraction of dose from the electron component in the first stage. As with the metaheuristic+gradient method, the solution from the first stage is then used to warm start the fmincon interior-point algorithm minimisation of the cost function. This method is described as follows and summarised as a flow chart in Figure 5.15.

First the electron dose distribution is optimised according to equation 5.3. Only the electron component of the weight vector, $x_{e,}$ is optimised and no dose is recognised from the X-ray photon component. The photon IMRT component is then optimised to fill in the gaps in the desired dose

distribution not covered by the electron dose. The total desired dose ${D_k}^{aim}$ is defined for each structure such that the desired photon dose at each voxel becomes.

$$ {D_{p,k}}^{aim} = ({D_k}^{aim} - m d_k(x_e)) \tag{5.6} $$

where $d_k(x_e)$ is the calculated dose from the electron component and *m* is the user input electron weighting. This weighting is required to allow the electron component to be reduced to allow for exit dose from the photon component. The photon beam weight vector x_p is then found to minimise the cost function given the objective $f_{p,k}(d)$.

$$ f_{p,k}(d(x)) = \sum_{n=1}^{N_k} \left(d_{k,j}(x_p) - {D_{p,k}}^{aim}\right)^2 \tag{5.7} $$

As with the electron component, minimisation is achieved with quadratic programming using the MATLAB quadprog trust-region-reflective solver.

By default the desired electron dose and photon dose are the same but they do not have to be. The electron dose can be set to a different value in order to use the electron component as an additional boost dose (see Chapter 6 for example of integrated breast boost).

This first stage very quickly produces an approximate solution to the problem. A second stage then uses the standard IMRT optimisation approach using fmincon and the cost function defined in Table 5.4 to further refine the combined electron and photon dose distribution.

The second stage refinement follows a first stage that is biased towards a solution that includes electron dose. If the global solution to the problem does not include electron beams then such a solution may not be found. This is not necessarily problematic for this study as it is the relative benefits of the combined electron and photon dose that is investigated. However, the amount of electron bias used is critical. To investigate the importance of the weighting factor associated with the electron component, the exIMRT problem was run with values of *m* between 0 (no electrons) and 1 (electrons only). The results of this investigation are shown in Figure 5.14.

For this particular exIMRT problem *F(x)* is reduced as *m* is increased up to a value of 0.85. There is a small increase of *F(x)* from *m*=0.85 to m=0.95 before a sharp increase at *m*=1. This suggests that the inclusion of the electron dose is beneficial but that some X-ray photon dose is required, with the optimum value being 85% electron dose. This is not unexpected as the problem

has been set as an exIMRT treatment plan. X-ray beam Gantry angles were set to maximise the benefit of the exIMRT plan (0, 62, 104, 256 and 298 degrees). These oblique beams do not pass through the posterior section of the phantom (minimising dose in this region) and are only effective due to the shape of the electron depth dose curve. Hence it is expected that the optimal plan includes a large electron dose contribution and this does not necessarily imply that the exIMRT plan is superior to an X-ray only IMRT plan (m=0) with an alternative gantry arrangement.

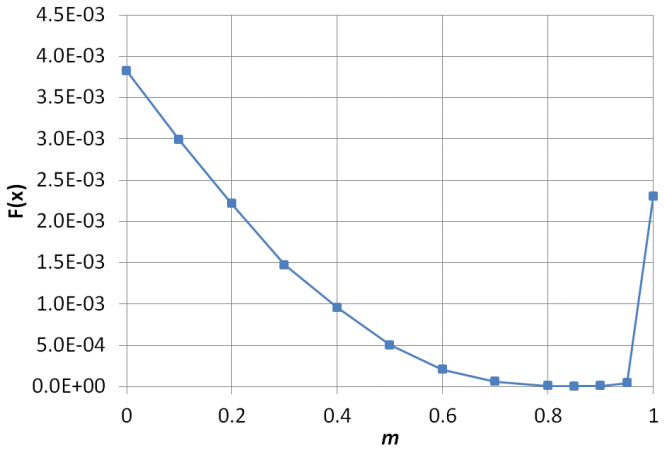

Figure 5.14 Plot of cost function value *F(x)* against the electron weighting factor *m*. X-ray beam Gantry angles have been set to maximise the benefit of the exIMRT plan (0, 62, 104, 256 and 298 degrees).

For all values of *m* the relative contribution of the electron dose is approximately maintained following the 2nd stage optimisation. The difference between *m* and the ratio of the electron contribution to the mean PTV dose and the total mean PTV dose is less than 5%. This suggests that only a slight modification of the electron contribution from the solution at the 1st stage is made by the 2nd stage.

For a value of *m*= 0.85, *F(x)* is reduced from 1.30E-05 to 5.55E-06 with the 2nd stage optimisation. Although this is a relatively small reduction it is sufficient to refine the dose distribution and bring the dose objectives within tolerance.

Table 5.5 Solutions to the IMRT and exIMRT problem. The final value of the cost function for objectives detailed in Table 5.4 is given along with the fraction of the PTV dose from the electron component.

Method		$F(x)$	$PTV^{e}_{mean}/PTV^{total}_{mean}$	Dose objectives met
5fld X-ray IMRT	gradient (fmincon)	1.54E-04	-	Y
exIMRT	gradient (fmincon)	7.09E-03	0.14	N
	metaheuristic (Firefly)	7.78E-01	0.30	N
	metaheuristic+gradient (Firefly+fmincon)	5.38E-03	0.31	N
	After 1st stage 1 (m=0.85)	1.30E-05	0.84	N
	After 2nd stage (m=0.85)	5.55E-06	0.84	Y

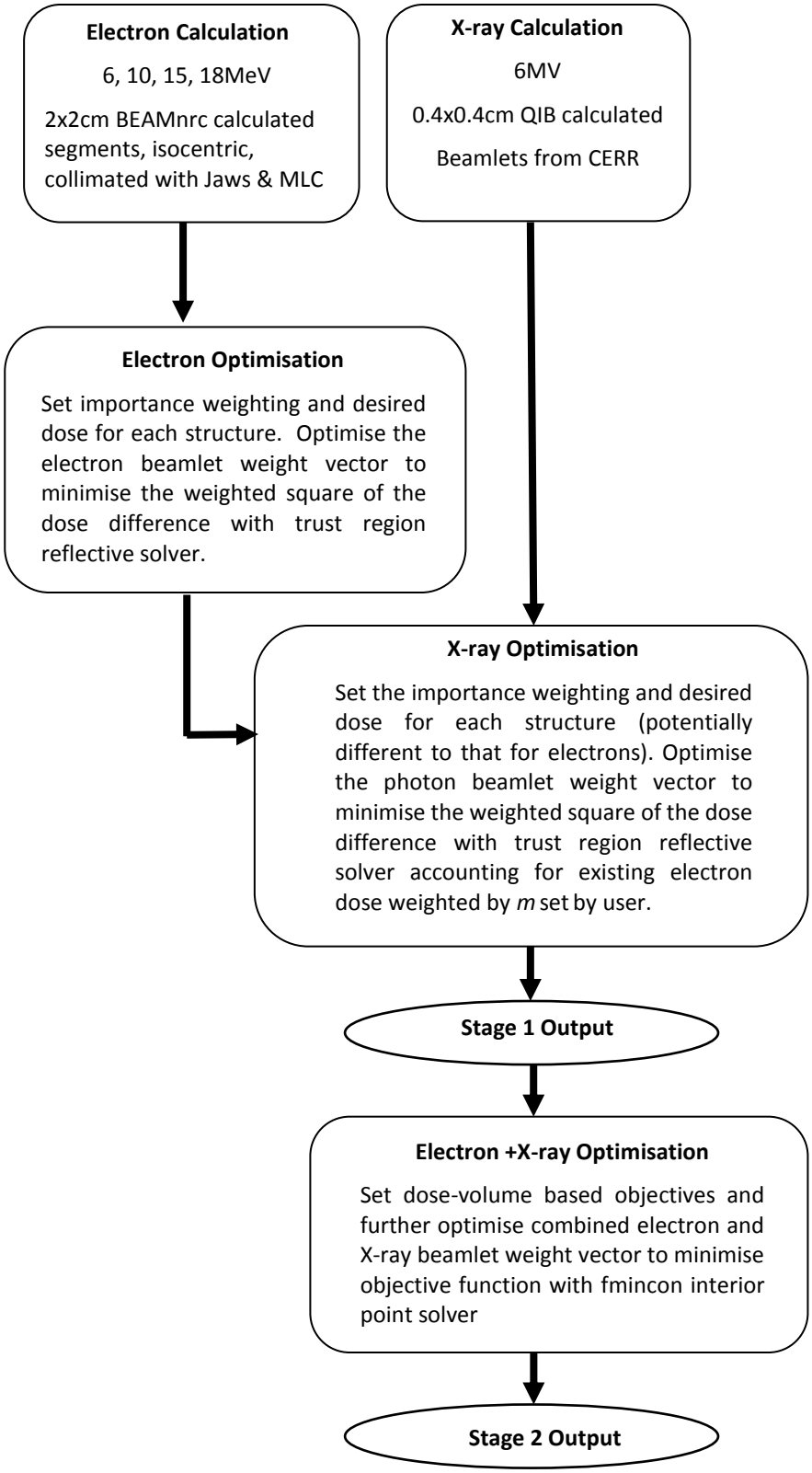

Figure 5.15 Flow chart depicting two stage exIMRT optimisation processes

5.6. Results of exIMRT comparison with IMRT

The optimal exIMRT plan created with the above two stage method has been compared to the optimal five field X-ray only IMRT plan. Dose-volume data are given in Table 5.6. Figure 5.16 shows the dose distribution for the IMRT plan and the exIMRT mixed modality plan (c) along with its electron (a) and 6 MV photon (b) components.

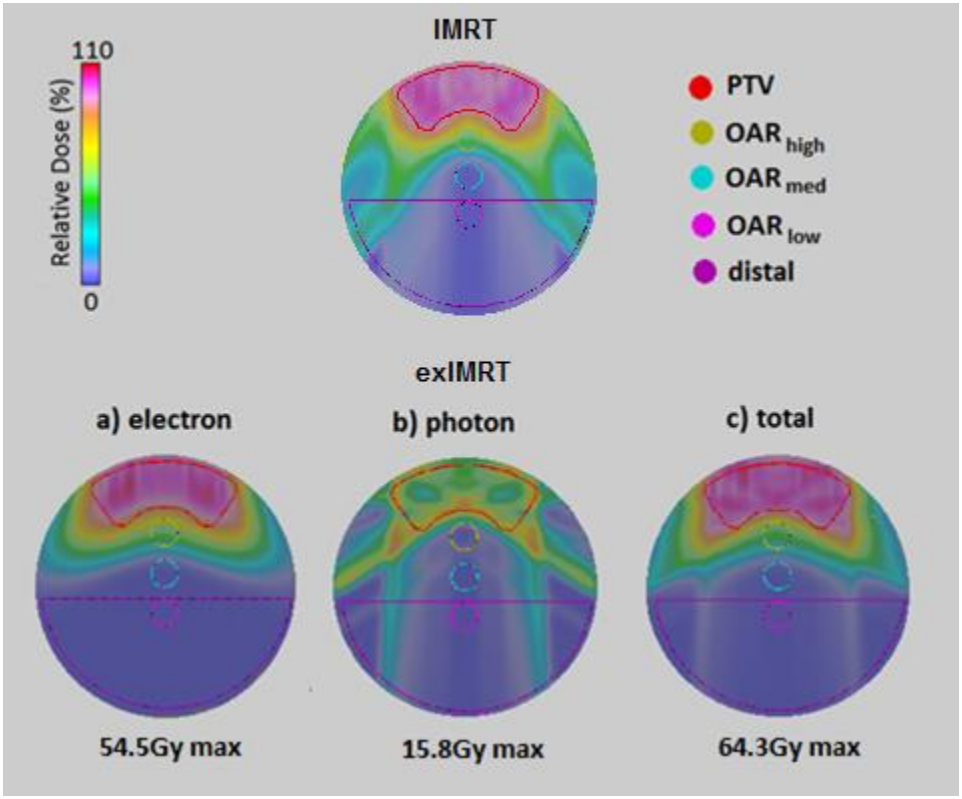

Figure 5.16 Dose distribution on the central slice for the phantom study for the 6MV X-ray photon IMRT plan and a) the MERT component, b) the 6MV X-ray photon IMRT component and c) the total dose for exIMRT (a+b=c).

The final exIMRT plan is able to meet all dose objectives with a reduced OAR dose compared to the IMRT plan. Doses to all OARs are reduced with the relative reduction increasing with distance from the PTV and largest improvement in the low dose demonstrated by a 79.0% reduction in mean dose to the distal volume.

Table 5.6 Dose-volume data for phantom study showing the benefits of using exIMRT

		achieved	
	target	IMRT	exIMRT
Dose to PTV (Gy)		Volume (%)	
57Gy	>95%	95.4	95.0
60Gy	50%	50	50
63Gy	<5%	4.7	2.7
Structure		Max Dose (Gy)	
OAR_{high}	<45Gy	44.2	38.9
OAR_{med}	-	5.2	3.3
OAR_{low}	-	1.7	0.5
		Mean Dose (Gy)	
distal	-	6.2	1.3

5.7. Discussion and conclusions

A two stage iterative optimisation procedure has been developed in this Chapter to optimise dose for combined photon and electron IMRT with fields of different modality and energy overlapping to produce depth modulation (exIMRT). The two stage iterative optimisation allows the user control over the electron contribution through a modifying factor and separate dose constraints at the first stage. The electron component is optimised for energy as well as intensity by allowing overlapping beamlets of three energies. It has been shown for a simple example that the optimal proportion of electron dose is 85% of the total dose, or m=0.85. Compared to a 6MV X-ray IMRT plan, the exIMRT technique has the potential to reduce the dose in the low dose wash whilst retaining target coverage.

Having demonstrated the benefits of the proposed optimisation scheme, this chapter provides the required evidence to extend the study from a phantom with artificially generated plans to clinical situations. The application of the proposed mix-beam mix-modality optimisation to re-plan previously delivered IMRT treatment plans is presented in the following chapter.

Chapter 6

Clinical treatment plan comparison

6.1. Introduction

This chapter presents four clinical cases to demonstrate the proposed technique and evaluate its potential. Treatment sites have been chosen that are appropriate to the physical properties of the electron beams as described in previous chapters. Specifically each plan includes a CTV that extends to within 5 to 10 mm of the skin surface and a PTV that is less than 7cm deep and less than 18cm in diameter.

Existing historical clinical treatment plans have been re-planned using the exIMRT method to a prescribed dose and dose objectives defined by clinical protocols for the given treatment site. Each exIMRT plan has been compared to the original clinical 6MV VMAT or ssIMRT plan created using the Elekta Monaco® treatment planning system at UHCW. Plans have been compared in terms of dose-volume data and the reduction in mean dose to organs at risk (OAR). The radiobiological impact of exIMRT has been considered by comparing equivalent uniform dose (EUD) for the PTV and normal tissue complication probability (NTCP) for selected OAR in each case. Secondary cancer induction has been considered by comparing the dose conformity and by calculating relative malignant induction probability (relMIP).

In reviewing the treatment plan comparisons there are a number of assumptions and approximations inherent to the exIMRT plan that we need to be aware of. These assumptions and approximations will be discussed in the first part of this chapter.

6.2. Assumptions and approximations

6.2.1. RBE

The first assumption made is that the radiobiological effectiveness (RBE) of the X-ray photon and electron components are equivalent. RBE is related to the linear energy transfer (LET) of the ionising radiation so there may be small differences for MeV electrons and MV X-rays. RBE may also vary with electron energy or even as a function of depth due to an increase in LET (Schwarz et al., 1966). However, the assumption that RBE for MeV electrons and MV X-rays is equivalent is supported by in-vitro studies (Zackrisson et al., 1991). There is also a long history in the effective use of electrons without RBE correction (Hogstrom and Almond, 2006). RBE variation is an issue that also affects proton therapy but in that field a generic RBE of 1.1 tends to be used (Giovannini et al., 2016). It is suggested that using a generic RBE of 1.0 for electrons in this study is not unreasonable.

6.2.2. X-ray photon dose calculation and segmentation

Some care has been taken to ensure that the dose calculation for the electron component of the exIMRT plans are representative of deliverable electron doses (Chapter 3 and 4). For the photon component the 6MV QIB Pencil beam algorithm as implemented in CERR has been used without modification (Deasy et al., 2003). The Monaco treatment planning system uses a clinically validated Monte Carlo dose calculation. In certain situation, these two algorithms will give different results. In particular the QIB pencil beam algorithm does not correctly predict the effects of lateral scatter (Knöös et al., 2006). The Monte Carlo dose calculation will therefore be more accurate in high or low density tissue and at the junction between dissimilar materials. Pencil beam dose calculations are particularly inaccurate in lung tissue which can lead to errors for a beam passing through the lung of up to 6% (Morgan et al., 2008).

As well as dose calculation, differences due to segmentation should be considered. The exIMRT treatment plans are constructed from idealised X-ray intensity maps whereas the Monaco plans represented deliverable plans with intensity maps segmented into MLC shapes or VMAT control points. Segmentation of the plan according to the physical constraints will limit the complexity of the final X-ray photon intensity maps. In addition, the accurate modelling of the

MLC and Jaws may result in increased penumbra widths, leakage etc. that further reduces plan quality.

The effect of X-ray dose calculation and segmentation errors should be reduced with the exIMRT calculation as the contribution of the photon component is relatively low. Of the four cases considered the biggest differences could be expected in the breast plan case where the photon dose contribution is largest and the incorrect calculation of lateral scatter from lung tissue with the QIB algorithm will lead to overestimate of the dose at the lung/chest interface.

To address the issue of comparing dissimilar treatment planning systems all cases have also been planned with the exIMRT system but with X-ray IMRT only. Hereafter the X-ray only IMRT plan will be referred to as the xIMRT plan. The xIMRT plan allows comparison of the exIMRT plan with an idealised X-ray IMRT plan. As this xIMRT plan is not limited by physical constraints it may be superior to the segmented IMRT plan. However the segmented IMRT plan, from the commercial treatment planning system, has the advantage of being independent of the exIMRT planning system. It will therefore be determined whether there is an improvement in mean OAR dose with the exIMRT plan as compared to the xIMRT plan as well as the segmented IMRT plan.

6.3. Case descriptions

6.3.1. Case descriptions: Introduction

The following sub-sections present a brief description of four clinical cases considered for the exIMRT technique. With the exception of Case 3 all cases use an initial electron photon weight of m=0.85, as described in Chapter 5. Case 3 uses a weighting of m=1.00 but separate electron and X-ray dose objectives in the first stage to create an electron ‘boost’ field. The contribution of the electron component to the total dose for each case is presented in Table 6.1 as the ratio of the mean dose to the PTV from the electron field to the mean dose to the PTV from combined electron and X-ray dose distribution. All cases exhibit a significant contribution from the electron component with > 72% of the dose from the electron field for Case 1, 2 and 4 and 34% of the dose from the electron field for Case 3.

6.3.2. Description: Case 1 - Paraspinal sarcoma

Sarcomas are malignant tumours that invade the soft tissues such as muscles nerves and fat. Sarcomas in the paraspinal muscles pose a technical challenge due to their proximity to the spinal cord. The treatment plan must irradiate the tumour to the prescribed dose whilst observing the dose constraint of maximum dose to the spinal cord and at the same time minimise dose to underlying organs at risk. For this reason paraspinal sarcomas are a potential area of expansion for adult proton therapy treatment (Weber et al., 2004, Weber et al., 2007)

This particular example includes a CTV approximately 13cm wide by 13cm long with a depth of up to 5.5cm. The CTV extends close to the skin surface and is overlying the spinal cord but not wrapped around the cord. The clinical plan is a 6MV VMAT 200^{o} partial arc to 60Gy in 30 fractions. The dose objectives of the plan are to cover the PTV defined as the CTV plus a 5mm isotropic margin maintaining a maximum of 50Gy to 1cc of the spinal cord planning risk volume (PRV) and minimising dose to normal tissue, in particular the underlying liver and kidneys. For optimisation the PTV was edited back 5mm from the skin surface. No bolus was added and the reduced surface dose was accepted by the Clinician. Clinically the dose to the actual PTV as well as the modified PTV was reported. Only dose to the modified PTV is reported here due to uncertainty in the dose calculation at the surface. The VMAT plan was created by an experienced member of staff using the Monaco treatment planning system with two arcs both arcing between 260^{o} and 100^{o}. The treatment was re-planned for this study using the exIMRT technique with a single anterior MERT field and an anterior and four oblique 6MV photon IMRT fields (gantry angles of 300^{o}, 270 ^{o}, 0 ^{o}, 60^{o} and 90^{o}). All fields share a single isocentre in the patient midplane. The field arrangement and dose objectives are similar to the non-clinical example in Chapter 5 and the same approach to optimisation has been used.

For comparison, an xIMRT plan was created with 6 fields equally spaced between 260^{o} and 100^{o} (mimicking the Monaco VMAT plan) with the isocentre in the centre of the PTV. This xIMRT plan has been optimised using the same objectives as the exIMRT plan.

6.3.3. Description: Case 2 – Brain

Brain tumours are amongst the most devastating of all malignant diseases. Glioblastoma multiform (GBM) is the most common primary brain tumour in adults. The standard therapy for GBM is

maximal surgical resection followed by radiotherapy and concurrent chemotherapy. In spite of extensive treatment the diseases is associated with poor clinical outcome (von Neubeck et al., 2015). The maximum radiation dose is limited by neurological toxicities so perhaps if the dose to normal brain tissue could be reduced with exIMRT there would be an opportunity to attempt dose escalation or at least make re-treatment following local recurrence more acceptable.

For low grade brain tumours where radiotherapy is potentially more successful, irradiation of normal brain tissue has been related to radiation induced cognitive impairment (Greene-Schloesser et al., 2012). In a similar manner to Case 1 there is some suggestion that reducing normal tissue dose with proton therapy could reduce side effects and the risk of secondary cancers (Arvold et al., 2012, Dennis et al., 2013, Brown et al., 2013). Although brain tumours can occur anywhere in the brain, they may be suitable for exIMRT if they are close to the surface.

In this example a right sided high grade glioblastoma multiform tumour with PTV 8 cm by 6 cm up to 6.6 cm deep extending 5mm to 9mm from the surface (no bolus or editing of PTV required) was treated with 6MV VMAT to 60 Gy in 30 fractions. The clinical treatment plan was created using the Monaco treatment planning system by an experienced planner with a start angle of 190 ^{o} and a finish angle of 340 ^{o}. The treatment was re-planned for this study using the exIMRT technique with a single MERT field and 5 X-ray fields at gantry angles of 190^{o}, 230^{o}, 270^{o}, 310^{o} and 340^{o}. All fields shared a single isocentre, level with the centre of the PTV in the superior inferior direction but in the centre of the brain to provide some reduction in SSD for the electron field. For comparison an xIMRT plan was created with 5 fields at the same gantry angles as the exIMRT plan, which cover the same arc as the Monaco VMAT plan. This xIMRT plan has been optimised using the same objectives as the exIMRT plan.

6.3.4. Description: Case 3 – Concomitant breast boost

Test Case 3 is slightly different to the first two in that the electron field is used as a boost dose within a larger X-ray photon dose distribution. Electron boosts have historically been used for breast treatments in order to take advantage of the dose drop off distal to the target to spare heart and lung tissue. Tangential X-ray field are used to treat the whole breast, angled to avoiding lung and heart tissue with additional electron fields added as boost to the tumour bed. This technique does have its drawback such as the limited control over dose conformity and the difficulties in

accurate set up (Davidson et al., 2015, De Santis et al., 2016). exIMRT could perhaps be used to create a more complex and stable integrated dose distribution still taking advantage of the dose drop off in the electron component.

The example is taken from the IMPORT-HIGH trial for dose escalated intensity modulated radiotherapy (Bliss, 2015). The trial protocol includes a concomitant boost to the tumour bed normally achieved with additional small X-ray boost fields on top of tangential whole breast fields. The more difficult planning test case from the trial QA process was selected. This case is the higher dose arm and is on the left side overlying the heart. The total desired dose was set to 53 Gy to the tumour bed (PTVtb) 40Gy to the partial breast (PTVpb) and 36Gy to the whole breast (PTVwb). Both the PTVwb and PTVpb were edited back 5mm from the patient surface. For the clinical Monaco step and shoot IMRT (ssIMRT) treatment plan virtual bolus was used in order to achieve a flash margin. For the IMRT and exIMRT treatment plan virtual bolus was not used, as robustness to set up was not considered as part of this study.

For the exIMRT plan tangential X-ray fields at the same gantry angles as the Monaco ssIMRT plan (307 ^{o} and 132^{o}) were used but no boost X-ray fields were added. In place of the boost X-ray fields a single MERT field was added to the tangential photon fields. To create the boost effect the initial desired electron dose was set to just 17Gy to the tumour bed and 4Gy to the partial breast. Dose objectives were taken from the IMPORT-HIGH protocol. All fields were placed with a single isocentre level with the centre of the PTV in the superior inferior direction but at the lung/chest interface to provide some reduction in SSD.

The exIMRT plan created was compared to the Monaco ssIMRT plan which used boost X-ray fields confined to the PTVpb volume as well as tangential fields to cover the whole breast volume. Boost X-ray fields were positioned at gantry angles 0^{o}, 45^{o} and 90^{o}. The Monaco ssIMRT treatment plan had previously been accepted by the trial validation team. The ssIMRT arrangement was replicated for an xIMRT plan which was optimised using the exIMRT objectives modified to create the boost with the X-ray fields.

6.3.5. Description: Case 4 – Head and Neck re-treatment

In this example a patient who has had previous radiotherapy treatment to a volume on the right side of their oropharynx has returned for treatment to new tumour that has developed on the left

side. This situation presents a technical challenge as it is difficult to assess the amount of repair to normal tissue between treatments and therefore determine what new dose can be safely given. If we assume no repair in-between treatment then the total dose received by OAR from the two treatments combined must be considered (McDonald et al., 2011).

For this example the maximum dose to the spinal cord was limited by the clinician to just 5 Gy in order to ensure a combined maximum dose for the original plan and retreatment plan of <50 Gy. The clinician also requested that the dose to the mandible be reduced as much as possible in order to reduce what is a significant risk of osteoradionecrosis (Nadella et al., 2015). 10mm thick wax bolus was added for the planning CT scan (and retained for treatment) to ensure adequate dose to the CTV in regions where it extends close to the patient surface. The bolus was added to an area indicated by the clinician using clinical judgment prior to the CTV being defined. Consequently the bolus covers a wider area than it would if it were determined by the proximity of the drawn CTV to the patient surface.

The clinical treatment plan was created using the Monaco treatment planning system by an experienced planner with 6 fields angled away from the spinal cord at gantry angles 300^{o}, 330^{o}, 0^{o}, 60^{o}, 90^{o} and 120^{o}. This plan was achieved after exploring multiple options including VMAT and a single direct electron field. The treatment was re-planned for this study using the exIMRT technique with a direct MERT field and X-ray fields at the same gantry angles as the Monaco ssIMRT plan. All fields shared a single isocentre level with the centre of the PTV in the superior inferior direction but on the patient midline to provide some reduction in SSD for the electron field. The ssIMRT arrangement was replicated for an xIMRT plan which was optimised using the exIMRT objectives.

Table 6.1 Contribution of the electron component to the mean PTV dose for exIMRT treatment plans

	Mean dose (Gy)					
	Case1 PTV	Case 2 PTV	Case 3			Case 4 PTV
			PTVtb	PTVpb-tb	PTVwb-pb	
Electron	49.53	44.56	18.03	10.36	2.25	44.10
Total	60.04	59.83	52.69	43.05	35.50	60.80
%electron	82.5%	74.5%	34.2%	24.1%	6.3%	72.5%

6.4. Results

6.4.1. Results: Introduction

A summary of results for the four clinical cases is presented in the following sub-sections. Although it is not always clinically relevant, the mean dose to the OAR is presented as an indicator of the reduction in OAR dose with exIMRT. Similarly, the average reduction in the mean dose with exIMRT has been calculated to summarise this reduction in a single quantitative value. A table of the full dose-volume data together with clinical dose objectives has been provided for each case in Appendix B.

6.4.2. Results: Case 1 - Paraspinal sarcoma

The Monaco VMAT, xIMRT and exIMRT plans meet all clinical dose objectives (Appendix B). The exIMRT technique is able to produce adequate target coverage with improved conformity. A representative dose distribution and DVHs are shown in Figure 6.1 and Figure 6.2 respectively. There is a reduction in the low dose wash with a corresponding improvement in dose for all OAR with the exIMRT plan. The reduction in the mean dose to OAR with exIMRT is 76.3% on average (see Figure 6.3). The X-ray only xIMRT plan is slightly more conformal than the clinical VMAT plan. In particular the xIMRT has an improved dose gradient between the spinal cord and the PTV than either the VMAT plan or the exIMRT plan. The dose to 1cc of the spinal cord PRV is therefore lower for the xIMRT plan than the exIMRT plan, 25.2 Gy compared to 33.0Gy. The exIMRT plan spinal cord dose is however within tolerance (1cc $\leq$ 50Gy) and there is reduction in the low dose wash and a corresponding reduction in the dose to the kidneys, spleen and liver when compared to the xIMRT plan. Compared to the xIMRT plan exIMRT achieves a reduction in mean dose to OAR of 66.1% on average (not including the spinal cord).

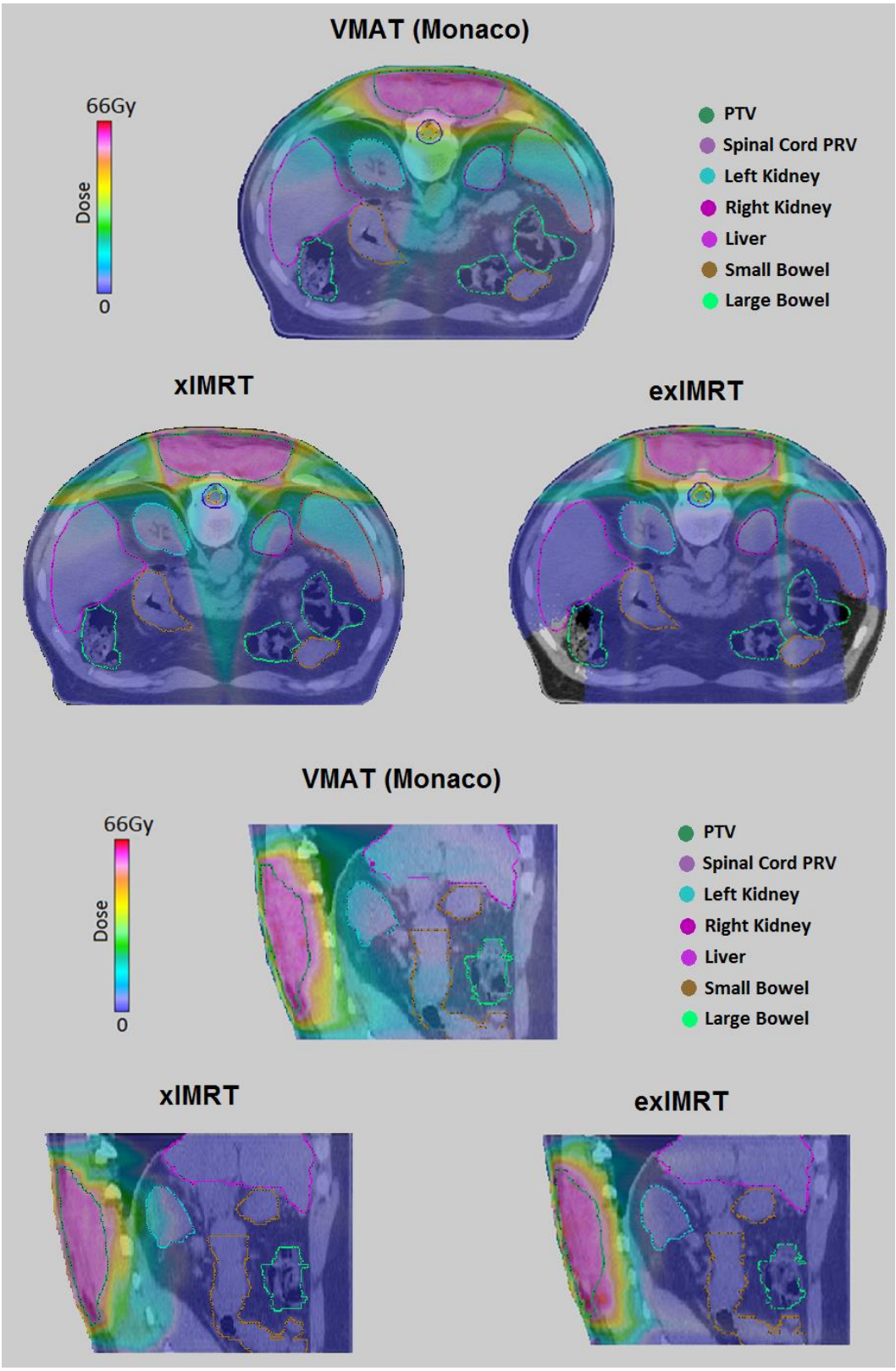

Figure 6.1 Case 1: Dose distribution on the isocentre slice for paraspinal sarcoma plan in the axial (top) and sagittal plane (bottom) for Monaco 6MV VMAT, xIMRT and exIMRT treatment plans.

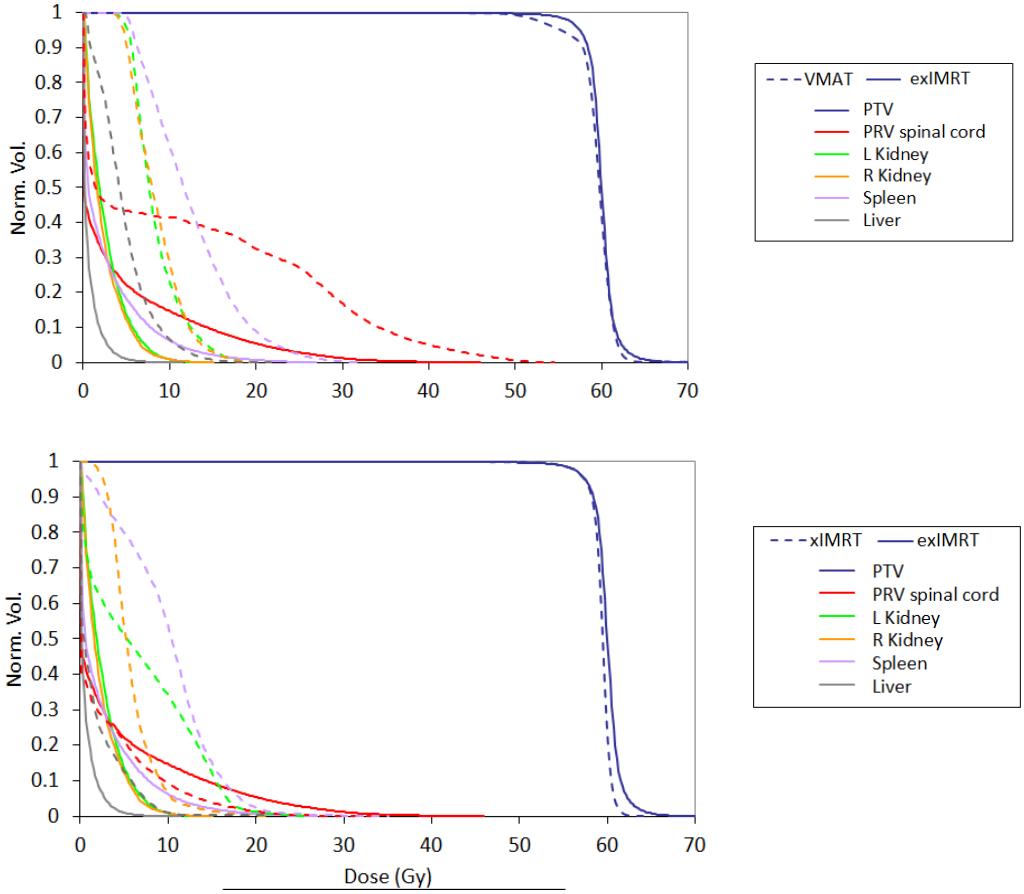

Figure 6.2 Case 1: DVH for paraspinal sarcoma plan Monaco 6MV VMAT (top), xIMRT (bottom) and exIMRT treatment plans.

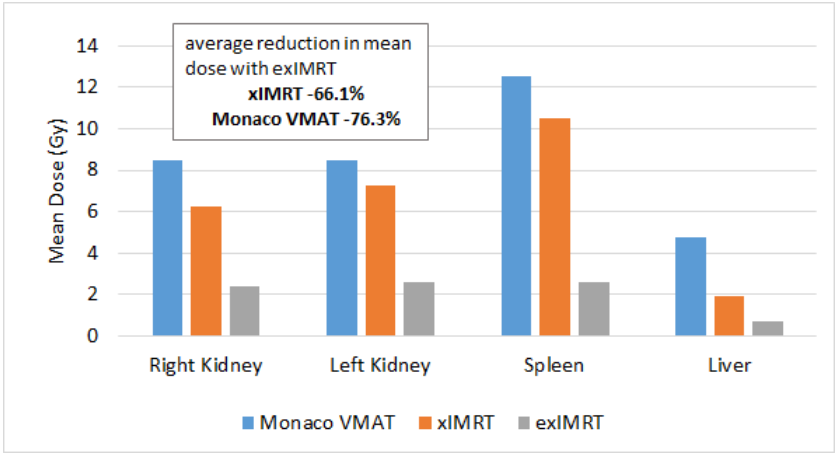

Figure 6.3 Case 1: OAR mean doses for Monaco 6MV VMAT, xIMRT and exIMRT treatment plans.

6.4.3. Results: Case 2 – Brain

The Monaco VMAT, xIMRT and exIMRT plans meet all clinical dose objectives (Appendix B). Dose distribution and DVHs are shown in Figure 6.4 and Figure 6.5 respectively. The exIMRT technique is able to produce adequate target coverage whilst avoiding the ocular apparatus with a reduction in dose to normal brain tissue. This reduction in normal brain dose can be seen in Figure 6.4 as a reduction in the exit dose beyond the tumour depth. In order to achieve this reduction the dose fall of the electron field is boosted by a posterior X-ray field resulting in a posterior hot streak. This streak is however thin and less than 70% of the prescribed dose. There is a 68.3% average reduction in the mean dose to all OAR with exIMRT (see Figure 6.6).

As with Case 1 the xIMRT plan is slightly more conformal than the clinical VMAT plan and the reduction with exIMRT is reduced to 61.2% on average. In particular the dose for normal brain tissue, defined as Brain-PTV, is lower for xIMRT than Monaco VMAT such that reduction in Brain dose with exIMRT is 55.5% when compared to Monaco VMAT but only 34.1% when compared to xIMRT.

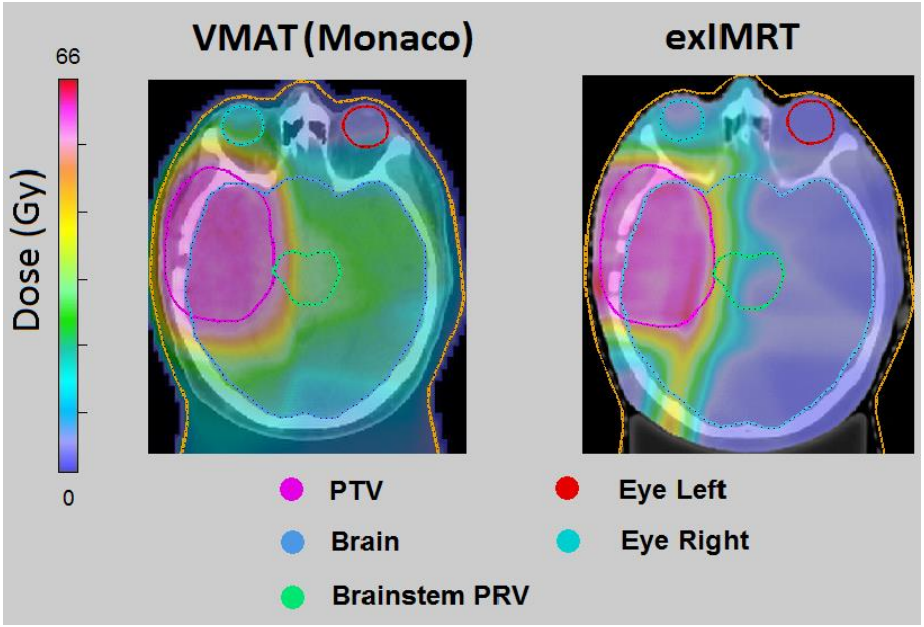

Figure 6.4 Case 2: Dose distribution on the isocentre slice for brain plan in the axial plane for Monaco 6MV VMAT (left) and exIMRT (right) treatment plans.

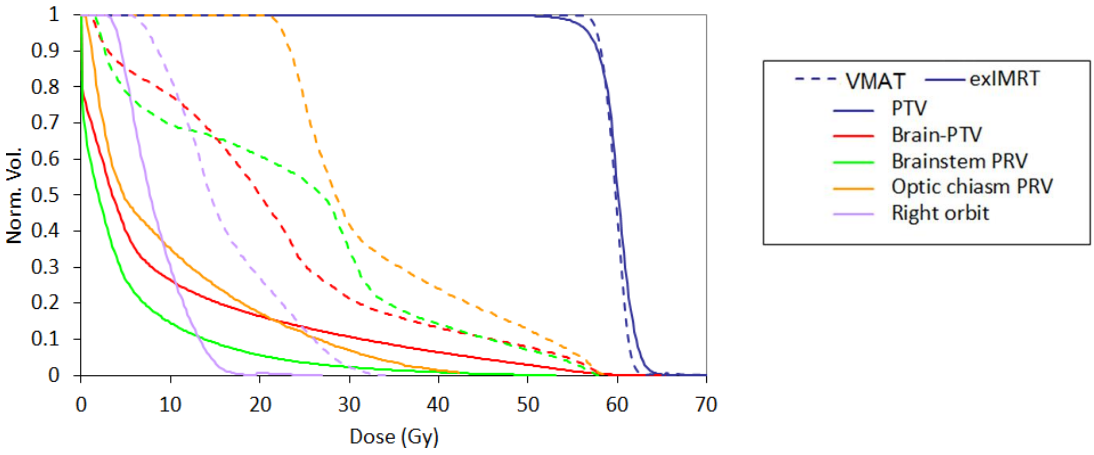

Figure 6.5 Case 2: DVH for Brain plan Monaco 6MV VMAT and exIMRT treatment plans.

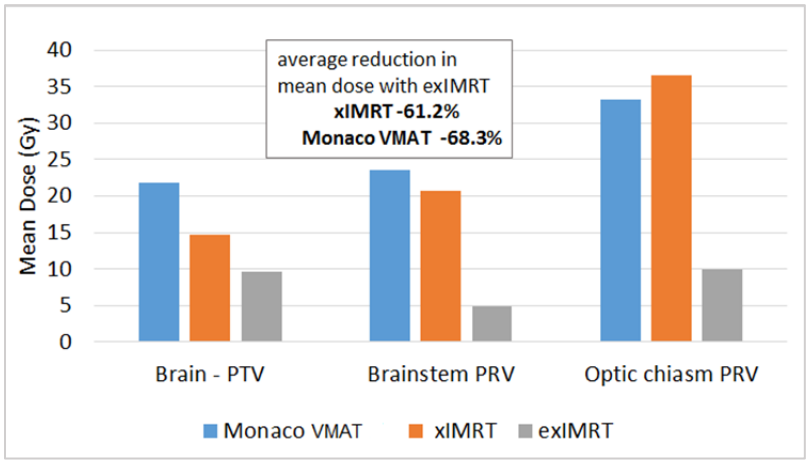

Figure 6.6 Case 2: OAR mean doses for Monaco 6MV VMAT, xIMRT and exIMRT treatment plans.

6.4.4. Results: Case 3 - Concomitant breast boost

The Monaco ssIMRT, xIMRT and exIMRT plans meet all clinical dose objectives (Appendix B). A representative dose distribution and DVHs are shown in Figure 6.7 and Figure 6.8 respectively. The Monaco plan and the X-ray only xIMRT plan compare well considering the numerous differences in the systems. The exIMRT plan is able to produce adequate target coverage but with only small improvements in the higher dose OAR values. The volume of ipsilateral heart or lung receiving 10 Gy or more is not significantly improved with exIMRT. However, as the exIMRT plan has no exit dose from X-ray boost fields there is a reduction in the low dose wash resulting in a reduction in the average dose to OAR. There is a 45.6% average reduction in the mean dose

to all OAR with exIMRT (see Figure 6.9). There is a reduction in the dose to the contralateral side with the mean dose for the Contralateral Lung and Contralateral Breast reduced from 1.0 Gy and 0.5Gy respectively to a negligible 0.1 Gy with exIMRT. These values should be viewed with caution due to the inaccuracies of dose calculations at these low levels (Huang et al., 2013) but demonstrate the fact that there is no exit dose to the contralateral side with exIMRT. As with Cases 1 and 2 the xIMRT plan is slightly more conformal than the clinical IMRT plan and the reduction with exIMRT is reduced to 59.3% on average.

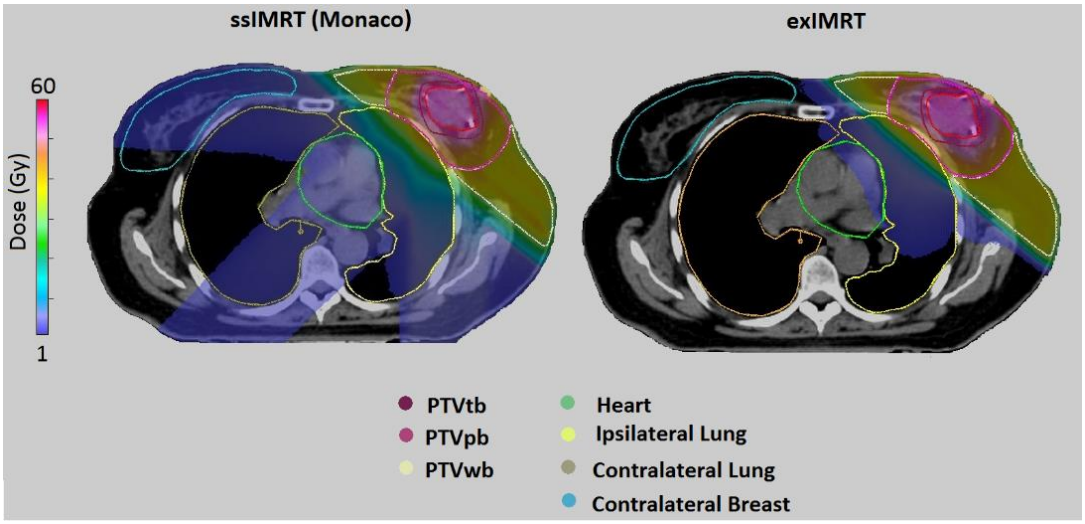

Figure 6.7 Case 3: Dose distribution on the isocentre slice for concomitant breast boost plan in the axial plane for Monaco 6MV ssIMRT (left) and exIMRT (right) treatment plans.

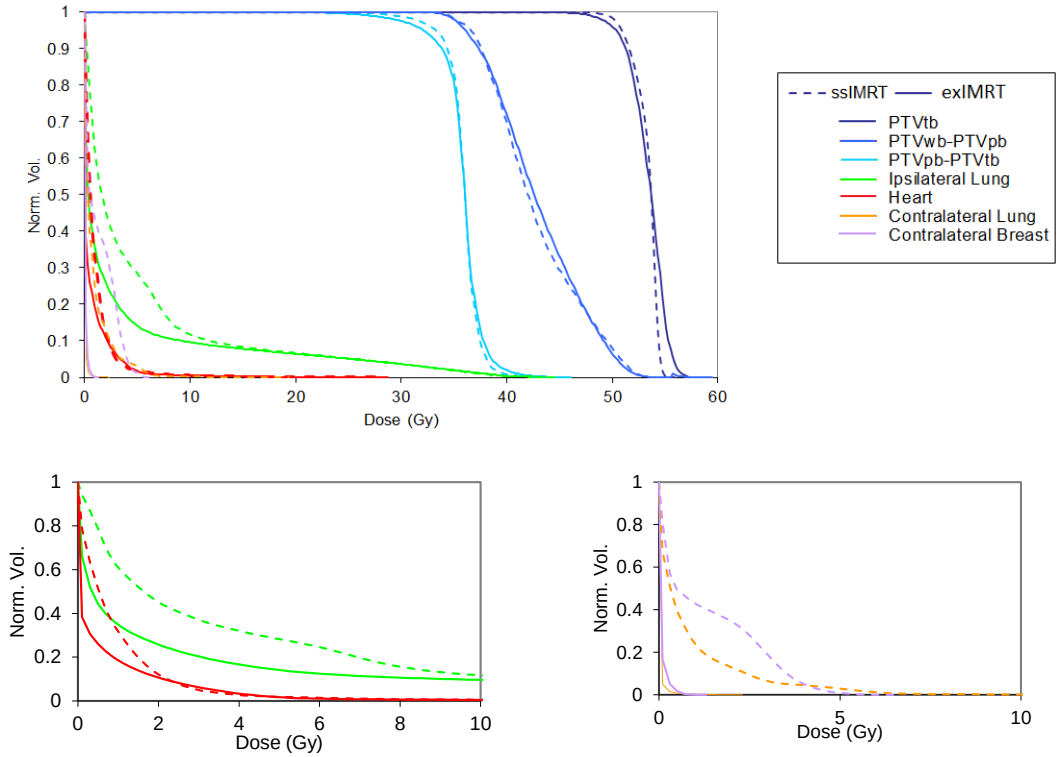

Figure 6.8 Case 3: DVH for concomitant breast boost plan Monaco 6MV ssIMRT and exIMRT treatment plans (with detail at under 10Gy).

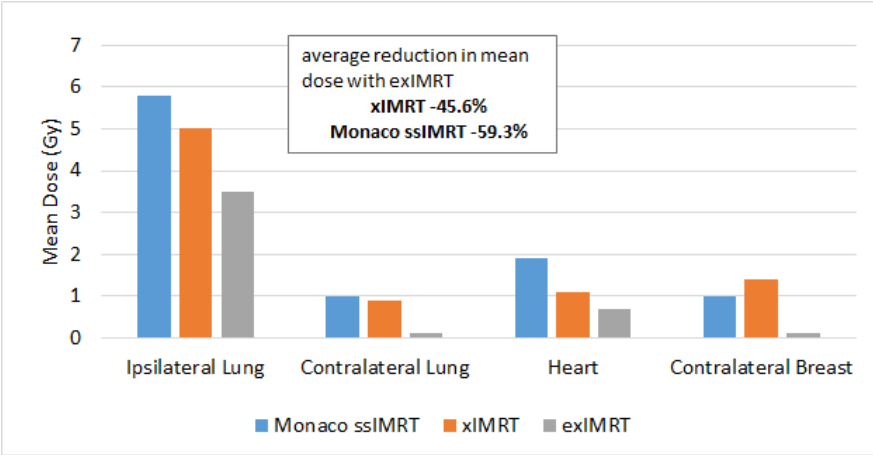

Figure 6.9 Case 3: OAR mean doses for Monaco 6MV ssIMRT, xIMRT and exIMRT treatment plans.

6.4.5. Results: Case 4 – Head and Neck re-treatment

This was a difficult case and not all clinical dose objectives were met by any of the three plans (Appendix B). The Monaco ssIMRT plans meets all objectives apart from the optimal objective of 1cc of the spinal cord PRV to ≤5Gy, where 5.9Gy was achieve and clinically accepted. The xIMRT plan meets all objectives apart from the dose to 99% of PTV which is just under the 54Gy tolerance at 53.5 Gy. The exIMRT plan meets all objectives apart from the objective of 1cc of the spinal cord PRV to ≤5Gy, which is just over at 5.1Gy, and the dose to 5% of the PTV which is just over the 63Gy tolerance at 63.5Gy. Representative dose distributions and DVHs are shown in Figure 6.10 and Figure 6.11 respectively. The exIMRT plan is able to match the Monaco ssIMRT plan for target coverage and low dose to the spinal cord but not without some dose from the X-ray photon component passing through the mandible. Having a very low objective on the spinal cord limits the amount of coverage achievable with the electron component and some X-ray dose is required to boost dose in the electron dose fall off region. As this X-ray dose is only required at the distal edge of the PTV some sparing of the mandible is achieved and the mean dose is reduced by 20.8% from 19.7Gy to 15.6Gy. The maximum dose to the mandible is not reduced as this is limited by the overlap between the mandible and the PTV. As with Case 1, 2 and 3 the xIMRT plan is slightly more conformal than the clinical IMRT plan and mean dose to the mandible is only reduced by 12.3% to 17.8Gy (see Figure 6.12). In addition the dose to the spinal cord is actually lower for the xIMRT plan than for the exIMRT plan, with 1cc of the spinal cord PRV receiving 3.3Gy compared to 5.1Gy.

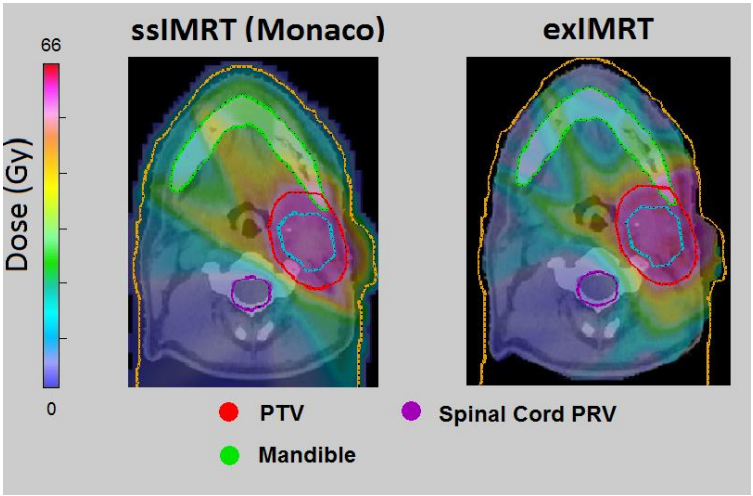

Figure 6.10 Case 4: Dose distribution on the isocentre slice for head and neck re-treatment plan in the axial plane for Monaco 6MV ssIMRT (left) and exIMRT (right) treatment plans.

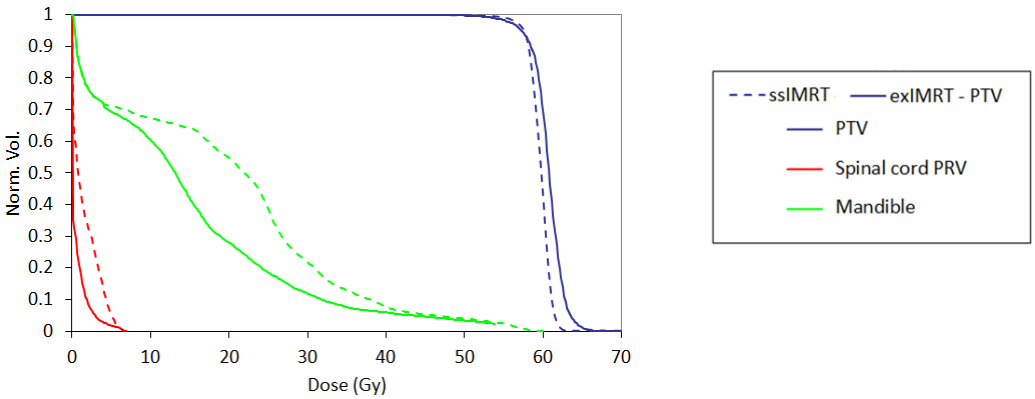

Figure 6.11 Case 4: DVH for head and neck re-treatment plan Monaco 6MV ssIMRT and exIMRT treatment plans.

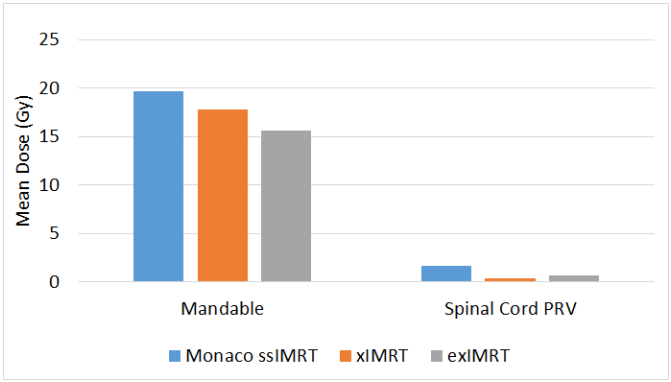

Figure 6.12 Case 4: OAR mean doses for Monaco 6MV ssIMRT, xIMRT and exIMRT treatment plans.

The dose to the mandible could be reduced further but only with some compromise in PTV coverage. A second plan was produced with a single direct mixed X-ray and MERT field. With no fields passing through the mandible this single field plan has a mean mandible dose of 8.2Gy. The PTV coverage is however reduced to 95% of the PTV volume receiving 50.1Gy (not 57Gy as required). The CTV is covered by the 90% isodose dose. This compromise could conceivably be clinically acceptable in a situation where mandible dose is a priority.

6.5. Radiobiology

The EUD for the PTV and the NTCP for relevant OAR have been calculated for all four cases above. For the PTV EUD a nominal value of a =-10 has been used as described in the report

of TG-66 for the comparison of planning systems (Allen Li et al., 2012). For NTCP an attempt has been made to find the most relevant data for each organ with the default being the LKB model with Emami-Burman parameters if no other values were found (Burman et al., 1991). Details of the models and parameters used have been provided in Appendix C.

6.5.1. Radiobiology: Case 1

For Case 1 the target coverage and uniformity of dose within the PTV with exIMRT is much the same as for the Monaco ssIMRT plan leading to similar values of EUD for the PTV. There is a reduction in the low dose wash leading to a reduction in EUD for the OAR with exIMRT. However, the dose received by these organs is already low and the predicted NTCP using the LKB model and Emami-Burman parameters is < 0.001 for all OAR with both ssIMRT and exIMRT (see Table 6.2).

Table 6.2 Radiobiology: Case 1

	ssIMRT (Monaco)	exIMRT	Ratio
	EUD		
PTV	59.02	59.51	1.01
Rt Kidney	8.36	2.12	0.25
Liver	4.03	0.29	0.07
	NTCP		
all OAR	<0.001	<0.001	-

6.5.2. Radiobiology: Case 2

In Case 2, as with Case, the target coverage and uniformity of dose with the PTV achieved with exIMRT is similar to that of the Monaco VMAT plan leading to similar values of EUD for the PTV. The EUD for the brain as a whole is reduced with exIMRT due to a reduction in low dose outside the PTV. Similar to the previous case the NTCP using the LKB model and Emami-Burman parameters is < 0.001 for both the VMAT and exIMRT plans (see Table 6.3).

Table 6.3 Radiobiology: Case 2

	VMAT (Monaco)	exIMRT	Ratio
	EUD		
PTV	59.75	59.43	0.99
Brain	20.47	4.62	0.23
	NTCP		
Brain	<0.001	<0.001	-

6.5.3. Radiobiology: Case 3

For Case 3 there are some differences in the distribution of dose within the PTV with the exIMRT plan leading to differences in EUD. In the tumour bed PTV there is an increase in cold spots but also an increase in hot spots resulting in higher EUD for exIMRT. In the whole breast volume there is a small reduction in EUD due to a reduction in coverage with the exIMRT plan.

A common side effect of breast radiotherapy is fibrosis. Modern radiotherapy attempts to reduce hot spots within the treated volume to try to minimise the risk of fibrosis. The impact of exIMRT on fibrosis risk should therefore be considered. The probability of fibrosis has been studied in detail in (Mukesh et al., 2013) by fitting NTCP curves to data from two trials and testing the models against data from a third trial. The best fit parameters from these curves have been used in this work to calculate a NTCP for the whole breast volume. Although there is an increase in hotspots with the tumour bed volume with exIMRT the EUD for the breast volume as a whole is lower for the exIMRT plan resulting in a reduction in NTCP.

One of the aims of breast radiotherapy is to minimise the dose to lung tissue in order to minimise the risk of radiation induced pneumonitis. There are a number of published models describing the risk of pneumonitis associated with breast cancer as outlined in a review by Svolos et al. (Svolos et al., 2011). In this work the model described in (Rancati et al., 2007) is used as it predicts the highest probability of complications. Using the parameters from (Rancati et al., 2007) the risk of Grade >=1 pneumonitis for the ipsilateral breast have been calculated. The exIMRT plan demonstrates a risk relative to the ssIMRT plan of 0.36, or 36% of the risk with the IMRT plan. Using the model in (Seppenwoolde et al., 2003) for the lung as a paired organ gives a much

lower absolute risk of Grade >=2 pneumonitis but with a similar reduction for exIMRT with a relative risk value of 0.36 (see Table 6.4).

The risk of cardiac mortality has been predicted using the relative seriality model suggested by Gagliardi (Gagliardi et al., 2000). Although the EUD for the Heart is reduced with exIMRT the calculated NTCP with both ssIMRT and exIMRT for this plan is already very low, <0.001, so a relative reduction is not relevant.

Table 6.4 Radiobiology: Case 3

	ssIMRT (Monaco)	exIMRT	Ratio
	EUD		
PTVtb	41.94	52.26	1.25
PTVpb-tb	40.69	40.72	1.00
PTVwb-pb	37.12	33.13	0.89
Ipsilateral lung	5.40	3.37	0.62
Lung paired organ	3.07	2.66	0.87
Heart	1.76	0.20	0.11
	NTCP		
PTVwb	0.105	0.086	0.82
Ipsilateral lung	0.031	0.014	0.36
Lung paired organ	0.007	0.004	0.37
Heart	<0.001	<0.001	-

6.5.4. Radiobiology: Case 4

For Case 4 the target coverage and uniformity of dose within the PTV with exIMRT is similar to that observed for the Monaco ssIMRT plan, leading to similar EUD for the PTV. The most clinically relevant issue associated with this treatment is the risk of osteoradionecrosis to the mandible. As this is a retreatment this will be the cumulative effect of this treatment and the original treatment. The cumulative effect has been estimated by assuming a uniform 30Gy dose wash to the mandible from the original 60Gy treatment. The total dose has therefore been calculated as the retreatment plan dose plus 30Gy. Using the LKB model and Emami-Burman values this leads to high complication probability with both methods but with exIMRT it is reduced by a factor of 0.72 (see Table 6.5).

Table 6.5 Radiobiology: Case 4

	ssIMRT (Monaco)	exIMRT	Ratio
	EUD		
PTV	59.68	60.84	1.02
	NTCP		
(Inc. 60Gy previous treatment)			
Mandible	0.813	0.584	0.72

6.5.5. Conformity and Malignant induction probability (MIP)

One of the aims of exIMRT is to minimise the exit dose from IMRT to reduce dose wash and improve conformity. This effect has been examined by calculating the conformity index (CI) defined as the ratio between the target volume and the volume irradiated to a certain dose level (Knöös et al., 1998). The CI is typically greater than 1, with values closest to 1 being the most conformal. CI is often used to describe the conformity of the 95% dose isodose to the PTV. The interest of this study is to determine where the improvement in conformity lies. Therefore, CI has been calculated for the 95% and 50% of the prescribed dose and at fixed dose levels of 20, 10, 5 and 2 Gy (see Table 6.6).

For Cases 1, 2 and 3 the conformity of the 95% isodose for the Monaco plan and the exIMRT plan is similar with less than 0.1 difference in CI. For Cases 1 and 2 the conformity of the 50% isodose is improved with exIMRT as is the conformity of the 20, 10, 5 and 2Gy dose levels with the relative improvement increasing at the lower dose levels. There is a relatively high low dose wash for the VMAT plan of Case 1 leading to the biggest improvement with exIMRT with CI_2 reduced from 24.75 to 8.14.

Case 3 is different to Case 1 and 2 in that the limitations of using the electron as a boost with fixed tangential fields leads to less of an improvement in conformity. There is some improvement in CI for the lowest dose levels for Case 2 with CI_2 reduced from 4.23 to 2.32.

Case 4 has not been included in this analysis as the improvement of conformity was not one of the aims of that planning study.

Table 6.6 Conformity index for clinical Case 1, 2 and 3

	Case 1		Case 2		Case 3	
Dose Level (Gy)	VMAT (Monaco)	exIMRT	VMAT (Monaco)	exIMRT	ssIMRT (Monaco)	exIMRT
95%	1.19 (57Gy)	1.10 (57Gy)	1.00 (57Gy)	1.02 (57Gy)	1.24 (32.4)	1.22 (32.4)
50%	2.88 (30Gy)	2.04 (30Gy)	1.53 (30Gy)	1.22 (30Gy)	-	-
20	4.47	2.57	4.38	2.13	1.61	1.53
10	8.53	4.82	6.26	2.81	1.94	1.67
5	15.28	5.40	6.78	3.58	2.47	1.81
2	24.75	8.14	7.41	5.28	4.23	2.21

It hypothesised that this improvement in conformity with exIMRT could result in a corresponding reduction in the probability of secondary cancer induction. In order to assess this effect the malignant induction probability (MIP) has been calculated according to the method of Timlin et al. (Timlin et al., 2011, Timlin et al., 2015). With reference to the work of Timlin et al. values of alpha = 0.09 and beta = 0.03 have been used in Cases 1 and 2 to give an alpha/beta = 3 whereas in Case 2 values of alpha = 0.06 and beta = 0.04 have been used. Details of the MIP calculation are given in Appendix C. The absolute value of MIP depends on parameters that must be tuned to clinical data for secondary cancer induction and should therefore be used with caution. Of most interest is the relative MIP value (relMIP). The relMIP is only weekly dependent on the model and parameters used (Timlin et al., 2011) so it is more useful for comparing similar plans. With exIMRT the relMIP is less than 1 in all cases and between 0.20 and 0.67 (see Table 6.7).

Table 6.7 Relative Malignant Induction Probability (relMIP) for exIMRT compared to the Monaco IMRT/VMAT plan

	relMIP
Case 1	
Liver	0.24
Kidney	0.49
Case 2	
Brain	0.67
Case 3	
Ipsilateral lung	0.64
Contralateral lung	0.20
Contralateral breast	0.35

6.5.6. Discussion and conclusion

In each of the four cases studied here the exIMRT technique was able to produce good quality plans that met the dose constraints. In all cases these exIMRT plans were able to reduce the dose to OAR when compared to the clinical Monaco 6MV IMRT or VMAT plan. In particular, on average, a mean dose reduction between 59.3% and 76.3% was observed. This comparison is perhaps optimistic resulting from the use of idealised X-ray photon intensity in the exIMRT plan, however, comparison with an idealised X-ray only still revealed OAR mean dose reduction of 45.6% to 66.1%. This suggest that a reduction in OAR dose distal to the target of around 50% is achievable with exIMRT.

As dose to these OAR is already low the actual clinical impact of exIMRT may also be low. The calculated NTCP is in most cases already small therefore the relative improvement is not clinically significant. However, calculations with the latest models for pneumonitis in breast cancer reveal a NTCP that is 36% of that for the standard plan. With future improvements to the sensitivity of NTCP models it might be possible to realise similar improvements in other cases.

As the dose gradient for the electron field is limited some X-ray photon dose may be required to boost dose at the distal edge of the PTV. This effect leads to streaking in Case 2 and to the requirement of X-ray beams through the mandible in Case 4. This however assumes no change to the PTV for exIMRT. True robust planning, rather than the use of planning target volumes, may yield further improvements due to the insensitivity of changes to the electron dose to movement along the field direction.

The greatest improvement with exIMRT in this study is the reduction of the low dose, seen as improvement in the conformity index at the 20Gy to 2Gy level. This is potentially associated with a relative reduction in secondary cancer induction as demonstrated by a relMIP of 20% to 67% for the exIMRT plans.

This study shows just four examples of possible applications of the exIMRT technique to carefully selected clinical cases. Although results are encouraging a full planning study would be required in order to determine conclusively whether or not the improvements with exIMRT over standard IMRT and VMAT are statistically significant.

Chapter 7

General conclusions and further research perspectives

This final chapter presents the overall conclusions that can be drawn from this research and suggests some of the future work that may follow-on from it.

7.1. General conclusions

The research described in this thesis aimed to answer the following question posed in Chapter 1:

- Is an isocentric combined X-ray and electron therapy treatment possible with no modifications to equipment and can it be used to improve radiotherapy dose distributions?

The first contribution of this work towards answering this question is the proposition that the linac is run in scattering foil free mode. Through measurement it has been demonstrated that improvements to dosimetry by removal of the scattering foils would allow delivery with xMLC without reducing SSD making a single isocentre and synergistic delivery of the electron and photon components a practical proposition.

The second contribution of this work is the demonstration that the dose distribution from the scattering foil free electron beam can be accurately calculated using Monte Carlo dose

calculations. The accuracy of Monte Carlo calculations for electron dose distributions is well established. In this study it has additionally been shown that the dose at extended SSD for small fields collimated with the xMLC can be accurately calculated by correctly accounting for the jaws and MLC and scatter in the air gap between the MLC and the patient.

The third contribution of this work is in the development of a two stage optimisation procedure to take advantage of the electron component of the mixed modality beam. In development of the optimisation routine a number of properties of the mixed modality plan have been highlighted. The issue of matching electron fields with effective widths greater than their geometric widths has been examined. The benefit of leaving gaps between electron segments was demonstrated and it was shown that by introducing gaps and optimising the field a uniform dose distribution can be built up in the central part of the electron field. It has been shown that these gaps are also useful when matching dissimilar energies and that the optimal way to combine multiple energies is by free optimisation rather than pre-determined selection by range. The option of overlapping matrices to produce a feathering effect was considered but found to provide only a small benefit for a large increase in computational time. Optimising the mixed modality treatment plan lead to multiple local minima dependent on the initial proportion of electron dose contribution. Using an 85% proportion of electrons relative to the total dose was found to be optimal. Optimisation of the mixed modality 'exIMRT' plan for geometric phantom demonstrated a potential improvement in OAR dose with the technique

The fourth contribution of this work is in demonstrating the clinical application of the exIMRT technique to clinical situations. For the four cases chosen the exIMRT technique has been shown to be able to reduce dose to organs at risk with the average improvement in mean dose between 45.6% and 76.3% using exIMRT. The absolute dose to these OAR is already low and the optimised clinical plan NTCP calculations, in most cases, produced a negligible value. It was however possible to identify a significant reduction in the relative risk of pneumonitis for the breast case, i.e. 0.36 with exIMRT. In all cases no appreciable change in target EUD was seen with exIMRT. A reduction in the low dose wash with exIMRT was converted to a relMIP value of between 0.20 and 0.67. This suggests that some reduction in the probability of secondary cancer induction is possible with exIMRT.

In summary this work has shown that an isocentric combined X-ray and electron therapy treatment is possible with no modifications to equipment and can potentially be used to improve radiotherapy dose distributions. In particular, exIMRT appears promising as a method to reduce the low dose wash with a corresponding reduction in secondary cancer risk for treatment sites close to the surface including breast, sarcoma and superficial brain treatments.

7.2. Further research perspectives

Although the results of this study are encouraging there are a number of questions that remain to be answered before exIMRT is put into clinical practice. These further research perspectives are described in the following sections.

7.2.1. Robustness

Throughout this study the concept of the planning target volume (PTV) has been used. The PTV is defined to take into consideration the net effect of all possible geometrical variation from the clinical target volume (CTV). The PTV includes a margin to account for set up uncertainties including patient positioning and patient movement during treatment. The effect of patient movement in particular may be different for exIMRT when compared to IMRT. Movement of the patient along the axis of the electron beam direction will result in less of a change in dose distribution than if the patient were moved within a uniformly distributed IMRT X-ray dose distribution. This effect could be beneficial in that perhaps PTV margins can be reduced at the distal edge of the PTV. However, the effect could also be problematic if it results in a mismatch with the X-ray field component. It is suggested that a study is required to artificially introduce geometric shifts into exIMRT plans to investigate their robustness to patient movement.

In addition to patient movement the robustness to air density should be studied. Henzen et al. (Henzen et al. 2014) suggest that changes in the order of 3% are possible due to the variation in scatter conditions with air density changes due to fluctuations in atmospheric pressure. Some of these variations would be accounted for by the output monitoring of the linac ionisation chamber. It is suggested therefore that robustness to air density for exIMRT is studied and should include measurement as well as modelling.

7.2.2. Planning studies

As part of this work clinical examples have been used to demonstrate the potential benefits of the exIMRT technique. Now for each treatment site of interest a full planning study is required to prove whether the exIMRT technique is statistically an improvement over standard techniques. Selecting multiple patients each with different characteristics would provide a more complete test of the technique

7.2.3. Clinical implementation and validation

Clinical implemented of the exIMRT requires further work in a number of areas. First a clinical implementation of the exIMRT treatment planning system would be required. This clinical exIMRT treatment planning system would include segmentation of the X-ray component and MU calculation and sequencing of the electron component. The system would also have to be integrated with the treatment machine record and verify system in order to deliver the exIMRT plan. Once a deliverable plan was achievable additional work is required to verify the accuracy of the treatment plan. Verification of the delivered dose distribution could be achieved either with radiochromic film measurements or with gel dosimetry. Calculation of dose to the skin from exIMRT should be verified with thermoluminescent dosimeters (TLD) placed on the surface of a phantom.

Additional work would then be required in order to integrate routine calibration of the scattering foil electron beam into clinical practice. It is likely that this would require each scattering foil free energy to be considered as a separate energy which would undergo calibration according to the electron codes of practice (Thwaites et al., 2003). Routine use of exIMRT would also require some form of pre-treatment quality control check of the calculated dosimetry. This check would be complicated by the fact that it is not possible to extract information from the exit beam of the electron component as is done with the X-ray component. Radiochromic film or gel dosimetry would be an option but would be difficult to implement efficiently in practice. Possible alternatives include measurement of the intensity maps for individual beams at shallow depths, measurement using a multi-layered ionisation chamber, independent calculation of dose distributions or some combination of these methods. Note that this issue is also applicable to proton therapy such that research into quality control methods for proton therapy may have overlap with work for exIMRT.

References

Ahnesjö, A., Saxner, M. and Trepp, A. (1992) 'A pencil beam model for photon dose calculation', *Med Phys,* 19(2), pp. 263-73.

Al-Yahya, K., Schwartz, M., Shenouda, G., Verhaegen, F., Freeman, C. and Seuntjens, J. (2005) 'Energy modulated electron therapy using a few leaf electron collimator in combination with IMRT and 3D-CRT: Monte Carlo-based planning and dosimetric evaluation', *Med Phys,* 32(9), pp. 2976-86.

Allen Li, X., Alber, M., Deasy, J. O., Jackson, A., Ken Jee, K. W., Marks, L. B., Martel, M. K., Mayo, C., Moiseenko, V., Nahum, A. E., Niemierko, A., Semenenko, V. A. and Yorke, E. D. (2012) 'The use and QA of biologically related models for treatment planning: short report of the TG-166 of the therapy physics committee of the AAPM', *Med Phys,* 39(3), pp. 1386-409.

Ardenfors, O., Josefsson, D. and Dasu, A. (2014) 'Are IMRT treatments in the head and neck region increasing the risk of secondary cancers?', *Acta Oncol,* 53(8), pp. 1041-7.

Arvold, N. D., Niemierko, A., Broussard, G. P., Adams, J., Fullerton, B., Loeffler, J. S. and Shih, H. A. (2012) 'Projected second tumor risk and dose to neurocognitive structures after proton versus photon radiotherapy for benign meningioma', *Int J Radiat Oncol Biol Phys,* 83(4), pp. e495-500.

Asell, M., Hyödynmaa, S., Söderström, S. and Brahme, A. (1999) 'Optimal electron and combined electron and photon therapy in the phase space of complication-free cure', *Phys Med Biol,* 44(1), pp. 235-52.

Barton, M. B., Gebski, V., Manderson, C. and Langlands, A. O. (1995) 'Radiation therapy: are we getting value for money?', *Clin Oncol (R Coll Radiol),* 7(5), pp. 287-92.

Bazalova-Carter, M., Qu, B., Palma, B., Hårdemark, B., Hynning, E., Jensen, C., Maxim, P. G. and Loo, B. W. (2015) 'Treatment planning for radiotherapy with very high-energy electron beams and comparison of VHEE and VMAT plans', *Med Phys,* 42(5), pp. 2615-25.

Bentzen, S. M., Constine, L. S., Deasy, J. O., Eisbruch, A., Jackson, A., Marks, L. B., Ten Haken, R. K. and Yorke, E. D. (2010) 'Quantitative Analyses of Normal Tissue Effects in the Clinic (QUANTEC): an introduction to the scientific issues', *Int J Radiat Oncol Biol Phys,* 76(3 Suppl), pp. S3-9.

Berger, M. (1964) 'Monte Carlo calculation of the penetration and diffusion of fast charged particles.', *Methods in Computational Physics,* 1.

Bjarngard, B. E., Piontek, R. W. and Svensson, G. K. (1976) 'Electron scattering and collimation system for a 12-MeV linear accelerator', *Med Phys,* 3(3), pp. 153-8.

Bliss, J. (2015) *IMPORT HIGH*. Available at: http://www.icr.ac.uk/our-research/our-research-centres/clinical-trials-and-statistics-unit/clinical-trials/import_high.

Bloquist, M., Karlsson, M. G., Zackrisson, B., Karlsson, M. (2002) 'Multileaf collimation of electrons – clinical effects on electron energy modulation and mixed beam therapy depending on treatment head design', *Phys. Med Biol,* 47(7), pp. 1013-24.

Bortfeld, T. (1999) 'Optimized planning using physical objectives and constraints', *Semin Radiat Oncol,* 9(1), pp. 20-34.

Bortfeld, T. (2006) 'IMRT: a review and preview', *Phys Med Biol,* 51(13), pp. R363-79.

Bortfeld, T., Bürkelbach, J., Boesecke, R. and Schlegel, W. (1990) 'Methods of image reconstruction from projections applied to conformation radiotherapy', *Phys Med Biol,* 35(10), pp. 1423-34.

Brown, A. P., Barney, C. L., Grosshans, D. R., McAleer, M. F., de Groot, J. F., Puduvalli, V. K., Tucker, S. L., Crawford, C. N., Khan, M., Khatua, S., Gilbert, M. R., Brown, P. D. and Mahajan, A. (2013) 'Proton beam craniospinal irradiation reduces acute toxicity for adults with medulloblastoma', *Int J Radiat Oncol Biol Phys,* 86(2), pp. 277-84.

Burman, C., Kutcher, G. J., Emami, B. and Goitein, M. (1991) 'Fitting of normal tissue tolerance data to an analytic function', *Int J Radiat Oncol Biol Phys,* 21(1), pp. 123-35.

Butson, M. J., Mathur, J. N. and Metcalfe, P. E. (1997) 'Skin dose from radiotherapy X-ray beams: the influence of energy', *Australas Radiol,* 41(2), pp. 148-50.

Cai, S. Y., Chao, T. C., Lin, M. J., Tung, C. J. and Lee, C. C. (2015) 'Depth dose characteristics of proton beams within therapeutic energy range using the particle therapy simulation framework (PTSim) Monte Carlo technique', *Biomed J,* 38(5), pp. 408-13.

Cashmore, J. (2008) 'The characterization of unflattened photon beams from a 6 MV linear accelerator', *Phys Med Biol,* 53(7), pp. 1933-46.

Chang, S. X., Cullip, T. J., Rosenman, J. G., Halvorsen, P. H. and Tepper, J. E. (2002) 'Dose optimization via index-dose gradient minimization', *Med Phys,* 29(6), pp. 1130-46.

Cheng, C. W. and Das, I. J. (1999) 'Treatment plan evaluation using dose-volume histogram (DVH) and spatial dose-volume histogram (zDVH)', *Int J Radiat Oncol Biol Phys,* 43(5), pp. 1143-50.

Coleman, T. F. and Li, Y. (2006) 'A Reflective Newton Method for Minimizing a Quadratic Function Subject to Bounds on Some of the Variables', *http://dx.doi.org/10.1137/S1052623494240456*.

Connell, T., Alexander, A., Evans, M. and Seuntjens, J. (2012) 'An experimental feasibility study on the use of scattering foil free beams for modulated electron radiotherapy', *Phys Med Biol,* 57(11), pp. 3259-72.

Cotrutz, C., Lahanas, M., Kappas, C. and Baltas, D. (2001) 'A multiobjective gradient-based dose optimization algorithm for external beam conformal radiotherapy', *Phys Med Biol,* 46(8), pp. 2161-75.

Craft, D., Bangert, M., Long, T., Papp, D. and Unkelbach, J. (2014) 'Shared data for intensity modulated radiation therapy (IMRT) optimization research: the CORT dataset', *Gigascience,* 3(1), pp. 37.

Das, S. K., Bell, M., Marks, L. B. and Rosenman, J. G. (2004) 'A preliminary study of the role of modulated electron beams in intensity modulated radiotherapy, using automated beam orientation and modality selection', *Int J Radiat Oncol Biol Phys,* 59(2), pp. 602-17.

Davidson, S., Kirsner, S., Mason, B., Kisling, K., Barrett, R. D., Bonetati, A. and Ballo, M. T. (2015) 'Dosimetric impact of setup accuracy for an electron breast boost technique', *Pract Radiat Oncol,* 5(5), pp. e499-504.

de Boer, S. F., Kumek, Y., Jaggernauth, W. and Podgorsak, M. B. (2007) 'The effect of beam energy on the quality of IMRT plans for prostate conformal radiotherapy', *Technol Cancer Res Treat,* 6(2), pp. 139-46.

de Moor, J. S., Mariotto, A. B., Parry, C., Alfano, C. M., Padgett, L., Kent, E. E., Forsythe, L., Scoppa, S., Hachey, M. and Rowland, J. H. (2013) 'Cancer survivors in the United States: prevalence across the survivorship trajectory and implications for care', *Cancer Epidemiol Biomarkers Prev,* 22(4), pp. 561-70.

De Santis, M. C., Nardone, L., Diletto, B., Canna, R., Dispinzieri, M., Marino, L., Lozza, L. and Valentini, V. (2016) 'Comparison of two radiation techniques for the breast boost in patients undergoing neoadjuvant treatment for breast cancer', *Br J Radiol,* 89(1066), pp. 20160264.

Deasy, J., O (2005) *CERR: A computational environment for radiotherapy research*. Available at: http://www.cerr.info/ (Accessed: 25/08/16 2016).

Deasy, J. O., Blanco, A. I. and Clark, V. H. (2003) 'CERR: a computational environment for radiotherapy research', *Med Phys,* 30(5), pp. 979-85.

Dennis, E. R., Bussiere, M. R., Niemierko, A., Lu, M. W., Fullerton, B. C., Loeffler, J. S. and Shih, H. A. (2013) 'A comparison of critical structure dose and toxicity risks in patients with low grade gliomas treated with IMRT versus proton radiation therapy', *Technol Cancer Res Treat,* 12(1), pp. 1-9.

Dias, J., Rocha, H., Ventura, T., Ferreira, B. and Lopes, M. o. C. (2016) 'Automated fluence map optimization based on fuzzy inference systems', *Med Phys,* 43(3), pp. 1083-95.

DOH (2012) *National Proton Beam Therapy Service Development Programme*. Available at: https://www.gov.uk/government/uploads/system/uploads/attachment_data/file/213045/national-

proton-beam-therapy-service-development-programme-value-for-money-addendum.pdf (Accessed: July 2016).

du Plessis, F. C., Leal, A., Stathakis, S., Xiong, W. and Ma, C. M. (2006) 'Characterization of megavoltage electron beams delivered through a photon multi-leaf collimator (pMLC)', *Phys Med Biol,* 51(8), pp. 2113-29.

Eldib, A., Jin, L., Li, J. and Ma, C. M. (2014) 'Investigation of the clinical potential of scattering foil free electron beams', *Phys Med Biol,* 59(4), pp. 819-36.

Eley, J. G., Hogstrom, K. R., Matthews, K. L., Parker, B. C. and Price, M. J. (2011) 'Potential of discrete Gaussian edge feathering method for improving abutment dosimetry in eMLC-delivered segmented-field electron conformal therapy', *Med Phys,* 38(12), pp. 6610-22.

Emami, B., Lyman, J., Brown, A., Coia, L., Goitein, M., Munzenrider, J. E., Shank, B., Solin, L. J. and Wesson, M. (1991) 'Tolerance of normal tissue to therapeutic irradiation', *Int J Radiat Oncol Biol Phys,* 21(1), pp. 109-22.

Engel, K. and Gauer, T. (2009) 'A dose optimization method for electron radiotherapy using randomized aperture beams', *Phys Med Biol,* 54(17), pp. 5253-70.

Ezzell, G. A. (1996) 'Genetic and geometric optimization of three-dimensional radiation therapy treatment planning', *Med Phys,* 23(3), pp. 293-305.

Gagliardi, G., Bjöhle, J., Lax, I., Ottolenghi, A., Eriksson, F., Liedberg, A., Lind, P. and Rutqvist, L. E. (2000) 'Radiation pneumonitis after breast cancer irradiation: analysis of the complication probability using the relative seriality model', *Int J Radiat Oncol Biol Phys,* 46(2), pp. 373-81.

Gentry, J. R., Steeves, R. and Paliwal, B. A. (2006) 'Inverse planning of energy-modulated electron beams in radiotherapy', *Med Dosim,* 31(4), pp. 259-68.

Gilio, J. P. (1998) 'Tabu search: An automatic treatment planning algorithm for conformal radiotherapy', *Medical Physics,* 25(5), pp. 796-796.

Giovannini, G., Böhlen, T., Cabal, G., Bauer, J., Tessonnier, T., Frey, K., Debus, J., Mairani, A. and Parodi, K. (2016) 'Variable RBE in proton therapy: comparison of different model predictions and their influence on clinical-like scenarios', *Radiat Oncol,* 11, pp. 68.

Goldman, S. P., Chen, J. Z. and Battista, J. J. (2005) 'Feasibility of a fast inverse dose optimization algorithm for IMRT via matrix inversion without negative beamlet intensities', *Med Phys,* 32(9), pp. 3007-16.

Greene-Schloesser, D., Robbins, M. E., Peiffer, A. M., Shaw, E. G., Wheeler, K. T. and Chan, M. D. (2012) 'Radiation-induced brain injury: A review', *Front Oncol,* 2, pp. 73.

Haas, O. C., Burnham, K. J. and Mills, J. A. (1998) 'Optimization of beam orientation in radiotherapy using planar geometry', *Phys Med Biol,* 43(8), pp. 2179-93.

Hall, E. J. and Wuu, C. S. (2003) 'Radiation-induced second cancers: the impact of 3D-CRT and IMRT', *Int J Radiat Oncol Biol Phys,* 56(1), pp. 83-8.

Henzen, D., Manser, P., Frei, D., Volken, W., Neuenschwander, H., Born, E. J., Vetterli, D., Chatelain, C., Stampanoni, M. F. and Fix, M. K. (2014) 'Monte Carlo based beam model using a photon MLC for modulated electron radiotherapy', *Med Phys,* 41(2), pp. 021714.

Hogstrom, K. R. and Almond, P. R. (2006) 'Review of electron beam therapy physics', *Phys Med Biol,* 51(13), pp. R455-89.

Hogstrom, K. R., Boyd, R. A., Antolak, J. A., Svatos, M. M., Faddegon, B. A. and Rosenman, J. G. (2004) 'Dosimetry of a prototype retractable eMLC for fixed-beam electron therapy', *Med Phys,* 31(3), pp. 443-62.

Hristov, D., Stavrev, P., Sham, E. and Fallone, B. G. (2002) 'On the implementation of dose-volume objectives in gradient algorithms for inverse treatment planning', *Med Phys,* 29(5), pp. 848-56.

Hu, A., Song, H., Chen, Z., Zhou, S. and Yin, F. (2008) *Evaluation of an electron Monte Carlo dose calculation algorithm for electron beam. 2008*.

Huang, J. Y., Followill, D. S., Wang, X. A. and Kry, S. F. (2013) 'Accuracy and sources of error of out-of field dose calculations by a commercial treatment planning system for intensity-modulated radiation therapy treatments', *J Appl Clin Med Phys,* 14(2), pp. 4139.

Hyödynmaa, S., Gustafsson, A. and Brahme, A. (1996) 'Optimization of conformal electron beam therapy using energy- and fluence-modulated beams', *Med Phys,* 23(5), pp. 659-66.

IAEA430 (2004)*: Commissioning and Quality Assurance of Computerized Planning Systems for Radiation Treatment of Cancer*: International atomic energy agency, Vienna (TRS 430).

ICRU44 (1989) *Tissue substitutes in radiation dosimetry and measurement.* Bethesda, Md., U.S.A.: International Commission on Radiation Units and Measurements.

ICRU50 (1993) *Prescribing, recording and reporting photon bem therapy : issued: 1 September 1993.* Bethesda, Md.: International Commission on Radiation Units and Measurements.

ICRU62 (1999) *Prescribing, recording and reporting photon beam therapy : (supplement to CRU report 50).* Bethesda, Md.: International Commission on Radiation Units and Measurements.

ICRU83 (2010) *Prescribing, recording, and reporting photon-beam intensity-modulated radiation therapy (IMRT).* Oxford: Oxford University Press.

IEC977 (1989)*: Medical electron accelerators-functional performance characteristics*: International Electrotechnical Commission, Geneva (IEC publication 977).

Israelski, E. W. and Muto, W. H. (2004) 'Human factors risk management as a way to improve medical device safety: a case study of the therac 25 radiation therapy system', *Jt Comm J Qual Saf,* 30(12), pp. 689-95.

James H, Beavis A, Budgell G et al (2008) 'IPEM Report 96: Guidance for the Clinical Implementation of Intensity Modulated Radiation Therapy', York, Institute of Physics and Engineering in Medicine

Jin, L., Ma, C. M., Fan, J., Eldib, A., Price, R. A., Chen, L., Wang, L., Chi, Z., Xu, Q., Sherif, M. and Li, J. S. (2008) 'Dosimetric verification of modulated electron radiotherapy delivered using a photon multileaf collimator for intact breasts', *Phys Med Biol,* 53(21), pp. 6009-25.

Jones, B. (2008) 'The potential clinical advantages of charged particle radiotherapy using protons or light ions', *Clin Oncol (R Coll Radiol),* 20(7), pp. 555-63.

Karaboga, D. and Basturk, B. (2007) 'A powerful and efficient algorithm for numerical function optimization: artificial bee colony (ABC) algorithm', *Journal of global optimization,* 39(3), pp. 459-471.

Karlsson, M., Nyström, H., Svensson, H. (1992) 'Electon beam charactersitics of the 50-MeV racetrack microtron', *Med Phys* 19(2), pp 307-15.

Karlsson, M. and Zackrisson, B. (1997) 'Exploration of new treatment modalities offered by high energy (up to 50 MeV) electrons and photons', *Radiother Oncol,* 43(3), pp. 303-9.

Karlsson, M. G., Karlsson, M., Ma .C. (1999) 'Treatment head design for multileaf collimated high-energy electrons', *Med Phys* 26(10), pp 2161-7.

Karmarkar, N. (1984) 'A new polynomial-time algorithm for linear programming', *Combinatorica,* 4, pp. 373-395.

Kawrakow, I. (2000) 'Accurate condensed history Monte Carlo simulation of electron transport. I. EGSnrc, the new EGS4 version', *Med Phys,* 27(3), pp. 485-98.

Kawrakow, I., Fippel, M. and Friedrich, K. (1996) '3D electron dose calculation using a Voxel based Monte Carlo algorithm (VMC)', *Med Phys,* 23(4), pp. 445-57.

Kirkpatrick, S., Gelatt, C. D. and Vecchi, M. P. (1983) 'Optimization by simulated annealing', *Science,* 220(4598), pp. 671-80.

Klein, E. E., Li, Z. and Low, D. A. (1996) 'Feasibility study of multileaf collimated electrons with a scattering foil based accelerator', *Radiother Oncol,* 41(2), pp. 189-96.

Klein, E. E., Mamalui-Hunter, M. and Low, D. A. (2009) 'Delivery of modulated electron beams with conventional photon multi-leaf collimators', *Phys Med Biol,* 54(2), pp. 327-39.

Klein, E. E., Vicic, M., Ma, C. M., Low, D. A. and Drzymala, R. E. (2008) 'Validation of calculations for electrons modulated with conventional photon multileaf collimators', *Phys Med Biol,* 53(5), pp. 1183-208.

Knöös, T., Wieslander, E., Cozzi, L., Brink, C., Fogliata, A., Albers, D., Nyström, H. and Lassen, S. (2006) 'Comparison of dose calculation algorithms for treatment planning in external photon beam therapy for clinical situations', *Phys Med Biol*, 51(22), pp. 5785-807.

Korevaar, E. W., Heijmen, B. J., Woudstra, E., Huizenga, H. and Brahme, A. (1999) 'Mixing intensity modulated electron and photon beams: combining a steep dose fall-off at depth with sharp and depth-independent penumbras and flat beam profiles', *Phys Med Biol*, 44(9), pp. 2171-81.

Korevaar, E. W., Huizenga, H., Löf, J., Stroom, J. C., Leer, J. W. and Brahme, A. (2002) 'Investigation of the added value of high-energy electrons in intensity-modulated radiotherapy: four clinical cases', *Int J Radiat Oncol Biol Phys*, 52(1), pp. 236-53.

Kry, S. F., Titt, U., Pönisch, F., Vassiliev, O. N., Salehpour, M., Gillin, M. and Mohan, R. (2007) 'Reduced neutron production through use of a flattening-filter-free accelerator', *Int J Radiat Oncol Biol Phys*, 68(4), pp. 1260-4.

Kudchadker, R. J., Hogstrom, K. R., Garden, A. S., McNeese, M. D., Boyd, R. A. and Antolak, J. A. (2002) 'Electron conformal radiotherapy using bolus and intensity modulation', *Int J Radiat Oncol Biol Phys*, 53(4), pp. 1023-37.

Kutcher, G. J., Burman, C., Brewster, L., Goitein, M. and Mohan, R. (1991) 'Histogram reduction method for calculating complication probabilities for three-dimensional treatment planning evaluations', *Int J Radiat Oncol Biol Phys*, 21(1), pp. 137-46.

Källman, P., Agren, A. and Brahme, A. (1992) 'Tumour and normal tissue responses to fractionated non-uniform dose delivery', *Int J Radiat Biol*, 62(2), pp. 249-62.

Larsen, E. W. (1992) 'In Honour of Jacques Devooght A theoretical derivation of the Condensed History Algorithm', *Annals of Nuclear Energy*, 19(10), pp. 701-714.

Laub, W. U. and Crilly, R. (2014) 'Clinical radiation therapy measurements with a new commercial synthetic single crystal diamond detector', *J Appl Clin Med Phys*, 15(6), pp. 4890.

Lee, M. C., Deng, J., Li, J., Jiang, S. B. and Ma, C. M. (2001) 'Monte Carlo based treatment planning for modulated electron beam radiation therapy', *Phys Med Biol*, 46(8), pp. 2177-99.

Li, J. G., Williams, S. S., Goffinet, D. R., Boyer, A. L. and Xing, L. (2000) 'Breast-conserving radiation therapy using combined electron and intensity-modulated radiotherapy technique', *Radiother Oncol*, 56(1), pp. 65-71.

Low, D. A., Harms, W. B., Mutic, S. and Purdy, J. A. (1998) 'A technique for the quantitative evaluation of dose distributions', *Med Phys*, 25(5), pp. 656-61.

Low, D. A., Starkschall, G., Bujnowski, S. W., Wang, L. L. and Hogstrom, K. R. (1992) 'Electron bolus design for radiotherapy treatment planning: bolus design algorithms', *Med Phys*, 19(1), pp. 115-24.

Lyman, J. T. (1985) 'Complication probability as assessed from dose-volume histograms', *Radiat Res Suppl*, 8, pp. S13-9.

Löf, J. (2000) *Development of a general framework for optimization of radiation therapy.* Stockholm University.

Ma, C. M., Ding, M., Li, J. S., Lee, M. C., Pawlicki, T. and Deng, J. (2003) 'A comparative dosimetric study on tangential photon beams, intensity-modulated radiation therapy (IMRT) and modulated electron radiotherapy (MERT) for breast cancer treatment', *Phys Med Biol*, 48(7), pp. 909-24.

Ma, C. M., Pawlicki, T., Lee, M. C., Jiang, S. B., Li, J. S., Deng, J., Yi, B., Mok, E. and Boyer, A. L. (2000) 'Energy- and intensity-modulated electron beams for radiotherapy', *Phys Med Biol*, 45(8), pp. 2293-311.

McDonald, M. W., Lawson, J., Garg, M. K., Quon, H., Ridge, J. A., Saba, N., Salama, J. K., Smith, R. V., Yeung, A. R., Yom, S. S., Beitler, J. J. and Cancer, E. P. o. R. O.-H. a. N. (2011) 'ACR appropriateness criteria retreatment of recurrent head and neck cancer after prior definitive radiation expert panel on radiation oncology-head and neck cancer', *Int J Radiat Oncol Biol Phys*, 80(5), pp. 1292-8.

Mikael, K. and Rockwell, M. T. (2013) *Electrons: are they underused in radiotherapy?* 2nd ESTRO Forum. Geneva, Switzerland. Available at: http://medicalphysicsweb.org/cws/article/opinion/53380 (Accessed: July 2016).

Mitchell, M. (1996) *An Introduction to Genetic Algorithms.* 5 edn. Cambridge, Massachusetts: Massachusetts Institute of Technology.

Morgan, A. M., Knöös, T., McNee, S. G., Evans, C. J. and Thwaites, D. I. (2008) 'Clinical implications of the implementation of advanced treatment planning algorithms for thoracic treatments', *Radiother Oncol,* 86(1), pp. 48-54.

Morgan, G., Ward, R. and Barton, M. (2004) 'The contribution of cytotoxic chemotherapy to 5-year survival in adult malignancies', *Clin Oncol (R Coll Radiol),* 16(8), pp. 549-60.

Mu, X., Olofsson, L., Karlsson, M., Sjögren, R. and Zackrisson, B. (2004) 'Can photon IMRT be improved by combination with mixed electron and photon techniques?', *Acta Oncol,* 43(8), pp. 727-35.

Mukesh, M. B., Harris, E., Collette, S., Coles, C. E., Bartelink, H., Wilkinson, J., Evans, P. M., Graham, P., Haviland, J., Poortmans, P., Yarnold, J. and Jena, R. (2013) 'Normal tissue complication probability (NTCP) parameters for breast fibrosis: pooled results from two randomised trials', *Radiother Oncol,* 108(2), pp. 293-8.

Nadella, K. R., Kodali, R. M., Guttikonda, L. K. and Jonnalagadda, A. (2015) 'Osteoradionecrosis of the Jaws: Clinico-Therapeutic Management: A Literature Review and Update', *J Maxillofac Oral Surg,* 14(4), pp. 891-901.

Nazareth, D. P., Brunner, S., Jones, M. D., Malhotra, H. K. and Bakhtiari, M. (2009) 'Optimization of beam angles for intensity modulated radiation therapy treatment planning using genetic algorithm on a distributed computing platform', *J Med Phys,* 34(3), pp. 129-32.

Nelder, J. A. and Mead, R. (1965) 'A Simplex Method for Function Minimization', *The computer journal,* 7(4), pp. 308-313.

Newhauser, W. D. and Zhang, R. (2015) 'The physics of proton therapy', *Phys Med Biol,* 60(8), pp. R155-209.

Niemierko, A. (1997) 'Reporting and analyzing dose distributions: a concept of equivalent uniform dose', *Med Phys,* 24(1), pp. 103-10.

Niemierko, A. (1999) 'WE-C2-10 A Unified Model of Tissue Response to Radiation', Med Phys, 26(6), pp. 1100.

Nutting, C. M., Morden, J. P., Harrington, K. J., Urbano, T. G., Bhide, S. A., Clark, C., Miles, E. A., Miah, A. B., Newbold, K., Tanay, M., Adab, F., Jefferies, S. J., Scrase, C., Yap, B. K., A'Hern, R. P., Sydenham, M. A., Emson, M., Hall, E. and group, P. t. m. (2011) 'Parotid-sparing intensity modulated versus conventional radiotherapy in head and neck cancer (PARSPORT): a phase 3 multicentre randomised controlled trial', *Lancet Oncol,* 12(2), pp. 127-36.

Olofsson, L., Mu, X., Nill, S., Oelfke, U., Zackrisson, B. and Karlsson, M. (2004) 'Intensity modulated radiation therapy with electrons using algorithm based energy/range selection methods', *Radiother Oncol,* 73(2), pp. 223-31.

Palma, B., Bazalova-Carter, M., Hårdemark, B., Hynning, E., Qu, B., Loo, B. W. and Maxim, P. G. (2016) 'Assessment of the quality of very high-energy electron radiotherapy planning', *Radiother Oncol,* 119(1), pp. 154-8.

Palma, B. A., Sánchez, A. U., Salguero, F. J., Arráns, R., Sánchez, C. M., Zurita, A. W., Hermida, M. I. and Leal, A. (2012) 'Combined modulated electron and photon beams planned by a Monte-Carlo-based optimization procedure for accelerated partial breast irradiation', *Phys Med Biol,* 57(5), pp. 1191-202.

Park, J. M., Choi, C. H., Ha, S. W. and Ye, S. J. (2011) 'The dosimetric effect of mixed-energy IMRT plans for prostate cancer', *J Appl Clin Med Phys,* 12(4), pp. 3563.

Poli, R. (2008) 'Analysis of the publications on the applications of particle swarm optimisation', 2008.

Rancati, T., Wennberg, B., Lind, P., Svane, G. and Gagliardi, G. (2007) 'Early clinical and radiological pulmonary complications following breast cancer radiation therapy: NTCP fit with four different models', *Radiother Oncol,* 82(3), pp. 308-16.

Ranganathan, V. and Maria Das, K. J. (2016) 'Determination of optimal number of beams in direct machine parameter optimization-based intensity modulated radiotherapy for head and neck cases', *J Med Phys,* 41(2), pp. 129-34.

Rocha, H., Dias, J. M., Ferreira, B. C. and Lopes, M. C. (2012) 'Discretization of optimal beamlet intensities in IMRT: A binary integer programming approach', *Mathematical and Computer Modelling,* 55(7–8), pp. 1969-1980.

Rogers, D. W., Faddegon, B. A., Ding, G. X., Ma, C. M., We, J. and Mackie, T. R. (1995) 'BEAM: a Monte Carlo code to simulate radiotherapy treatment units', *Med Phys,* 22(5), pp. 503-24.

Rosca, F. (2012) 'A hybrid electron and photon IMRT planning technique that lowers normal tissue integral patient dose using standard hardware', *Med Phys,* 39(6), pp. 2964-71.

Salari, E. and Unkelbach, J. (2013) 'A column-generation-based method for multi-criteria direct aperture optimization', *Phys Med Biol,* 58(3), pp. 621-39.

Sayre, G. A. and Ruan, D. (2013) 'Dose-shaping using targeted sparse optimization', *Med Phys,* 40(7), pp. 071711.

Schwarz, G., Berg, R. and Botstein, C. (1966) 'Changes in the relative biological effectiveness (RBE) of a 35 Mev. electron beam as a function of tissue depth', *Am J Roentgenol Radium Ther Nucl Med,* 97(4), pp. 1049-52.

Seppenwoolde, Y., Lebesque, J. V., de Jaeger, K., Belderbos, J. S., Boersma, L. J., Schilstra, C., Henning, G. T., Hayman, J. A., Martel, M. K. and Ten Haken, R. K. (2003) 'Comparing different NTCP models that predict the incidence of radiation pneumonitis. Normal tissue complication probability', *Int J Radiat Oncol Biol Phys,* 55(3), pp. 724-35.

Shepard, D. M., Earl, M. A., Li, X. A., Naqvi, S. and Yu, C. (2002) 'Direct aperture optimization: a turnkey solution for step-and-shoot IMRT', *Med Phys,* 29(6), pp. 1007-18.

Silva, A., Neves, A. and Costa, E. (2002) 'An Empirical Comparison of Particle Swarm and Predator Prey Optimisation', in O'Neill, M., Sutcliffe, R.F.E., Ryan, C., Eaton, M. & Griffith, N.J.L. (eds.) *Artificial Intelligence and Cognitive Science: 13th Irish Conference, AICS 2002 Limerick, Ireland, September 12–13, 2002 Proceedings*. Berlin, Heidelberg: Springer Berlin Heidelberg, pp. 103-110.

Smilowitz, J. B., Das, I. J., Feygelman, V., Fraass, B. A., Kry, S. F., Marshall, I. R., Mihailidis, D. N., Ouhib, Z., Ritter, T., Snyder, M. G., Fairobent, L. and Group, A. M. P. P. G. T. (2015) 'AAPM Medical Physics Practice Guideline 5.a.: Commissioning and QA of Treatment Planning Dose Calculations - Megavoltage Photon and Electron Beams', *J Appl Clin Med Phys,* 16(5), pp. 5768.

Spirou, S. V. and Chui, C. S. (1998) 'A gradient inverse planning algorithm with dose-volume constraints', *Med Phys,* 25(3), pp. 321-33.

St-Hilaire, J., Sévigny, C., Beaulieu, F., Gingras, L., Tremblay, D. and Beaulieu, L. (2009) 'Optimization of photon beam energy in aperture-based inverse planning', *J Appl Clin Med Phys,* 10(4), pp. 3012.

Su, S., Moran, K. and Robar, J. L. (2014) 'Design and production of 3D printed bolus for electron radiation therapy', *J Appl Clin Med Phys,* 15(4), pp. 4831.

Sun, C., Cheng, C. W., Shimm, D. S. and Cassady, J. R. (1998) 'Dose profiles in the region of abutting photon and electron fields in the irradiation of head and neck tumors', *Med Dosim,* 23(1), pp. 5-10.

Surucu, M., Klein, E. E., Mamalui-Hunter, M., Mansur, D. B. and Low, D. A. (2010) 'Planning tools for modulated electron radiotherapy', *Med Phys,* 37(5), pp. 2215-24.

Svolos, P., Tsougos, I., Kyrgias, G., Kappas, C. and Theodorou, K. (2011) 'On the use of published radiobiological parameters and the evaluation of NTCP models regarding lung pneumonitis in clinical breast radiotherapy', *Australas Phys Eng Sci Med,* 34(1), pp. 69-81.

Teoh, M., Clark, C. H., Wood, K., Whitaker, S. and Nisbet, A. (2011) 'Volumetric modulated arc therapy: a review of current literature and clinical use in practice', *Br J Radiol,* 84(1007), pp. 967-96.

Thwaites, D. I., DuSautoy, A. R., Jordan, T., McEwen, M. R., Nisbet, A., Nahum, A. E., Pitchford, W. G. and Party, I. W. (2003) 'The IPEM code of practice for electron dosimetry for radiotherapy beams of initial energy from 4 to 25 MeV based on an absorbed dose to water calibration', *Phys Med Biol,* 48(18), pp. 2929-70.

Thwaites, D. I. and Tuohy, J. B. (2006) 'Back to the future: the history and development of the clinical linear accelerator', *Phys Med Biol,* 51(13), pp. R343-62.

Timlin, C., Houston, M. and Jones, B. (2011) 'Malignant induction probability maps for radiotherapy using X-ray and proton beams', *Br J Radiol,* 84 Spec No 1, pp. S70-8.

Timlin, C., Warren, D. R., Rowland, B., Madkhali, A., Loken, J., Partridge, M., Jones, B., Kruse, J. and Miller, R. (2015) '3D calculation of radiation-induced second cancer risk including dose and tissue response heterogeneities', *Med Phys,* 42(2), pp. 866-76.

Unkelbach, J., Menze, B. H., Konukoglu, E., Dittmann, F., Le, M., Ayache, N. and Shih, H. A. (2014) 'Radiotherapy planning for glioblastoma based on a tumor growth model: improving target volume delineation', *Phys Med Biol,* 59(3), pp. 747-70.

van der Laan, H. P., Korevaar, E. W., Dolsma, W. V., Maduro, J. H. and Langendijk, J. A. (2010) 'Minimising contralateral breast dose in post-mastectomy intensity-modulated radiotherapy by incorporating conformal electron irradiation', *Radiother Oncol,* 94(2), pp. 235-40.

van't Riet, A., Mak, A. C., Moerland, M. A., Elders, L. H. and van der Zee, W. (1997) 'A conformation number to quantify the degree of conformality in brachytherapy and external beam irradiation: application to the prostate', *Int J Radiat Oncol Biol Phys,* 37(3), pp. 731-6.

Verellen, D. and Vanhavere, F. (1999) 'Risk assessment of radiation-induced malignancies based on whole-body equivalent dose estimates for IMRT treatment in the head and neck region', *Radiother Oncol,* 53(3), pp. 199-203.

Verhey, L. J. (2002) 'Issues in optimization for planning of intensity-modulated radiation therapy', *Semin Radiat Oncol,* 12(3), pp. 210-8.

von Neubeck, C., Seidlitz, A., Kitzler, H. H., Beuthien-Baumann, B. and Krause, M. (2015) 'Glioblastoma multiforme: emerging treatments and stratification markers beyond new drugs', *Br J Radiol,* 88(1053), pp. 20150354.

Webb, S. (1989) 'Optimisation of conformal radiotherapy dose distributions by simulated annealing', *Phys Med Biol,* 34(10), pp. 1349-70.

Webb, S. (2003) 'Use of a quantitative index of beam modulation to characterize dose conformality: illustration by a comparison of full beamlet IMRT, few-segment IMRT (fsIMRT) and conformal unmodulated radiotherapy', *Phys Med Biol,* 48(14), pp. 2051-62.

Weber, D. C., Mirimanoff, R. O. and Miralbell, R. (2007) '[Proton beam therapy: clinical indications and summary of the Swiss experience]', *Bull Cancer,* 94(9), pp. 807-15.

Weber, D. C., Trofimov, A. V., Delaney, T. F. and Bortfeld, T. (2004) 'A treatment planning comparison of intensity modulated photon and proton therapy for paraspinal sarcomas', *Int J Radiat Oncol Biol Phys,* 58(5), pp. 1596-606.

Weinberg, R. (2007) *Electron Intensity Modulation for Mixed-Beam Radiation Therapy with an X-Ray Multi-leaf Collimator.* PhD, The University of Texas.

Wu, X. and Zhu, Y. (2001) 'An optimization method for importance factors and beam weights based on genetic algorithms for radiotherapy treatment planning', *Phys Med Biol,* 46(4), pp. 1085-99.

Yang, X.-S. (2008) *Nature-inspired metaheuristic algorithms.* Frome, U.K.: Luniver Press.

Yu, C., Shepard, D., Earl, M., Cao, D., Luan, S., Wang, C. and Chen, D. Z. (2006) 'New developments in intensity modulated radiation therapy', *Technol Cancer Res Treat,* 5(5), pp. 451-64.

Zackrisson, B., Johansson, B. and Ostbergh, P. (1991) 'Relative biological effectiveness of high-energy photons (up to 50 MV) and electrons (50 MeV)', *Radiat Res,* 128(2), pp. 192-6.

Zhang, Y., Feng, Y., Ming, X. and Deng, J. (2016) 'Energy Modulated Photon Radiotherapy: A Monte Carlo Feasibility Study', *Biomed Res Int,* 2016, pp. 7319843.

Zou, W., Fisher, T., Zhang, M., Kim, L., Chen, T., Narra, V., Swann, B., Singh, R., Siderit, R., Yin, L., Teo, B. K., McKenna, M., McDonough, J. and Ning, Y. J. (2015) 'Potential of 3D printing technologies for fabrication of electron bolus and proton compensators', *J Appl Clin Med Phys*, 16(3), pp. 4959.

Appendix A

Optimisation Algorithms

This Appendix presents a description of the heuristic optimisation algorithms and parameters used in Chapter 5. A description of the function used for benchmarking the algorithm is presented in Table A1. This work was conducted in collaboration with undergraduate students Paul Johnson and Thomas Roussi.

A.1. Genetic Algorithm

The Genetic algorithm is a heuristic search method that is inspired by the natural process of evolution. Genetic algorithms (GA) have been used extensively for the optimisation of problems where gradient based solutions can become trapped into local minima. The general method of a genetic algorithm is to randomly create an initial population of solutions in a search space then enable these solutions to mutate and combine with each other to create an overall solution that meets the required criteria. Each solution in this population has a set of properties that control its overall ability. Each property in the solution is referred to as a gene that can be mutated or altered. If just one of these genes is changed it has the ability to change the overall solution. Each gene is assessed by a fitness factor and the most successful genes selected to progress (Mitchell, 1996). The basic algorithm for the GA used in this work consists of the following:

Step 1. Generate: The initial population of random solutions is created with each gene being part of the search space.

Step 2. Evaluate: The fitness function is used to rate the initial population and evaluates their ability to solve the problem

Step 3. Select: The most effective solutions of the problem are selected from the fitness function

Step 4. Combine: The selected solutions are then have their properties combined by the process of crossover to create 'children' that contain propertied of each of the 'parents'.

Step 5. Mutate: A proportion of children are allowed to randomly mutate.

Step 6. Evaluate: These solutions are then evaluated by the fitness function

Step 7. Destroy: The old less effective solutions are destroyed and replaced by newer solutions

Step 8. Finish or repeat: If the fitness function produces a result the meets the needed criteria then the program is stopped. If the system has not reached this criteria then the system resets back to step 3

The parameters used for the GA algorithm are given Table A2.

A.2. Particle Swarm Optimisation (PSO)

Particle Swarm Optimisation is a method based on the swarming intelligence that can occur in flocks of birds or shoals of fish. The population of this swarm consists of particles. Each particle assesses its current fitness value within the search space it is inside and communicates its own with neighbours in the swarm. The movement of each particle is controlled by a movement vector that is controlled by the history of fitness factors of it and its neighbours and also random permutations (Poli, 2008)

The basic algorithm of the particle swarm used in this work consists of the following:

Step 1. Initialize : Create a swarm of Particles uniformly distributed around the search space

Step 2. Evaluation: Particles asses their fitness and asses the best know position compared to their initial condition

Step 3. Update: The swarm updates the best know position

Step 4. Movement: Each particle calculates their vector movement (mixture of random movement and best known position)

Step 5. End or Repeat: Repeat to step 2 if the system requirements are not met. If they are met the algorithm finishes.

The parameters used for the PSO algorithm are given Table A2.

A.1. Firefly Algorithm

The Firefly Algorithm is a nature inspired algorithm, inspired by the behaviour of fireflies (Yang, 2008). In reality, fireflies emit light to attract fireflies of the other sex and to find a loving partner. The Firefly Algorithm is inspired by this behaviour but with some modifications:

1) All fireflies are unisexual, so that any individual firefly will be attracted to all other fireflies;
2) Attractiveness is proportional to their brightness, and for any two fireflies, the less bright one will be attracted by (and thus move towards) the brighter one; however, the intensity (apparent brightness) decrease as their mutual distance increases;
3) If there are no fireflies brighter than a given firefly, it will move randomly;

With these known factors is in now possible to describe the algorithm for the Firefly algorithm. Which follows as:

Step 1. Initialize: Create a swarm of fireflies uniformly distributed around the search space with randomly created initial velocities.

Step 2. Evaluation: Asses the fitness of the Fireflies through a fitness function and then produce the equivalent brightness for each firefly. Including the idea of distance change.

Step 3. Movement: Each firefly moves in the direction of search space that has the brightest firefly compared to them.

Step 4. Repeat and End: This cycle repeats to Step 2 until the criteria for the fitness value is best and so the best solution is chosen.

A summary of the parameters used for the Firefly algorithm are given Table A2.

Table A1 Functions used for tuning and evaluation of the optimisation algorithms

Function	Equation	1D or 2D representation of function
Second order PID	$\frac{y}{u} = \frac{1}{s^2 + 2s + 4}$	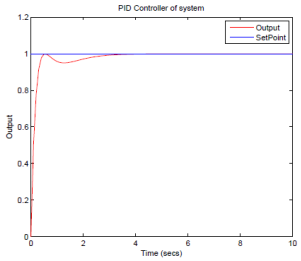
Third order PID	$\frac{y}{u} = \frac{1}{s^3 + 6s^2 + 2s + 4}$	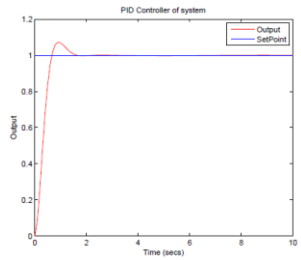
Griewank function	$f_1(\vec{x}) = \frac{1}{4000}\left(\sum_{i=1}^{D}(x_i^2)\right) - \left(\prod_{i=1}^{D} cos\left(\frac{x_i}{\sqrt{i}}\right)\right) + 1$	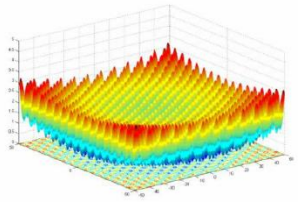
Rosenbrock function	$f_2(\vec{x}) = \sum_{i=1}^{D} 100(x_i^2 - x_{i+1})^2 + (1 - x_i)^2$	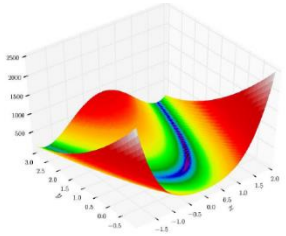
Ackley function	$f_3(\vec{x}) = 20 + e - 20e^{\left(-0.2\sqrt{\frac{1}{D}\sum_{i=1}^{D} x_i^2}\right)} - e^{\frac{1}{D}\sum_{i=1}^{D} cos(2\pi x_i}$	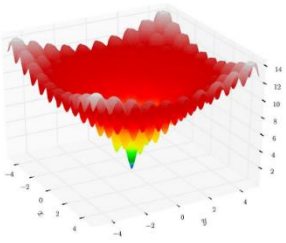

Table A2 Optimisation algorithm parameters used for IMRT problem

Algorithm	Parameter	Description
GA	PopulationSize: 1000	Size of the population
	CrossoverFraction: 0.8	The fraction of the population at the next generation created by the crossover function
	MigrationFraction:0.2	Fraction of individuals in each subpopulation that migrates to a different subpopulation
	MigrationInterval:20	Number of generations that take place between migrations of individuals between subpopulations
PSO	MaxGen: 400	Maximum number of generations of each particle
	D:200	Swarm size
	1.0	Inertia weight
	C1,C2: 2.0	Learning factor
PPO	MaxGen: 300	Maximum number of generations of each particle
	D:50	Swarm Size
	R: 3	Search Range
	α:0.1	Alpha Velocity
	Imax: 10	Inertia Max
	Imin: 0	Inertia Min
	C1:2	Learning factor
	C2:8	Learning factor
	Fa:1	Fear range: maximum amplitude
	Fb:1	Fear range: drop off characteristic
	FL:0.7	Fear level
	Ev:5	Exploratory move: vector size
	Es:0.01	Exploratory move: step size
	Ed:1	Exploratory move: number dimensions
Firefly	MaxGen : 200	Maximum number of generations of each particle
	n:400	Number of fireflies.
	β :1	Adjusts the importance of the move term over the precedent location.
	γ :0.1	Absorption coefficient: The higher it is, the less the fireflies will be attracted by each other.
	α :0.8	Adjusts the importance of the random term (0-1).
	δ :0.99	Randomness reduction

Appendix B

Dose-volume data

This Appendix presents the dose objectives used for the treatment plan evaluation in Chapter 6 along with the dose-volume data achieved for the clinical plan (Monaco), the X-ray only plan (xIMRT) and the combined electron and X-ray plan (exIMRT).

Table B1 Dose-volume data: Case 1 Paraspinal Sarcoma (a.l.a.p. = as low as possible)

	Dose Objective	6MV VMAT (Monaco)	xIMRT	exIMRT
Volume to PTV (Gy)		Dose (Gy)		
98%	≥54Gy	54.0	56.0	55.9
95%	≥57Gy	57.2	57.9	57.3
50%	=60Gy	60	60	60
5%	≤63	61.7	61.3	62.4
2%	≤66	62.4	61.8	63.4
Structure		Dose to 1cc (Gy)		
Spinal cord PRV	≤50Gy	50.0	25.2	33.0
		Dose to 100cc		
Small Bowel	a.l.a.p	6.9	4.3	2.2
Large Bowel	a.l.a.p	7.1	6.3	1.2
		Mean Dose (Gy)		
Right Kidney	a.l.a.p	8.5	6.3	2.4
Left Kidney	a.l.a.p	8.5	7.3	2.6
Spleen	a.l.a.p	12.5	10.5	2.6
Liver	a.l.a.p	4.7	1.9	0.7

Table B2 Dose-volume data: Case 2 Brain

	Dose Objective	6MV VMAT (Monaco)	xIMRT	exIMRT
Dose to PTV (Gy)		Dose (Gy)		
99%	≥54Gy	57	57.1	54.2
95%	≥57Gy	57.8	58.2	57.1
50%	=60Gy	60	60	60
5%	≤63	61.6	61.0	62.7
2%	≤66	62.0	61.5	63.4
Structure				
Brain stem PRV	D_{1cc}≤60Gy (54Gy optimal)	56.4	55.3	32.6
	V_{59Gy}<10cc	0	0	0
Chiasm PRV	D_{max}<60Gy (54Gy optimal)	59.3	58.7	47.7
Optic Nerve Left	D_{max}<60Gy (54Gy optimal)	23.1	23.2	9.1
Optic Nerve Right	D_{max}<60Gy (54Gy optimal)	57.5	40.1	45.4
Orbit Left	D_{max}<50	11.1	9.3	2.5
Orbit Right	D_{max}<50	34.9	6.7	19.5
Lens Left	D_{max}<6	3.9	5.7	1.1
Lens Right	D_{max}<6	8.1	1.5	5.3

Table B3 Dose-volume data: Case 3 Breast

Volume	Dose Objective		6MV ssIMRT (Monaco)	xIMRT	exIMRT
	Volume	Dose			
PTV_{WB}-PTV_{PB}	>90%	32.4Gy	98.3	96.8	94.3
	median dose = 34 - 37Gy		37.0	36.1	35.6
	< 5%	> 40Gy	0.9	0.8	1.8
PTV_{PB}-PTV_{TB}	> 90%	36.0Gy	97.0	97.5	99.4
	median dose = 40 - 44Gy		40.8	39.7	43.2
	< 3%	> 53Gy	0.4	0.1	0.2
PTV_{TB}	> 95%	50.4Gy	96.9	97.4	95.1
	median dose = 52.5 - 53.5 Gy		53.0	53.6	53.5
	< 3%	> 56.7 Gy	0.1	0.0	0.6
	Global max < 58.3 Gy		57.4	57.9	58.2
	Dose (Gy)	%Max allowable volume (Optimal)			
Ipsilateral Lung	18	15 (10)	9.3	7.2	6.9
	9	-	18.2	13.0	10
	2	-	51.1	45.0	25.7
	Mean	6	5.8	5.0	3.5
Contralateral Lung	2.5	15 (5)	11.2	9.7	0.1
	Mean	(1)	1.0	0.9	0.1
Heart	13	10 (2)	0.7	0.4	0.3
	2	-	15.5	12.0	10.4
	Mean	(3)	1.9	1.1	0.7
Contralateral Breast	Mean	1.5 (0.5)	1.0	1.4	0.1

Table B4 Dose-volume data: Case 4 Head and Neck re-treatment

	Dose Objective	6MV ssIMRT (Monaco)	xIMRT	exIMRT
Dose to PTV (Gy)		Dose (Gy)		
99%	≥54Gy	55.4	53.5	54.0
95%	≥57Gy	57.7	57.0	57.2
50%	=60Gy	60	60	60
5%	≤63	61.5	61.5	63.5
2%	≤66	61.9	62.5	64.5
Structure				
Cord PRV	D_{1cc}≤5Gy Optimal	5.9	3.3	5.1
	D_{max} <10Gy	7.5	15.1	8.6
Mandible	D_{1cc} a.l.a.p.	56.8	54.8	57.4
	D_{mean} a.l.a.p.	19.7	17.8	15.6

Appendix C

Radiobiology

This Appendix presents a description of the radiobiology models and parameters used for the treatment plan evaluation in Chapter 6.

C1. NTCP

Two normal tissue complication (NTCP) models have been used for the calculations in Chapter 6. The Lyman-Kutcher-Burman (LKB) model and the relative seriality model. Both models are described in detail in TG-166 (Allen Li et al., 2012). They are formulated as described below with parameters used for these models presented in Table C1.

LKB NTCP model

$$EUD = \left(\sum v_i D_i^{1/n}\right)^n$$

$$t = \frac{EUD - TD_{50}}{mTD_{50}}$$

$$NTCP = \frac{1}{\sqrt{2\pi}} \int_{-\infty}^{t} e^{\frac{x^2}{2}}\, dx$$

where *EUD* is the dose that, if given uniformly to the entire volume, will lead to the same NTCP as the actual non-uniform dose distribution, TD_{50} is the uniform dose given to the entire organ that

results in 50% complication risk, *m* is a measure of the slope of the sigmoid curve, *n* is the volume effect parameter, and v_i is the fractional organ volume receiving a dose D_i.

Relative Seriality Model

$$NTCP = \left[1 - \prod \left(1 - \left[2^{-e\gamma\left(1-{D_i}/{TD_{50}}\right)}\right]\right)^{{vi}/{V}}\right]^{1/s}$$

where v_i is the volume irradiated to a homogeneous dose D_i , V the total volume, TD_{50} is the uniform dose that causes 50% probability of complication, γ is the slope of the curve, and s is the relative seriality.

Table C1Parameters for NTCP calculations

Organ	Complication	Model	TD_{50}	a	m	Reference
Kidney	Renal dysfunction	LKB	28	0.7	0.1	Emami-Burman (1991)
Liver	Radiation induced liver disease	LKB	40	0.32	0.15	Emami-Burman (1991)
Brain	Necrosis	LKB	60	0.25	0.15	Emami-Burman (1991)
Breast	Fibrosis	LKB ($BEUD_3$)	132	0.012	0.35	Mukesh et al. (2013)
Lung	Grade ≥ 1 pneumonitis	LKB	16.4	0.86	0.36	Rancati et al., (2007)
Lungs as a paired Organ	Grade ≥ 2 pneumonitis	LKB	30.8	0.99	0.37	Seppenwoolde et al. (2003)
Heart	Cardiac mortality	Relative seriality	52.3	γ=1.28	s=0.87	Gagliardi (2007)
Mandible	Osteoradionecrosis	LKB	72	0.07	0.1	Emami-Burman (1991)

C2. Malignant Induction probability (MIP)

Malignant induction probability has been calculated according to Timlin et al. (Timlin et al., 2011, Timlin et al., 2015). The calculation has been formulated as described below with parameters used for this model presented in Table C2.

$$MIP \approx \epsilon n \sum_{i=1}^{N} C_{oi}(\gamma_i d_i + \delta_i d_i^2) e^{-n(\alpha_i d_i + \beta_i d_i^2)}$$

$$reMIP = \frac{MIP_{plan1}}{MIP_{plan2}}$$

where d_i, is the dose per fraction in voxel i, N is the number of voxels and α, β, γ, and δ are the radiobiological parameters. The number of fractions, n, the probability that a transformed cell becomes an overt malignancy, ϵ, and the number of cells pre-treatment in voxel i, C_{0i} , all cancel in the calculation of relative MIP.

Table C2 Parameters for relMIP calculations

	α,	β	γ	δ
Case 1&3	0.09	0.03	$10^{-6}\alpha$	$10^{-6}\beta$
Case 2	0.06	0.03	$10^{-6}\alpha$	$10^{-6}\beta$